



**UNIVERSIDADE FEDERAL DE MINAS GERAIS  
INSTITUTO DE GEOCIÊNCIAS  
PROGRAMA DE PÓS-GRADUAÇÃO EM GEOLOGIA**



# **DISSERTAÇÃO DE MESTRADO**

**GEOCRONOLOGIA U-PB, ANÁLISES ISOTÓPICAS LU-HF E LITOQUÍMICA DA  
REGIÃO DE RIBEIRÃO DA FOLHA, NORDESTE DE MINAS GERAIS:  
IMPLICAÇÕES TECTONOSSEDIMENTARES PARA A ZONA DE SUTURA DO  
ORÓGENO ARAÇUAÍ**

**AUTOR:** Leandro Silva dos Santos Amaral

**ORIENTAÇÃO:** Prof. Dr. Fabrício de Andrade Caxito

**COORIENTAÇÃO:** Prof. Dr. Antônio Carlos Pedrosa Soares

Nº 200

**BELO HORIZONTE  
DATA (29/03/2019)**

**Leandro Silva dos Santos Amaral**

**GEOCRONOLOGIA U-PB, ANÁLISES ISOTÓPICAS LU-HF E LITOQUÍMICA  
DA REGIÃO DE RIBEIRÃO DA FOLHA, NORDESTE DE MINAS GERAIS:  
IMPLICAÇÕES TECTONOSSEDIMENTARES PARA A ZONA DE SUTURA  
DO ORÓGENO ARAÇUAÍ**

**Dissertação apresentada ao programa de pós-graduação em geologia do Instituto de Geociências da Universidade Federal de Minas Gerais como requisito para a obtenção do título de mestre em geologia.**

**Área de concentração:** Geologia Regional

**Orientador:** Fabrício de Andrade Caxito

**Coorientador:** Antônio Carlos Pedrosa Soares

Belo Horizonte  
Instituto de Geociências  
Março de 2019

A485g  
2019

Amaral, Leandro Silva dos Santos.  
Geocronologia U-Pb, análises isotópicas Lu-Hf e litoquímica da Região de Ribeirão da Folha, Nordeste de Minas Gerais [manuscrito] : implicações tectonossedimentares para a zona de sutura do Orógeno Araçuaí / Leandro Silva dos Santos Amaral – 2019.  
102 f., enc.: il. (principalmente color.)

Orientador: Fabrício de Andrade Caxito.

Coorientador: Antônio Carlos Pedrosa Soares.

Dissertação (mestrado) – Universidade Federal de Minas Gerais, Instituto de Geociências, 2019.

Área de concentração: Geologia Regional.

Bibliografia: f. 71- 83.

Inclui anexos.

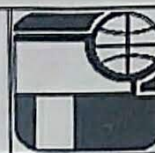
1. Geologia estrutural – Minas Gerais – Teses. 2. Tempo geológico – Teses. 3. Geoquímica – Minas Gerais – Teses. I. Caxito, Fabrício de Andrade. II. Pedrosa-Soares, Antônio Carlos. III. Universidade Federal de Minas Gerais. Instituto de Geociências. IV. Título.

CDU: 551.24 (815.1)



**UNIVERSIDADE FEDERAL DE MINAS GERAIS**

**PROGRAMA DE PÓS-GRADUAÇÃO EM GEOLOGIA**



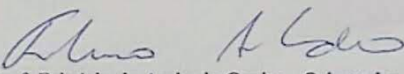
## FOLHA DE APROVAÇÃO

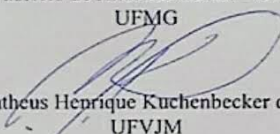
**GEOCRONOLOGIA U-PB, ANÁLISES ISOTÓPICAS LU-HF E GEOQUÍMICA DA REGIÃO DE RIBEIRÃO DA FOLHA, NORDESTE DE MINAS GERAIS: IMPLICAÇÕES TECTONOSSEDIMENTARES PARA A ZONA DE SUTURA DO ORÓGENO ARAÇUAÍ**

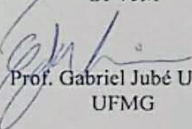
**LEANDRO SILVA DOS SANTOS AMARAL**

Dissertação submetida à Banca Examinadora designada pelo Colegiado do Programa de Pós-Graduação em GEOLOGIA, como requisito para obtenção do grau de Mestre em GEOLOGIA, área de concentração GEOLOGIA REGIONAL.

Aprovada em 29 de março de 2019, pela banca constituída pelos membros:

  
Prof. Fabrício de Andrade Caxito - Orientador  
UFMG

  
Prof. Matheus Henrique Kuchenbecker do Amaral  
UFVJM

  
Prof. Gabriel Jubé Uhlein  
UFMG

Belo Horizonte, 29 de março de 2019.

## AGRADECIMENTOS

Agradeço ao meu orientador Fabrício Caxito – sempre com sua praticidade e agilidade características – pelo apoio intelectual, pelas ideias compartilhadas e pelas mais diversas colaborações dadas durante a realização deste trabalho.

Ao meu coorientador Antônio Carlos Pedrosa Soares por todas as correções e sugestões dadas, pelas discussões durante o trabalho, e especialmente por ter me apresentado a riqueza geológica da região Ribeirão da Folha e me proposto um trabalho na área.

À D. Lia e ao “Seu” Antônio José, por terem me emprestado os aposentos de sua residência durante as campanhas de campo.

Aos técnicos e responsáveis do Laboratório de Laminação do Centro de Pesquisa Manoel Teixeira da Costa (CPMTC-IGC-UFGM), dos laboratórios de Preparação de Amostras para Geocronologia (LOPAG), Geoquímica Isotópica e Microscopia e Microanálises (LMic) da Universidade Federal de Ouro Preto, pelas dúvidas esclarecidas e pelas diversas colaborações.

Aos amigos e geólogos, Bruno Alcântara pelo apoio nos trabalhos de campo, Henrique Joncew, Pedro Leonardo Vieira, Laura Wisniowski e Ramon Aranda pelas análises e opiniões dadas durante as etapas de laboratórios, bem como pelos apoios nas ideias e em eventuais leituras do manuscrito.

À Janaina pela companhia, pelo apoio emocional concedido e pelo que representa.

Aos demais amigos dos anos de graduação e de pós-graduação que de alguma maneira colaboraram para que esse trabalho se tornasse possível.

## RESUMO

O Orógeno Araçuaí, localizado no sudeste do Brasil, é parte de um sistema orogênico Neoproterozoico desenvolvido entre os crátons do São Francisco e do Congo no contexto do Gondwana Ocidental. Nas proximidades da zona de sutura desse orógeno, ocorre a região de Ribeirão da Folha e o seu complexo ofiolítico homônimo. Este trabalho visa apresentar uma síntese desse complexo e destina especial atenção à sua seção superior – relativa à sedimentação turbidítica oceânica de margem passiva distal – com investigações acerca de suas proveniências sedimentares. Foram selecionadas três amostras (LC-004, LC-019 e LC-037) para análises de zircões detríticos com dados isotópicos combinados (U-Pb e Lu-Hf) e dez amostras para análises de geoquímica de rocha total. A amostra LC-037, representativa da Unidade A (predominantemente metapelítica), e a amostra LC-019 representativa da Unidade B (predominantemente metapsamítica), exibem idades máximas de sedimentação de 741 Ma e 673 Ma, respectivamente. Ambas apresentam grande similaridade em seus espectros de idades e em suas assinaturas isotópicas de Hf, as quais são compatíveis com a Formação Ribeirão da Folha, unidade de topo da bacia Macaúbas e precursora do Orógeno Araçuaí. A amostra LC-004 exibe zircões detríticos de idades ediacaranas e criogenianas com  $\epsilon_{\text{Hf}}$  de -7,2 a -6,3, provenientes do arco magmático Rio Doce e que são condizentes com as contribuições características da bacia sin-orogênica Salinas. A geoquímica de rocha total mostra que a maior parte das rochas metapelíticas analisadas possuem enriquecimento dos ETRL leves em relação aos ETRP ( $[\text{La}/\text{Yb} = 11,9 - 5,3]_N$ ), anomalia negativa de Eu ( $[\text{Eu}/\text{Eu}^* = 0,8 - 0,4]_N$ ) e padrão de distribuição relativamente plano para os ETRP ( $[\text{Gd}/\text{Yb} = 1,8 - 1,3]_N$ ), mas que distintas contribuições sedimentares também são parte do contexto, com padrões destoantes das demais. As amostras com características geoquímicas similares exibem razões Th/U (4,3 a 7,8) e Rb/Sr ( $> 0,5$ ) que indicam importante história de reciclagem sedimentar e de processos intempéricos, e as razões Th/Sc (0,5 a 1,2) e Zr/Sc (5,6 a 8,2) sugerem que as contribuições sedimentares são derivadas principalmente de rochas ígneas evoluídas. Diagramas geoquímicos multidimensionais indicam que as contribuições sedimentares são oriundas sobretudo de ambientes geotectônicos colisionais, com menor participação dos ambientes de arco magmático e de rifte continental. Por meio de análises microestruturais nos metapelitos foram reconhecidas três fases de deformações, com pico do metamorfismo progressivo na fácies anfíbolito, reconhecido na associação mineral de sua fase de deformação principal ( $D_n$ ). Os dados e as interpretações estruturais de  $D_n$  sugerem uma zona de cisalhamento de topo para SSW a SW, dominada por transpressão dextral. Dada a grande variabilidade litológica em área reduzida, com o envolvimento de diversos estágios evolutivos do Orógeno Araçuaí (da bacia precursora à bacia sin-orogênica, com presença de corpos ofiolíticos e granitos intrusivos tardi- à pós-colisionais), além de sua

complexa história deposicional e deformacional, é possível apontar o complexo ofiolítico de Ribeirão da Folha como a possível região de *mélange* tectônica do Orógeno Araçuaí.

**Palavras-chave:** *Mélange* tectônica; Geocronologia U-Pb; Isótopos Lu-Hf; Geoquímica de rocha total; Orógeno Araçuaí.

## ABSTRACT

*The Araçuaí Orogen, located in southeastern Brazil, is part of a Neoproterozoic orogenic system developed between the São Francisco and Congo cratons in the Western Gondwana setting. In the vicinity of this orogen's suture zone, the Ribeirão da Folha region and its homonymous ophiolitic complex occur. This work aims to present a synthesis of this complex, and address particular attention to its upper section – related to the oceanic turbidite sedimentation of distal passive margin – with investigations concerning its sedimentary origins. Three samples (LC-004, LC-019 and LC-037) were selected for detrital zircons analyzes with combined isotopic data (U-Pb and Lu-Hf), and ten samples for whole rock geochemistry analyzes. Sample LC-037, representative of Unit A (predominantly metapelitic), and sample LC-019, representative of Unit B (predominantly metapsamitic), exhibit maximum sedimentation ages of 741 Ma and 673 Ma, respectively. Both present great similarity in their age spectra and in their Hf isotopic signatures, which are compatible with the Ribeirão da Folha Formation, top unit of the Macaúbas Basin, and precursor to the Araçuaí Orogen. Sample LC-004 exhibits detrital zircons of Ediacaran and Cryogenian ages (599 Ma to 648 Ma), with  $\epsilon_{\text{Hf}}(t)$  of -7.2 to -6.3, derived the Rio Doce Magmatic Arc, and consistent with the characteristic contributions of the syn-orogenic Salinas Basin. The whole rock geochemistry reveals that most of the analyzed metapelitic rocks show enrichment of LREE in relation to HREE ( $[\text{La}/\text{Yb} = 11.9 - 5.3]_{\text{N}}$ ), negative Eu anomaly ( $[\text{Eu}/\text{Eu}^* = 0.8 - 0.4]_{\text{N}}$ ), and a relatively flat distribution pattern for the HREE ( $[\text{Gd}/\text{Yb} = 1.8 - 1.3]_{\text{N}}$ ), though that different sedimentary contributions are also part of the of setting, with contrasting patterns to the others. Samples with similar geochemical characteristics exhibit Th/U (4.3 to 7.8) and Rb/Sr ( $>0.5$ ) ratios which indicate an important history of sediment recycling and weathering processes, and Th/Sc (0.5 to 1.2) and Zr/Sc (5.6 to 8.2) ratios suggest that sedimentary contributions are derived mainly from evolved igneous rocks. Multidimensional geochemical diagrams indicate that the sedimentary contributions are mainly derived from collisional geotectonic environments, with minor participation of magmatic arc and continental rift environments. By means of microstructural analyzes in the metapelites, three deformation phases were recognized, with the progressive metamorphic peak in the amphibolite facies, recognized in the mineral association of its main deformation phase ( $D_n$ ). The data and structural interpretations of  $D_n$  suggest a top to SSW-SW shear, dominated by dextral transpression. Given the large lithological variability in a reduced area, with the involvement of several evolutionary stages of the Araçuaí Orogen (from the precursor basin to the syn-orogenic basin, with presence of ophiolitic bodies and late to post-collisional intrusive granites), as well as its complex depositional and*



*deformational history, it is possible to point out the ophiolitic complex of Ribeirão da Folha as the possible tectonic mélange region of the Araçuaí Orogen.*

**Keywords:** *Tectonic mélange; U-Pb Geochronology; Lu-Hf isotopes; Whole rock geochemistry; Araçuaí Orogen.*

## SUMÁRIO

1.	INTRODUÇÃO .....	15
1.1	Estrutura da dissertação.....	15
1.2	Premissa e objetivos .....	15
2.	LOCALIZAÇÃO E VIAS DE ACESSO .....	17
3.	O ESTADO DA ARTE DA REGIÃO DE RIBEIRÃO DA FOLHA.....	19
3.1	Formação Ribeirão da Folha .....	19
3.2	Formação Capelinha.....	22
3.3	Formação Salinas .....	23
4.	ARTIGO CIENTÍFICO: <i>EVIDENCE OF TECTONIC MÉLANGE IN THE RIBEIRÃO DA FOLHA OPHIOLITE COMPLEX (ARAÇUAÍ OROGEN, SE BRAZIL): INSIGHTS FROM LITHOCHEMISTRY, AND IN-ZIRCON U-PB AND LU-HF DATA</i> .....	25
1.	INTRODUCTION.....	27
2.	GEOTECTONIC SETTING .....	29
3.	MATERIALS AND METHODS .....	32
3.1.	Whole rock geochemistry .....	32
3.2.	U-Pb geochronology and Lu-Hf isotopic analyzes in detrital zircons .....	33
3.3.	Mineral chemistry .....	34
4.	RESULTS .....	35
4.1.	The tectonic <i>mélange</i> of Ribeirão da Folha .....	35
4.1.1.	The metavolcano-sedimentary ophiolitic Section.....	37
4.1.2.	The meta-mafic and meta-ultramafic ophiolitic section and the meta-plagiogranite of Ribeirão da Folha.....	41
4.1.3.	Late- to post-collisional intrusions.....	42
4.2.	Tectonic structures .....	44

4.3.	Deformation and metamorphism phases .....	45
4.4.	Mineral chemistry .....	48
4.4.1.	Garnet zoning .....	48
4.5.	Whole rock geochemistry .....	50
4.5.1.	Nature of the protolith and general geochemical characteristics .....	51
4.6.	U-Pb geochronology and Lu-Hf isotopic analysis in detrital zircons .....	53
4.6.1.	Sample LC-004 (staurolite-garnet-muscovite-biotite schist): U-Pb and Lu-Hf in detrital zircons.....	54
4.6.2.	Sample LC-019 (quartzite): U-Pb and Lu-Hf in detrital zircons .....	55
4.6.3.	Sample LC-037 (quartzite): U-Pb and Lu-Hf in detrital zircons .....	58
5.	DISCUSSIONS .....	59
5.1.	REE geochemical signature .....	59
5.2.	Intensity of weathering and sediment recycling.....	61
5.3.	Sedimentary provenance and tectonic ambience: geochemical perspective .....	62
5.4.	Sedimentary provenance: U-Pb and Lu-Hf analyzes .....	63
5.4.1.	Samples LC-019 and LC-037.....	64
5.4.2.	Sample LC-004 .....	66
6.	CONCLUSION AND TECTONIC MODEL .....	67
	REFERÊNCIAS BIBLIOGRÁFICAS.....	71

## ÍNDICE DE FIGURA

Figura 1. Localização e vias de acesso para a região de Ribeirão da Folha. .... 17

### ÍNDICE DE FIGURAS: ARTIGO CIENTÍFICO

Figure 1. The Araçuaí-West Congo Orogen (AWCO) and its simplified geological map with its lithotectonic assemblages..... 28

Figure 2. Units distribution of the Macaúbas Group precursor basin and the syn-orogenic Salinas Basin in the Araçuaí Orogen setting. .... 31

Figure 3. Simplified map and cross-section of the study area.. .... 36

Figure 4. The tectono-stratigraphic column of the study area.. .... 37

Figure 5. Lithologies and tectonic structures of the Ribeirão da Folha metasedimentary sequence.. .... 39

Figure 6. Photomicrographs of the Ribeirão da Folha peraluminous mica schists and orthoamphibolite. .... 43

Figure 7. Stereograms with plots and densities contours (equal-area) for the main tectonic structures observed..... 44

Figure 8. Diagram of relative ages of the commonly found minerals in the Ribeirão da Folha peraluminous mica schists in relation to the deformation phases..... 46

Figure 9. Chemical profiles along garnet porphyroblasts..... 49

Figure 10. Classification of the pelitic rocks of Ribeirão da Folha according to the Herron log ( $\text{SiO}_2/\text{Al}_2\text{O}_3$ ) vs.  $\log(\text{Fe}_2\text{O}_3^{(t)}/\text{K}_2\text{O})$  diagram ..... 52

Figure 11. Chondrite-normalized REE diagram ..... 53

Figure 12. Cathodoluminescence (CL) images of the detrital zircons..... 55

Figure 13. Frequency and probability curves histograms of the U-Pb geochronological analyzes57

Figure 14. Hf isotopic diagram. .... 59

Figure 15. Chondrite-normalized REE diagram, comparing sample LC-039 with data compiled from Pedrosa-Soares et al. (1998)..... 60

Figure 16. Verma and Armstrong-Altrin multi-dimensional diagram (2013) for tectonic discrimination of siliciclastic sediments. .... 63

Figure 17. Evolutionary model illustrating the development of the tectonic mélange of Ribeirão da Folha..... 69

## ÍNDICE DE TABELA

Tabela 1. Coordenadas dos vértices do polígono da área de estudo .....	18
--	----

## ÍNDICE DE TABELA: ARTIGO CIENTÍFICO

Table 1. Geochemical data of the mica schists of Ribeirão da Folha. ....	51
--	----

## 1. INTRODUÇÃO

### 1.1 Estrutura da dissertação

Esta dissertação de mestrado é apresentada no modelo de artigo científico, com base no que é proposto pelo programa de pós-graduação em Geologia do Instituto de Geociências da Universidade Federal de Minas Gerais (IGC-UFMG), e encontra-se estruturada em duas partes. A primeira (capítulos 1, 2 e 3) apresenta considerações preliminares acerca do trabalho realizado, com a premissa e os objetivos desta dissertação, a localização e as vias de acesso da área de estudo, na região de Ribeirão da Folha e, por fim, um levantamento do histórico dos trabalhos realizados nos seus arredores. A segunda parte (capítulo 4) contém o artigo científico – principal produto deste estudo – intitulado de “*Evidence of tectonic mélange in the Ribeirão da Folha ophiolite complex (Araçuaí orogen, SE Brazil): insights from lithochemistry, and in-zircon U-Pb and Lu-Hf data*”. No corpo do artigo estão contidas todas as informações necessárias para o entendimento deste estudo, com descrições acerca do contexto geológico regional e local, das metodologias utilizadas, bem como dos resultados obtidos e de suas discussões e conclusões resultantes. Todas as informações referidas no artigo como *Supplementary Files* se encontram em anexo à esta dissertação.

### 1.2 Premissa e objetivos

Situada nas proximidades da zona de sutura do Orógeno Araçuaí, a região de Ribeirão da Folha recebeu maior atenção após a descoberta de remanescentes oceânicos neoproterozoicos em meio às suas sequências metassedimentares. Os primeiros estudos que seguiram a essa descoberta se empenharam em compreender a região no contexto regional, que passou a ser interpretada como um complexo ofiolítico. Esse complexo ocorre de maneira desmembrada e deformada, com seções suboceânicas e seções oceânicas tectonicamente encaixadas em meio à seção metavulcanossedimentar da margem passiva distal da bacia Macaúbas. Os estudos subsequentes se dedicaram preferencialmente às seções ofiolíticas em separado, ou apenas a partes dessas seções.

Este estudo tem como objetivo principal promover uma melhor caracterização da porção superior desse complexo – representativa da seção metavulcanossedimentar – com atenção especial destinada às

rochas das sequências siliciclásticas. A partir da aquisição de novos dados, buscou-se uma melhor compreensão acerca da derivação dessas rochas metassedimentares, do seu ambiente deposicional e de suas proveniências sedimentares, das idades de sedimentação e do seu ambiente paleotectônico. Com isso, realizou-se uma integração entre os novos dados obtidos e parte dos disponíveis na literatura, os quais a partir das interpretações culminaram em consequências tectonossedimentares diretas para a zona de sutura do Orógeno Araçuaí.

Desse modo, os resultados e as interpretações das seções do complexo ofiolítico de Ribeirão da Folha serão apresentados no artigo científico apresentado nesta dissertação, com a utilização de dados petrográficos, estruturais e estratigráficos, também suportados por análises laboratoriais que envolvem geocronologia U-Pb e isotópicas Lu-Hf em zircões detríticos, e de litoquímica e química mineral das rochas metassedimentares da seção metavulcanossedimentar do ofiolito.

As despesas laboratoriais e os trabalhos de campo foram custeados pelos contratos de auxílio à pesquisa do Conselho Nacional de Desenvolvimento Científico e Tecnológico (CNPq), pela Fundação de Amparo à Pesquisa do Estado de São Paulo (FAPESP) e pelo Centro de Pesquisa Manoel Teixeira da Costa, vinculado ao Instituto de Geociências da Universidade Federal de Minas Gerais (CPMTC-IGC-UFMG).



## 2. LOCALIZAÇÃO E VIAS DE ACESSO

A área de estudo se localiza nos arredores do distrito de Ribeirão da Folha, município de Minas Novas, situado na porção nordeste do estado de Minas Gerais (Figura 1). O distrito de Ribeirão da Folha dista em linha reta cerca de 40 km da cidade de Minas Novas e Capelinha.

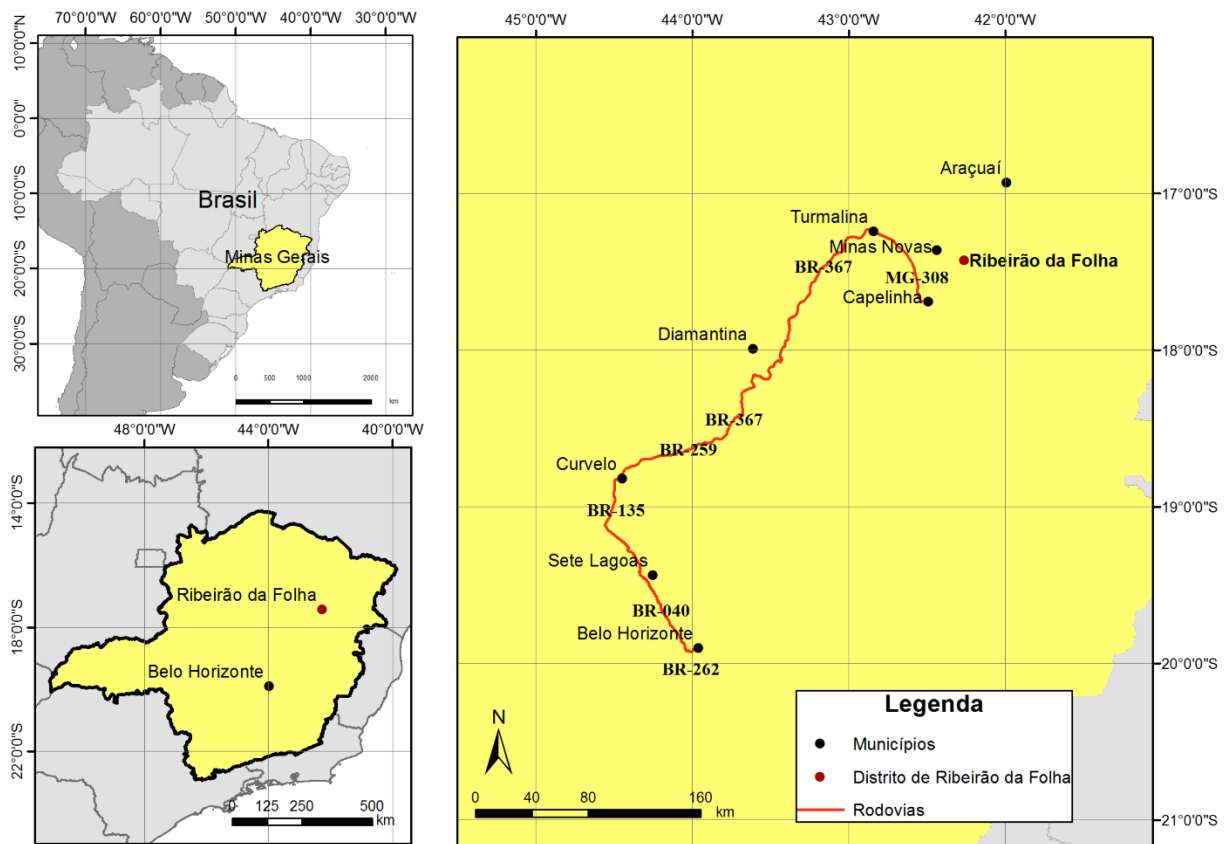


Figura 1. Localização e vias de acesso para a região de Ribeirão da Folha.

A área encontra-se inserida em sua maior parte na folha Jenipapo (SE-23-X-D-III, escala 1:100.000), mas também ocupa a porção noroeste da folha Malacacheta (SE-23-XD-VI, escala 1:100.000). As coordenadas dos vértices do polígono são dadas na Tabela 1.

<b>Vértice</b>	<b>UTM E</b>	<b>UTM N</b>
SW	765750	8051915
NW	765750	8085871
NE	799268	8085871
E	799268	8064040
Central	786078	8064040
S	786078	8051915

Tabela 1. Coordenadas dos vértices do polígono da área de estudo - UTM, Zona 24S, no datum WGS1984.

O acesso utilizado para o distrito de Ribeirão da Folha (Figura 1), partindo-se de Belo Horizonte, passa pela cidade de Capelinha, em um percurso total de aproximadamente 580 km. Inicialmente se percorre as rodovias BR-040, BR-135 e BR-259 até Diamantina. Posteriormente, toma-se a BR-367 passando por Turmalina e depois a MG-308 até Capelinha. A partir daí, são percorridos aproximadamente 50 km por estrada não pavimentada até o distrito de Ribeirão da Folha.

Outros acessos possíveis são:

- Belo Horizonte – Diamantina – Minas Novas – Ribeirão da Folha;
- Belo Horizonte – Governador Valadares – Teófilo Otoni – Novo Cruzeiro – Ribeirão da Folha.

### **3. O ESTADO DA ARTE DA REGIÃO DE RIBEIRÃO DA FOLHA**

Três unidades litoestratigráficas são historicamente descritas na região de Ribeirão da Folha: a unidade homônima Ribeirão da Folha, a unidade Capelinha e a unidade Salinas. Com o avanço dos estudos na região, as mesmas receberam hierarquias estratigráficas diferentes e, portanto, um resumo histórico dos estudos na região se faz importante, de modo a melhor compreender a evolução das ideias e não gerar confusões estratigráficas. Destaca-se de antemão que no estudo realizado nesta dissertação de mestrado, ocorre o predomínio da Formação Ribeirão da Folha, com ocorrência restrita – e pioneira – da Formação Salinas (como representante da bacia sin-orogênica do Orógeno Araçuaí).

Os subtítulos que se seguem utilizam da nomenclatura estratigráfica atual.

#### **3.1 Formação Ribeirão da Folha**

O primeiro trabalho documentado na região de Ribeirão da Folha foi realizado por Luciano Jacques de Moraes, entre os anos de 1920 e 1930. O autor descreveu as rochas da região e as incluiu no Grupo Macaúbas (apud Pedrosa-Soares et al. 1995).

Ferrari (1985), utilizando os dados do Projeto Jequitinhonha (Fontes et al., 1978) coordenado pela Companhia de Pesquisa de Recursos Minerais (CPRM) e pelo Departamento Nacional de Produção Mineral (DNPM), sugere, nos arredores dos distritos de Ribeirão da Folha e Baixa Quente, a ocorrência de mineralizações de ouro. Estas estariam associadas às sequências com contribuições vulcânicas ácida, básica e ultrabásica, associadas com variedades filíticas, quartzíticas e de chert, possivelmente de idades arqueanas.

Pedrosa-Soares et al. (1986) caracterizam as sequências de Ribeirão da Folha como uma sucessão metavulcanossedimentar, que contém ricas camadas sulfetadas. Um novo posicionamento estratigráfico foi proposto, e a região passou a ser incluída na “Unidade Salinas”, correlata do Grupo Macaúbas.

Três trabalhos de graduação foram realizados por alunos do curso de Geologia da Universidade Federal de Minas Gerais (Freitas-Silva e Pereira, 1987; Lagoeiro e Menegasse, 1987; Silva et al., 1987), com o objetivo de realizar o mapeamento geológico da região de Ribeirão da Folha em escala 1:25.000. Foi então caracterizada a subunidade metapelítica P<sub>sx</sub>, pertencente a “Unidades Salinas”, na qual

predominam quartzo-mica-xistos granatíferos (com presença de feldspato e/ou de carbonatos), com eventual presença de estauroлита, cianita ou sillimanita, e que estariam intercalados em menor quantidade por rochas calciossilicáticas, grafita-xistos, quartzitos, metacherts, anfibolitos e diopsidito, todos possivelmente sulfetados. Situadas a leste do leito Ribeirão da Folha, foram também descritas as rochas do corpo metaultramáfico do Córrego do Rubinho.

Pedrosa-Soares et al. (1990a, 1990b) passaram a interpretar a “Unidade Salinas” como margem passiva do Grupo Macaúbas e questionaram a natureza exclusivamente ensiálica atribuída à bacia Macaúbas nos estudos da época. A subunidade Psx, por sua vez, passou à hierarquia de “Fácies”, sendo então nomeada de “Fácies Ribeirão da Folha”.

Uhlein (1991), incluiu a região de Ribeirão da Folha como uma unidade do seu “Complexo Salinas” a partir de estudos regionais, e considerou que a bacia Macaúbas teria se depositado em ambiente exclusivamente ensiálico.

Pedrosa-Soares et al. (1992) propuseram um novo modelo tectônico para a bacia Macaúbas, contrapondo o modelo exclusivamente ensiálico vigente, destacando evidências mesmo que parciais de oceanização. Muitos dos argumentos em defesa do novo modelo se basearam nas rochas da “Unidade Salinas” (chamada de “Formação Salinas” no mesmo trabalho), que consistiam de turbiditos distais relacionados a leques submarinos, e que continham as sequências metavulcanossedimentares da fácies Ribeirão da Folha como as típicas representantes de um ambiente situado próximo da abertura oceânica. Nesse trabalho foram apresentadas idades isocrônicas Sm-Nd das rochas metaultramáficas e dos anfibolitos de Ribeirão da Folha, que forneceram idades de  $793 \pm 90$  Ma.

Pedrosa-Soares (1995, 1997), Pedrosa-Soares et al. (1998, 2001) e Pedrosa-Soares e Wiedemann-Leonardos (2000) realizaram estudos acerca do ambiente deposicional e paleotectônico da “Fácies (ou “Membro”) Ribeirão da Folha”, já considerando o modelo de oceanizado da bacia Macaúbas. Como consequência, o acervo litológico de Ribeirão da Folha recebeu descrições mais detalhadas, passando a ser caracterizado por micaxisto peraluminoso (com granada, estauroлита, cianita e/ou sillimanita) e quartzo-micaxisto, com intercalações de formações ferríferas bandadas ricas em silicatos (granada e anfibólito), óxidos (magnetita e hematita) e sulfetos (principalmente pirita), metachert, diopsidito sulfetado com corpos de sulfeto maciço, xisto grafitoso e rocha calciossilicática. Realizaram-se também análises qualitativas do metamorfismo com base nas paragêneses minerais do micaxisto peraluminoso, que indicaram fácies anfibolito médio (na zona da cianita, com a presença de estauroлита), e análises quantitativas a partir de cálculos geotermobarométricos, cujas temperaturas se situam entre 550°C e

570°C (com pico de 600°C) e as pressões litostáticas entre 5,0 e 5,5 kbar. A partir de análises geoquímicas, os anfíbolitos da “Fácies” Ribeirão da Folha, foram caracterizados como derivados de magmas toleíticos, com assinatura de assoalho oceânico, e idade de cristalização magmática (Sm-Nd em rocha total) de  $816 \pm 72$  Ma. As formações ferríferas bandadas, o metachert e o diopsidito foram interpretados como sedimentos químico-exalativos, originados a partir de fontes vulcânicas oceânicas, com variados teores de contaminações por sedimentos argilosos e por matéria orgânica pelágica. As rochas metaultramáficas do Córrego do Rubinho passaram a ser interpretadas como lascas suboceânicas tectonicamente encaixadas na “Fácies” Ribeirão da Folha e em suas sequências quartzíticas sobrepostas.

Lima et al. (2002), estudando as sequências turbidíticas localizadas nas proximidades da cidade de Salinas, obtiveram idades U-Pb em zircões detríticos que indicam idade máxima de sedimentação de 568 Ma. Como essas idades são mais jovens que as comumente encontradas para o Grupo Macaúbas, os pacotes turbidíticos dos arredores de Salinas passaram a ser interpretados como resquícios de uma bacia tardi-orogênica, sobreposta à bacia Macaúbas. Com isso, a “Fácies Ribeirão da Folha” passou a ser entendida como Formação Ribeirão da Folha – representante da margem passiva distal do Grupo Macaúbas.

Brandani e Costa (2004) em trabalho de graduação pela Universidade Federal de Minas Gerais, realizam o mapeamento em escala 1:25.000 da região de Baixa Quente – distrito situado a norte de Ribeirão da Folha – e observaram a continuidade de suas sucessões metassedimentares.

Queiroga (2006) e Queiroga et al. (2006), realizaram a caracterização minerográfica das diversas fases sulfetadas das rochas de Ribeirão da Folha e identificaram pelo menos três estágios de sulfetação nas variedades de metachert e diopsidito. Apresentaram também novas análises litoquímicas – sobretudo das sequências químicas – que indicam que os metacherts apresentam contribuições pelíticas; que os diopsiditos se tratam de rochas híbridas com componentes exalativos (quartzo + sulfetos), os quais possuem marcante contribuição máfico-ultramáfica; que as formações ferríferas do tipo silicato estão intimamente associadas com os xistos pelíticos; e que as formações ferríferas do tipo óxido exibem assinatura de elementos terras raras (ETR) com forte anomalia negativa de cério, o que sugere origem em ambiente submarino com herança das rochas da pilha ofiolítica. Apresentaram também novas análises do metamorfismo, baseada qualitativamente nas paragêneses minerais da xistosidade principal ( $S_n$ ), que indica o metamorfismo como pertencente a fácies anfíbolito (zona da cianita), e quantitativamente pela geotermobarometria em  $S_n$ , cujos valores indicam um intervalo de temperatura e pressão situados na fácies anfíbolito intermediário (530°C - 600°C e 4,9 - 5,3 kbar).

Queiroga (2010) realizou a caracterização petrográfica, geoquímica e isotópica dos remanescentes oceânicos do Orógeno Araçuaí, incluindo as rochas metamáficas e metaultramáficas de Ribeirão da Folha. As características petrográficas e geoquímicas dessas rochas indicam afinidade ofiolítica e origem em ambiente de fundo oceânico. Os dados isotópicos Sm-Nd indicam assinaturas positivas de  $\epsilon\text{Nd}$  (+1,8 a +6,3) e suas idades modelo  $T_{\text{DM}}$  sugerem desenvolvimento de crosta oceânica durante o Neoproterozoico. Esse trabalho propôs que as vênulas leucocráticas presentes nos anfibolitos tratam-se de plagiogranito oceânico e apresentou estudos geocronológicos U-Pb em seus zircões. As idades obtidas indicam idade de cristalização magmática em aproximadamente 640 Ma, as quais passaram a ser consideradas como os indícios das idades da geração de crosta oceânica da bacia Macaúbas.

### **3.2 Formação Capelinha**

O Projeto Jequitinhonha (Fontes et al., 1978) foi pioneiro em descrever e a individualizar as espessas sequências quartzíticas que predominam nos altos topográficos situados nas proximidades do município de Capelinha, situada a sudoeste e a cerca de 40 km de Ribeirão da Folha.

Nos trabalhos de graduação de Freitas-Silva e Pereira (1987), Menegasse e Lagoeiro (1987) e Silva et al. (1987), as sequências quartzíticas situadas na região de Ribeirão da Folha foram caracterizadas como a subunidade Psq, pertencente a “Unidade Salinas”. Segundo os autores, a subunidade é constituída por quartzitos puros ou micáceos e, em menor proporção, por quartzitos ferruginosos, quartzitos feldspáticos e quartzo-muscovita xisto.

Grossi-Sad et al. (1991) em trabalho realizado para a ACESITA-GEOSOL nos arredores dos municípios de Capelinha, Turmalina e Minas Novas, caracterizou informalmente a Formação Capelinha. Os autores sugeriram que a Formação Capelinha estaria sobreposta aos xistos da “Unidade Salinas” e corresponderia a unidade de topo do Grupo Macaúbas.

Grossi-Sad et al. (1993), caracterizaram de fato a Formação Capelinha como uma nova unidade litoestratigráfica do Grupo Macaúbas, e a dividiu em dois membros, inferior e superior. O membro inferior é constituído majoritariamente por protoquartzito micáceo, ferruginoso, feldspático e/ou grafitoso, intercalado com quartzo-mica xisto rico em plagioclásio e xisto carbonoso-grafitoso. Já o

membro superior, apresenta predomínio de ortoquartzito laminado, com ocorrências locais de quartzito ferruginoso que podem ou não conter micas e/ou feldspatos.

Pedrosa-Soares (1995, 1997) demonstrou a distribuição territorial da Formação Capelinha no vale do Rio Araçuaí e vizinhanças. O autor também considera a Formação Capelinha como sobreposta à Formação Ribeirão da Folha, destacando a ocorrência de discordância, de contatos tectônicos, e do marcante contraste sedimentológico entre ambas. Nesses trabalhos o autor também considerou a Formação Capelinha como o registro sedimentológico do fechamento da bacia Macaúbas, e sugeriu que as proveniências sedimentares estariam predominantemente relacionadas aos blocos arqueanos do embasamento – sobretudo ao bloco Guanhães – situado a sudeste e relativamente próximo da região de Ribeirão da Folha.

Brandani e Costa (2004) em trabalho de graduação, relataram em mapa geológico em escala 1:25.000 a continuidade da Formação Capelinha na região de Baixa Quente, situada nas proximidades e a norte de Ribeirão da Folha.

Castro (2014), em trabalho nos arredores da cidade de Capelinha separou a formação em duas unidades: uma basal, predominantemente metapsamítica, constituída por mica xistos, xistos quartzosos e quartzitos, puros ou micáceos, com magmatismo básico associado, e uma superior, majoritariamente metapelítica, composta por xistos peraluminosos granatíferos, que podem conter estaurolita e/ou cianita. A partir de análises geocronológicas realizadas na unidade inferior (idade máxima de sedimentação em torno de 970 Ma) e superior (idade máxima de sedimentação em torno de 1123 Ma), bem como em amostras de anfibolito (cristais de zircão com idades de cristalização magmática em *ca.* 956 Ma), considera que a Formação Capelinha está posicionada estratigraficamente na base do Grupo Macaúbas, com ocorrência de magmatismo sinsedimentar, contemporâneo ao estágio de rifteamento que levou a abertura da bacia Macaúbas no período Toniano.

### **3.3 Formação Salinas**

Lima et al. (2002) caracterizou a Formação Salinas como representante da bacia orogênica do Orógeno Araçuaí, constituída por grauvasca, arenito grauvaquiano, pelito e conglomerado clasto-suportado, que representam depósitos sedimentares de plataforma, talude e bacia, correspondentes da sedimentação plataformal rasa até turbidítica. Antes desse trabalho, o nome “Salinas” era atribuído às

sequências metassedimentares predominantemente pelito-arenosas relacionadas à margem passiva da bacia Macaúbas.

A redefinição da Formação Salinas e a sua retirada do Grupo Macaúbas são sustentadas por indícios diversos: o metamorfismo regional da pilha grauvaquiana evidenciam fácies xisto verde (zona da biotita, principalmente), o que configura contraste com a zoneografia metamórfica do Grupo Macaúbas nas proximidades da zona de sutura, onde há predomínio da fácies anfibolito; o acamamento sedimentar das sequências da Formação Salinas apresenta mergulho baixo para norte, ao passo que as sequências do Grupo Macaúbas apresentam mergulhos comumente para leste, sugerindo uma discordância angular entre as unidades; os atributos geoquímicos e as idades obtidas pelos zircões detríticos extraídos de grauvacas e de seixos de rochas vulcânicas e sub-vulcânicas félsicas contidos nos conglomerados, indicam proveniência sedimentar relacionada ao arco magmático do Orógeno Araçuaí.



**4. ARTIGO CIENTÍFICO: *EVIDENCE OF TECTONIC MÉLANGE IN THE RIBEIRÃO DA FOLHA OPHIOLITE COMPLEX (ARAÇUAÍ OROGEN, SE BRAZIL): INSIGHTS FROM LITHOCHEMISTRY, AND IN-ZIRCON U-PB AND LU-HF DATA***

---

**Evidence of tectonic mélange in the Ribeirão da Folha ophiolite complex (Araçuaí orogen, SE Brazil): insights from lithochemistry, and in-zircon U-Pb and Lu-Hf data**

Leandro Silva dos Santos Amaral <sup>a, \*</sup>, Fabrício de Andrade Caxito <sup>a, 1</sup>, Antônio Pedrosa Soares <sup>a, 1</sup>,  
Ricardo Trindade <sup>b, 1</sup>, Marly Babinski <sup>b, 1</sup>, Gláucia Queiroga <sup>c, 1</sup>,  
Cristiano Lana <sup>c, 1</sup>

<sup>a</sup> Universidade Federal de Minas Gerais, Programa de Pós-Graduação em Geologia, CPMTc-IGC-UFMG, Av. Antônio Carlos 6627, Pampulha, 31270-901, Belo Horizonte, MG, Brazil

<sup>b</sup> Instituto de Geociências, Universidade de São Paulo, Rua do Lago, 562, 05580-080, São Paulo, SP, Brazil

<sup>c</sup> Departamento de Geologia, Escola de Minas, Universidade Federal de Ouro Preto, Morro do Cruzeiro, 35400-000, MG, Brazil

\* Corresponding author.

<sup>1</sup> Research fellow of the Brazilian Scientific Council (CNPq).

E-mail addresses: leandrosamaral@outlook.com (L. Amaral), facaxito@yahoo.com.br (F. Caxito), pedrosasoares@gmail.com (A. Pedrosa Soares), ritrindad@gmail.com (R. Trindade), babinski@usp.br (M. Babinski), glauciaqueiroga@yahoo.com.br (G. Queiroga), cristianodeclana@gmail.com (C. Lana)

**Abstract**

The Araçuaí orogen (SE Brazil) and the West Congo belt (SW Africa) make up a confined orogenic system (AWCO) developed between the São Francisco and Congo cratons from the Ediacaran to Cambrian. The AWCO, embraced by cratonic land to the north, east and west, but connected to Brasiliano – Pan-African orogens to the south, includes a northern ensialic sector and a southern sector that experienced limited ocean spreading. The Late Cryogenian (c. 650 Ma) Ribeirão da Folha ophiolitic complex, located close to the northern segment of the AWCO suture zone, roughly marks the boundary between those distinct sectors. Although strongly deformed and tectonically dismembered, the Ribeirão da Folha complex includes ophiolitic meta-ultramafic and meta-mafic rocks with meta-plagiogranite

bodies, and a well-preserved sedimentary section composed, at the base, of metamorphosed chemical-exhalative sediments (cherts, massive sulphides, diopsidites, banded iron formations), followed, to the top, by a thick package of siliciclastic sediments (pelites, semipelites, psammites). This work aims to present a synthesis of this complex, and address particular attention to its upper section – related to the oceanic turbidite sedimentation of distal passive margin – with investigations concerning its sedimentary origins. Three deformation phases were recognized, with the peak of progressive metamorphism in the amphibolite facies related to the main deformation phase ( $D_n$ ) on metapelites. Kinematic indicators from  $D_n$  suggest a top to SSW-SW shear zone, dominated by dextral transpression. Analytical studies, together with data from the literature, include ten samples selected for lithochemical analyses, and three samples (LC-004, LC-019 and LC-037) for U-Pb (LA-ICPMS) geochronology coupled with isotopic Lu-Hf analysis on detrital grains of zircon. Sample LC-037, representative of the predominantly pelitic Unit A, and sample LC-019, representative of the predominantly psammitic Unit B, exhibit maximum sedimentation ages around 741 Ma and 673 Ma, respectively. Both present great similarity in their age spectra and Hf isotopic signatures, being compatible with published data for the Ribeirão da Folha Formation. Besides Cryogenian zircon grains, sample LC-004 also exhibits detrital zircons of Ediacaran age with  $\epsilon_{Hf}$  from -7.2 to -6.3, similar to those from the Rio Doce magmatic arc (630 – 580 Ma), similar to published data from metasedimentary units related to that arc and the syn-orogenic Salinas Formation. Most metapelitic rocks shows enrichment of light rare earth elements in relation to heavy ones ( $[La/Yb = 11.9 - 5.7]_N$ ), negative Eu anomaly ( $[Eu/Eu^* = 0.8 - 0.4]_N$ ), and a relatively flat distribution pattern for the heavy rare earth elements ( $[Gd/Yb = 1.8 - 1.3]_N$ ), though that different sedimentary contributions are also part of the of the setting, with contrasting patterns to the others. Samples with similar geochemical characteristics exhibit Th/U (4.3 to 7.8) and Rb/Sr ( $>0.5$ ) ratios which indicate an important history of sediment recycling and weathering processes, and Th/Sc (0.5 to 1.2) and Zr/Sc (5.6 to 8.2) ratios suggest that sedimentary contributions are derived mainly from evolved igneous rocks. Multidimensional geochemical diagrams indicate sedimentary contributions mainly derived from collisional environments, with minor participation of magmatic arc and continental rift sources. Actually, the distinct sediment provenances together with the large lithological variability in a reduced area and presence of meta-magmatic ophiolitic bodies, involved in a complex depositional and deformational history, suggest a tectonic *mélange* related to the Ribeirão da Folha ophiolite complex, marking a segment of the suture zone of the Araçuaí orogen.

**Keywords:** Tectonic *mélange*; Sedimentary provenance; U-Pb Geochronology; Lu-Hf isotopes; Whole rock geochemistry; Araçuaí Orogen.

## 1. INTRODUCTION

Collisional orogens result from converging tectonic movements which succeed the subduction and culminate in the collision of two or more continental blocks. The suture zone is the extension which joins these lands, presents a diverse lithological assemblage, and involves, other than the blocks in collision, the sedimentation of the passive and of deep sea margin, the rocks of the ocean floor, the sedimentation related to the volcanic arc and the syn-orogenic sedimentation (flysch). When these contents of distinct origins and characteristics are arranged in a region of mappable scale, which presents diverse rock bodies arranged in a chaotic manner, usually surrounded by a clayey, sandy or ophiolitic matrix and with no clear continuity of their strata and/or contacts, the region can also be characterized as a tectonic *mélange* (Festa et al., 2010a, 2010b, 2012). Based on these premises, this study aims to point out the evidences of the tectonic *mélange* of the Araçuaí Orogen, from a comprehensive tectonic analysis.

The Araçuaí Orogen (Fig. 1) is a collisional orogen developed from the Ediacaran to the Cambrian, located in southeastern Brazil, between the 15°S and 21°S parallels, surrounded by the São Francisco Craton (Pedrosa-Soares et al., 2001, 2007, 2011). For more than four decades of systematic studies, with most of its area covered by geological maps and extensive laboratory data, the Araçuaí Orogen is one of the most investigated geological settings in the Brazilian territory, with a robust theoretical foundation (e.g. Pedrosa-Soares et al., 2001, 2007, 2008, 2011; Alkmim et al., 2006, 2007; Tedeschi et al., 2016). Regarding the paleogeographic reconstructions of Western Gondwana (Porada, 1989; Brito Neves and Cordani, 1991; Trompette, 1997), the Araçuaí Orogen corresponds to the western counterpart of an orogenic system, separated from its eastern counterpart, the West Congo Orogen, located on the African continent.

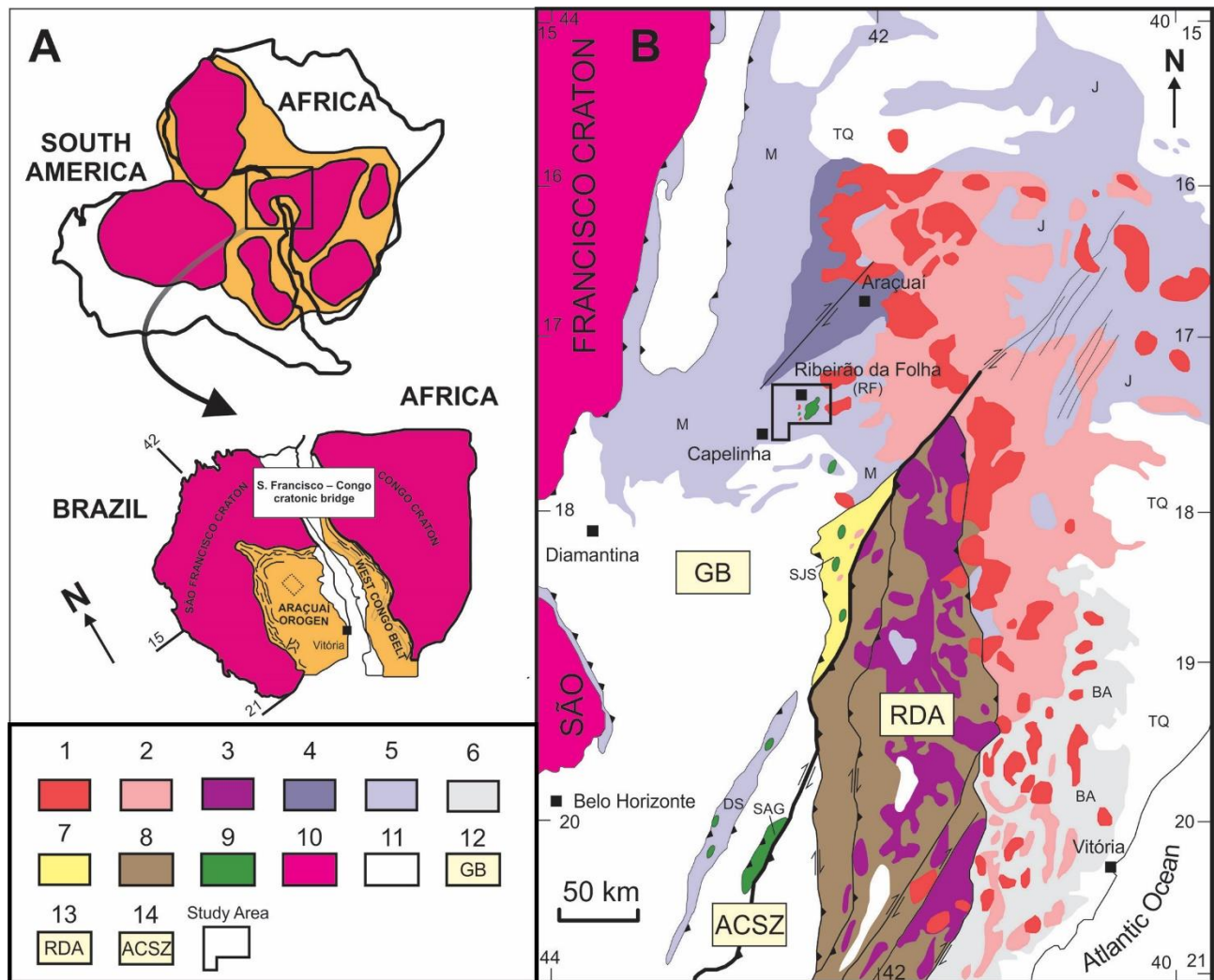


Figure 1. (A). The Araçuaí-West Congo Orogen (AWCO) and the surrounding São Francisco-Congo Craton in the setting of Western Gondwana (modified from Alkmim et al., 2006). (B) Simplified geological map of the Araçuaí Orogen with its lithotectonic assemblages: 1, late to post-collisional granitic intrusions (545 to 480 Ma); 2, collisional granitic intrusions (585 to 540 Ma); 3, pre-collisional intrusions of the Rio Doce Magmatic Arc (630 to 580 Ma); 4, the syn-orogenic Salinas Basin (or Salinas Formation); 5, rift and passive margin sequences of the Macaúbas Basin and its related units (M: Macaúbas Group, DS: Dom Silvério Group, J: Jequitinhonha Complex); 6, back-arc deposits; 7, accretionary wedge; 8, volcano-sedimentary arc deposits; 9, ophiolitic complexes (RF: Ribeirão da Folha, DS: Dom Silvério, SJS: São José da Safira, SAG: Santo Antônio do Grama); 10, São Francisco Craton; 11, pre-neoproterozoic and Cenozoic units (TQ); 12, Guanhanes Block; 12, Rio Doce Magmatic Arc; 13, Abre Campo Shear Zone. Modified from Pedrosa-Soares et al. (2008).

With the definition of the Abre Campo shear zone as the suture zone of the Araçuaí Orogen (Alkmim et al., 2006, 2007), by joining the Paleoproterozoic and Archean-Paleoproterozoic basements (Cunningham et al., 1996, 1998; Peres et al., 2004), a better characterization of its adjacent terrains became necessary (e.g. Peixoto et al., 2015), given that in areas of Precambrian sutures it is always complicated to distinguish a suture zone from any shear zone, since great part of the evidences may have

been destroyed or remodeled by more recent events. For this study, the region of Ribeirão da Folha (state of Minas Gerais, southeastern Brazil) was selected, where there is the presence of a dismembered and deformed ophiolitic complex, with suboceanic and oceanic mantle sections tectonically encased in the metavolcano-sedimentary section of the Macaúbas Basin, with also evidence of syn-orogenic sedimentation related to the Salinas Basin (Fig. 1 and 3). Thus, this study aims to present contributions to the surrounding area of the Araçuaí Orogen suture zone, highlighting its vast lithological and structural setting, its sedimentary provenances, and the depositional environment of the Ribeirão da Folha region, which can be considered a representative of the tectonic *mélange* region of the Araçuaí Orogen, supporting the compatibility of the spatial geotectonic relations to the suture zone. For this, in this study there will be presented investigations and interpretations of petrographic, stratigraphic and structural nature, with the support of laboratory analyzes involving U-Pb geochronology and Lu-Hf isotopic studies (LA-ICP-MS) in detrital zircons, as well as mineral chemistry and lithochemistry in metasedimentary rocks of the metavolcano-sedimentary section of the Ribeirão da Folha ophiolite.

## 2. GEOTECTONIC SETTING

The study area is part of the Araçuaí Orogen (Fig. 1), an Ediacaran collisional orogen which conserves, along with its earlier stages, evidences of a complete Wilson Cycle. Therefore, it can be well comprehended based on its lithotectonic assemblages, temporarily summarized as follows: 1) Archean-Paleoproterozoic and Paleoproterozoic-Mesoproterozoic basement complexes; 2) Tonian-Cryogenian succession of the Macaúbas Group, representative of the orogen's precursor basin, with associated ophiolitic sequences; 3) The Ediacaran Rio Doce Magmatic Arc and its associated metavolcano-sedimentary deposits; 4) The syn-orogenic Salinas Basin; 5) The syn- to post-collisional magmatic suites.

The Araçuaí Orogen's basement is composed by the Archean-Paleoproterozoic assemblage (Noce et al., 2007; Teixeira et al. 2000, 2016; Aguilar et al., 2017; Degler et al., 2018) represented by the complexes originated from the paleocontinental counterparts of the São Francisco-Congo Craton (Guanhães, Gouveia, Porteirinha, Mantiqueira, Juiz de Fora e Pocrane), and the Paleoproterozoic-Mesoproterozoic assemblage related to aulacogens (Noce et al., 2007; Pedrosa-Soares e Alkmim, 2011; Chemale et al., 2012; Guadagnin et al., 2015) with anorogenic granites (Borrachudos and Lagoa Real Suites) and sedimentary records of a paleo-mesoproterozoic continental rift (Espinhaço Supergroup).

The Macaúbas Group (Fig. 2), of Tonian-Cryogenian age, represents the precursor basin system of the Araçuaí Orogen, comprised of two Neoproterozoic rifting stages: rift 1, in the Early Tonian (c. 935-875 Ma), which resulted in the opening of the Macaúbas Basin, and rift 2, in the Late Tonian to Late Cryogenian (c. 735-650 Ma), which led its extensive development, with the establishment of its passive margin and consequent oceanization, with the occurrence of at least one glacial event in the Neoproterozoic (Pedrosa-Soares and Alkmim, 2011; Pedrosa-Soares et al., 2011a; Babinski et al., 2012; Caxito et al., 2012; Kuchenbecker et al., 2015). Among the upper sequences of the Macaúbas Group, representative of the oceanic sedimentation, there are tectonically dismembered ophiolitic complexes, in which fragments of metamafic-ultramafic rocks exhibit lithochemical and isotopic data indicative of oceanic signatures (Pedrosa-Soares et al., 1992, 1998, 2001; Pedrosa-Soares, 1995, 1997; Aracema et al., 2000; Suita et al., 2004; Queiroga et al., 2007; Queiroga, 2010; Peixoto et al., 2015), as recorded in the schist belts of Ribeirão da Folha, São José da Safira and Dom Silvério, as well as in the Santo Antônio do Grama Suite. Zircon crystals extracted from the meta-plagiogranite bodies of Ribeirão da Folha and the amphibolite of Santo Antônio do Grama, provide U-Pb ages of approximately 660 and 600 Ma, respectively, and have been interpreted as an indication of the oceanic crust production of the Macaúbas Basin (Queiroga et al., 2007; Queiroga, 2010). Further NE, the paragneisses of the Jequitinhonha Complex represent a high-grade metamorphic equivalent of the distal, post-glacial deep sea Macaúbas Group (Gonçalves-Dias et al., 2016).

The assemblage related to the inversion stage, with the shortening of the Macaúbas Basin, now under the setting of an active continental margin, is represented by the rocks that constitute the Ediacaran Rio Doce Magmatic Arc (Pedrosa-Soares et al., 2011b; Gonçalves et al., 2016, 2017; Tedeschi et al., 2016; Novo et al., 2018). The Rio Doce arc is characterized by an expanded calc-alkaline series, with Type I plutons, and predominance of crustal magmas under mantelic ones, which indicate the subduction process of the pre-collisional stage of the orogen, developed from 630 to 580 Ma (Pedrosa-Soares et al., 2001; Nalini Jr. et al., 2005; Pedrosa-Soares et al., 2008, 2011b; Tedeschi et al., 2016). Metavolcano-sedimentary successions accumulated in the marginal basins related to the magmatic arc. The forearc and intra-arc sequences are associated with the Rio Doce Group, which include mica schists and paragneisses with intercalation of quartzites, meta-graywackes, meta-volcanics, meta-volcanoclastics, calc-silicatics and pyroclastics, with U-Pb magmatic crystallization ages of about 595 Ma, and of approximately 584 Ma for volcanic protoliths (Vieira, 2007; Novo et al., 2018). The back-arc basin contains predominantly paragneisses with intercalation of calc-silicatic rocks from the Nova Venécia Complex, with a maximum sedimentation age of 600 Ma (Noce et al., 2004).

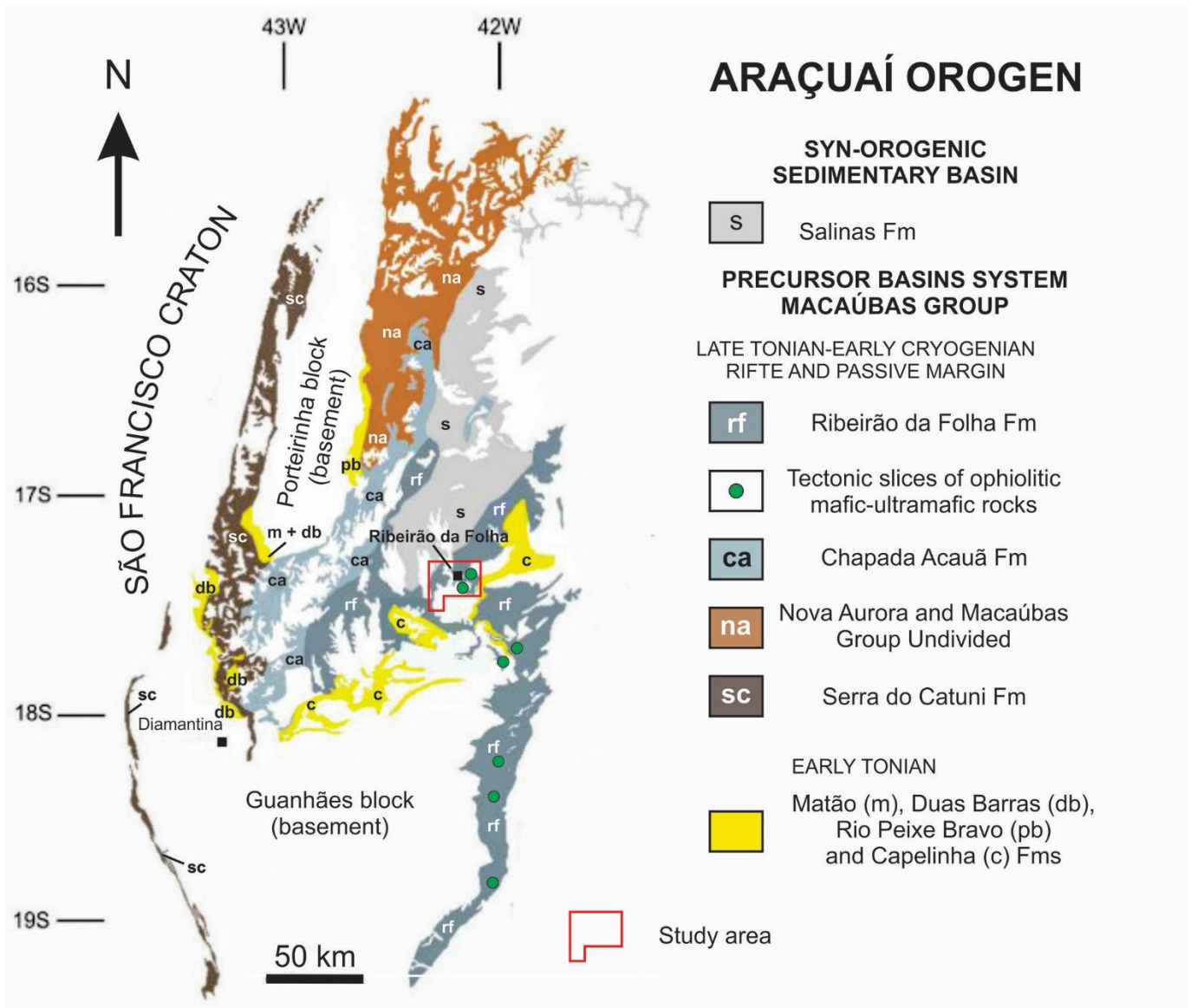


Figure 2. Units distribution of the Macaúbas Group precursor basin and the syn-orogenic Salinas Basin in the Araçuaí Orogen setting (modified from Castro (2014) after Pedrosa-Soares et al., (2011)).

Overlapping the Macaúbas precursor basin lies the Salinas Formation, representative of a syn-orogenic sedimentary basin, with an important sedimentary contribution from the Rio Doce Magmatic Arc (Santos et al., 2009). The Salinas Formation (or Salinas Basin) consists of a thick sandy-pelitic turbidite sequence, which contains lenses of conglomerates with volcanic rock pebbles of the magmatic arc, and calc-silicatic rocks, with a maximum sedimentation age of approximately 588 Ma (Lima et al., 2002; Pedrosa-Soares et al., 2008; Santos et al., 2009).

The collisional stage of the Araçuaí Orogen occurred under extensive production of peraluminous granites with ages between 585 and 540 Ma, and other granitic intrusions aged between 545 and 480 Ma,

known as late to post-collisional products (Pedrosa-Soares et al., 2001, 2011b; Gradim et al., 2014; Peixoto et al., 2015; Richter et al., 2016; Serrano et al., 2018). The magmas which originated the peraluminous granites of the syn-collisional stage might be related to a complex combination of tectonic processes related to the subduction and the continental collision (Gradim et al., 2014; Tedeschi et al., 2016), as well as to the crustal thickening and the tangential tectonic processes of the continental blocks (Pedrosa-Soares et al., 2007). The late to post-collisional products are interpreted based on the mantle delamination and the extensional gravitational collapse of the orogen's final stages, with the production of plutons composed of granites and mafic rocks, which characterizes a bimodal assemblage (Pedrosa-Soares et al., 2001, 2011b; Gradim et al., 2014; Tedeschi et al., 2016).

From the tectonic array point of view, the Araçuaí Orogen can be well understood with two domains: external and internal. The external domain exhibits greenschist facies metamorphism, predominantly, covers the fold and thrust belt which borders the São Francisco Craton and extends until the orogen's suture zone, while the internal domain, representative of the crystalline nucleus of the orogen, presents granulite facies metamorphism, with voluminous granitoid bodies and extensive anatexis (Pedrosa-Soares et al., 2001; Alkmim et al., 2006; Noce et al., 2007). The recorded structures demonstrate centrifugal vergences directed towards the cratonic areas, with the western sector of the crystalline nucleus registering a predominantly top-to-west tectonic transport, towards the São Francisco Craton, whereas the eastern sector presents its vergence mostly to the east (Alkmim et al., 2006). The continental suture zone of the orogen is marked by the Abre Campo shear zone, which limits the occurrence of the granitoids of the magmatic arc to the east, and the ophiolitic complexes to the west (Fig. 1B). To the west of the Abre Campo shear zone, the orogen's accretionary wedge occurs, which is architected under a schist belt arranged in dextral shear zones of N-NE direction, situated between an elevation of the Archean-Paleoproterozoic basement (Guanhães block) and the plutonic rocks of the Rio Doce Magmatic Arc (Cunningham et al., 1996, 1998; Peres et al., 2004; Alkmim et al., 2006; Peixoto et al., 2015).

### **3. MATERIALS AND METHODS**

#### **3.1. Whole rock geochemistry**

The samples received previous treatment of washing and cutting, for a better selection of portions free from weathering and secondary hydrothermal alterations, as well as for a better choice of the most



homogeneous and representative mineral portions. The analyzes were performed in the SGS Geosol laboratories by ICP-MS (Inductively Coupled Plasma Mass Spectrometry), and by ICP-OES (Inductively Coupled Plasma Optical Emission Spectrometry) for the major, trace and rare earth elements. The loss on ignition (LOI) was determined by weighing the difference after ignition at 450°C and/or 1,000°C. The complete results of these analyzes are displayed in Supplementary Files.

### **3.2. U-Pb geochronology and Lu-Hf isotopic analyzes in detrital zircons**

Ten to fifteen kilograms for each sample of the metasedimentary rocks analyzed were collected, free from weathering and hydrothermal changes. Two samples (LC-019 and LC-037) had their preparation and preliminary cares executed at the laboratory of High-Purity Mineral Separation, in the Manoel Teixeira da Costa Research Center, of the Federal University of Minas Gerais (SEPURA-CPMTC-UFMG), followed by grain separation, imaging and analyzes at the Laboratory of Samples Preparation for Geochemistry and Geochronology, in the Geology Department of the Federal University of Ouro Preto (LOPAG-DEGEO-UFOP). Sample LC-004 endured the same procedures as the two samples mentioned above, though carried out at the Geochronological Research Center, of the Geosciences Institute of the University of São Paulo (CPGeo-IGc-USP).

Initially, the samples were washed with the purpose of removing superficial impurities. Subsequently, heavy minerals concentrates were extracted from the samples through the conventional crushing, milling, gravimetric and magnetic separation (*Frantz* isodynamic separator) procedures. The collection of the detrital zircon grains was performed by manual picking, with grains selection in a binocular loupe. About 200 grains were randomly collected from each one of the quartzite samples (LC-019 and LC-037), in order to obtain the greatest variability of zircons generations possible, so to better identify their distinct sedimentary provenances. In the staurolite-garnet-muscovite-biotite schist sample (LC-004), it was attempted to collect the same amount of grains, however, the sample was found to be poor in zircons, having only 32 grains collected. The grains were then mounted in epoxy resin discs, and afterwards polished for the better exposure of their centers. The grains were then imaged by cathodoluminescence (CL) and by backscattered electron (BSE), using the JEOL 6510 Scanning Electron Microscope for the recognition of the morphological features, internal structures, presence of inclusions, cracks or damaged areas in the collected grains. Finally, the U-Pb and Lu-Hf analyzes were performed

in LA-MC-ICP-MS (Laser Ablation Multi-Collector Inductively Coupled Plasma Mass Spectrometry), Neptune Plus model, with coupled Laser Photo Machines.

In the U-Pb analyzes, the analytical routines used the zircon grain BB-9 (560 Ma; Santos et al., 2017) as primary reference, and Plešovice (337 Ma; Sláma et al., 2008) as secondary, for quality control. The spots diameter in the grains was of 30  $\mu\text{m}$ , and no spot was performed in the vicinity of the inclusions, fractures and/or metamictic features. The data reduction was performed in the Glitter software (van Achterbergh et al., 2001). In all samples, the data for each spot took into account the contents of common Pb, the errors of the isotope ratios, percentages of discordant ages and Th/U ratios. Among the performed spots, only those with disagreement less than 15% for the samples were used to plot the histograms. The histograms were obtained by using the IsoplotR software (Vermeesch, 2018).

A total of 71 Lu-Hf isotopic analyzes were performed, which used the same spots as the U-Pb isotopic analyzes. The analytical routines used the zircon grain BB-9 (560 Ma,  $^{176}\text{Hf} / ^{177}\text{Hf} = 0.2816713$ ) as the primary reference, and the Mudtank grains (732 Ma,  $^{176}\text{Hf} / ^{177}\text{Hf} = 0.282504$ ; e.g. Woodhead and Hergt, 2005), GJ-1 (602 Ma,  $^{176}\text{Hf}/^{177}\text{Hf} = 0.282000$ ; Jackson et al., 2004; Morel et al., 2008) and Plešovice (337 Ma,  $^{176}\text{Hf}/^{177}\text{Hf} = 0.282482$ ) as secondary references. The laser was operated with a spot of 40  $\mu\text{m}$  in diameter (65% power), fluence of 3  $\text{J}/\text{cm}^2$  36s, and a pulse rate of 5 Hz. Helium was used as carrier gas to minimize oxide formation and increase Hf sensitivity (Bahlburg et al., 2011). For the calculation of the  $\varepsilon_{\text{Hf}(t)}$  values, a constant decay of  $1.867 \times 10^{-11}$  was adopted for the  $^{176}\text{Lu}$  (Söderlund et al., 2004) and the current chondrite ratios of  $^{176}\text{Hf}/^{177}\text{Hf} = 0.282785$  plus  $^{176}\text{Lu}/^{177}\text{Hf} = 0.0336$  (Bouvier et al., 2008). The Hf evolution curve from the depleted mantle was determined from its current values, with  $^{176}\text{Hf} / ^{177}\text{Hf}$  ratio of 0.282525 and  $^{176}\text{Lu}/^{177}\text{Hf}$  ratio of 0.0388 (Griffin et al., 2000; updated by Andersen et al., 2009). The continental model of the felsic continental crust was calculated by using the initial  $^{176}\text{Hf}/^{177}\text{Hf}$  zircon ratio and the  $^{176}\text{Lu}/^{177}\text{Hf} = 0.022$  ratio (Pietranik et al., 2008).

The complete results of the Lu-Hf isotopic and U-Pb geochronological analyzes are displayed in Supplementary Files.

### 3.3. Mineral chemistry

Four-sample garnet crystals were analyzed in a JEOL-JXA 8230 SuperProbe Electron Probe Microanalyzer (EPMA), equipped with five WDS spectrometers, installed in the Microanalysis Laboratory, of the Geology Department of the Federal University of Ouro Preto (LMic-DEGEO-UFOP).

The analyzes were performed with the following operating conditions: spot of 5  $\mu\text{m}$  diameter, 15 kV voltage, and 20 nA current. The contents analyzed in garnet crystals were:  $\text{SiO}_2$ ,  $\text{Al}_2\text{O}_3$ ,  $\text{MgO}$ ,  $\text{MnO}$ ,  $\text{CaO}$ ,  $\text{FeO}$ ,  $\text{TiO}_2$ ,  $\text{SrO}$ ,  $\text{BaO}$ ,  $\text{K}_2\text{O}$ ,  $\text{Cr}_2\text{O}_3$ ,  $\text{Na}_2\text{O}$ , F and Cl. The results of the mineral chemistry analyzes on the garnets and further details on the mineral chemistry, reference values, and analytical conditions are available in Supplementary Files.

## 4. RESULTS

### 4.1. The tectonic *mélange* of Ribeirão da Folha

The study area is located in the vicinity of the Ribeirão da Folha district (state of Minas Gerais, southeastern Brazil), to the west of the Araçuaí Orogen suture zone (Fig. 1B and 3). The Ribeirão da Folha region received considerable attention since the discovery of Neoproterozoic oceanic remnants, parts of an ophiolitic complex, with subsequent studies that investigated and highlighted its metalogenetic potential and its present sections separately. Thus, with the support of these works, greater attention can be directed to the regional geotectonic setting, which presents a potential tectonic *mélange* environment of the Araçuaí Orogen, as well as to its sedimentary provenance, with a main focus directed towards the rocks of the ophiolitic metavolcano-sedimentary section.

The existing rocks in the study area belong to the Ribeirão da Folha ophiolitic complex, of the homonymous formation, and representative of the Macaúbas Group oceanic sedimentation (Fig. 2), besides post-collisional intrusions, with the whole array metamorphosed in amphibolite facies. They are:

i) Rocks of the metavolcano-sedimentary ophiolitic section, represented by the siliciclastic (sandy-pelitic turbidites and quartzites) and chemical (banded iron formations, sulfated metacherts, diopsidites and calc-silicatic) sequences, which correspond to the oceanic sedimentation of the passive margin;

ii) Rocks of the meta-mafic and meta-ultramafic section, representative of the oceanic lithosphere and the upper mantle;

iii) Late- to post-collisional granite intrusions, of the Mangabeiras Suite.

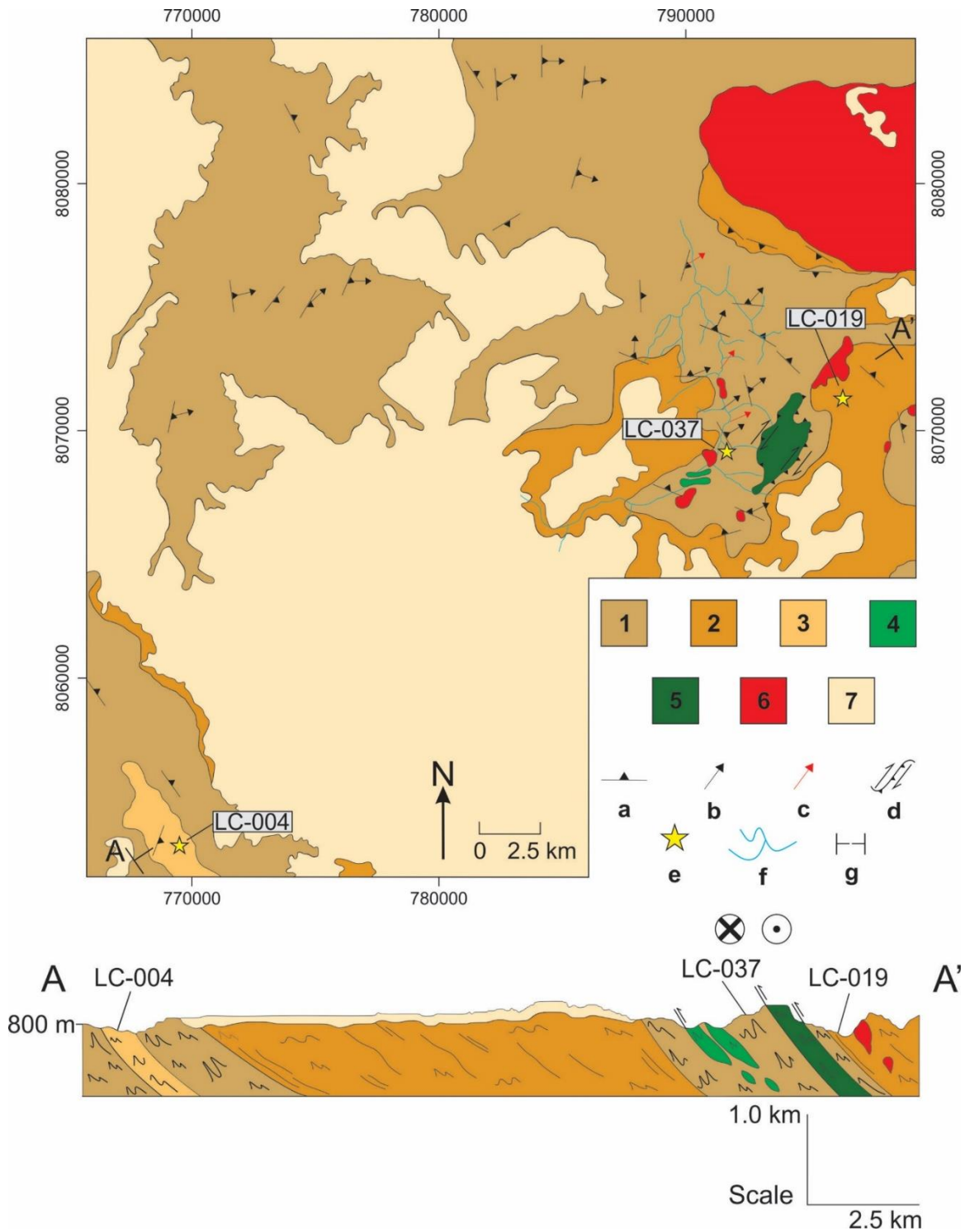


Figure 3. Simplified map and cross-section of the study area. 1, Unit A; 2, Unit B; 3, Salinas Formation; 4, meta-mafic section (orthoamphibolite); 5 meta-ultramafic section (tremolite schist, anthophyllite-dolomite schist and ultramafic metabreccia); 6, post-collisional intrusions (granite and pegmatite granite); 7, Quaternary sediments; a, regional foliation ( $S_n$ ); b, physical lineation ( $L_n$ ); c, fold axis ( $B_n$ ); d, oblique shear zone; e, U-Pb geochronological and Lu-Hf isotopic analyzes; f, Ribeirão da Folha Creek; g, A-A' cross-section. Simplified map modified from Pedrosa-Soares (1997).

#### 4.1.1. The metavolcano-sedimentary ophiolitic Section

The metavolcano-sedimentary section of the Ribeirão da Folha ophiolitic complex encompasses siliciclastic and chemical sequences, with predominance of the first, which, together, represent the deep sea turbidite sedimentation (Fig. 3 and 4). There is an expressive variation in the sedimentary content of the depositional environment, which presents packages with coarsening upward of the siliciclastic content and expressive decrease of the chemical sequences to the top (Fig. 4). Thus, based on the field distribution of the rocks, it was possible to recognize and divide the area into Units A and B. Unit A occurs at the bases of the stratigraphic column and presents a large predominance of pelitic sequences, with a recurrent presence of chemical sequences, whereas Unit B, present at the top of the column, has a large predominance of psammitic sequences, with few chemical horizons.

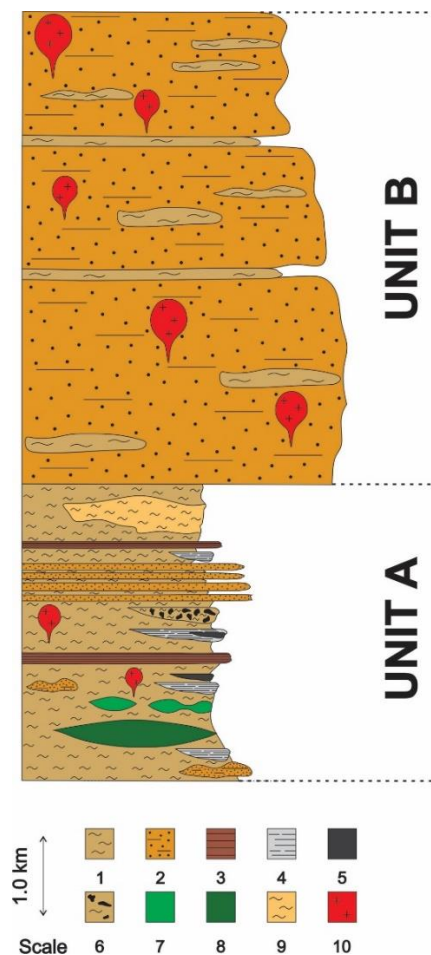


Figure 4. The tectono-stratigraphic column of the study area. 1, mica schists from the Ribeirão da Folha Formation; 2, quartzites; 3, banded iron formations; 4, metacherts; 5 diopsidites; 6, monomictic metabreccia; 7, meta-mafic section (orthoamphibolites); 8, meta-metaultramafic section (tremolite schist, anthophyllite-dolomite schist and ultramafic metabreccia); 9, Salinas Formation mica schists; 10, post-collisional intrusions (granite and pegmatite granite).

#### 4.1.1.1. Siliciclastic sequences

The siliciclastic sequences are represented by sandy-pelitic turbidite sedimentation, represented by mica schists (with variable mineral content) and quartzites.

Unit A (Fig. 4) presents the mica schists as the typical rocks of its fine-grain sedimentation. Its best exposures occur especially in the Ribeirão da Folha Creek riverbed (Fig. 3). The mica schists vary in quantity and mineral content, with occurrence of quartz-mica schists, peraluminous mica schists and graphite schists, which occur in an intercalated manner. In every domain occupied by the mica schists, there is a recurrent gradation, especially between the quartz-mica schists and the peraluminous mica schists. Cycles with alternating pelitic and psamitic sedimentation, of outcrop-scale, also occur in this Unit, in which the thicknesses of the psamitic layers vary from a few tens of centimeters to about 1.0 meter, and are intercalated by reduced pelitic layers (Fig. 5C).

The quartz-mica schists (Fig. 5A) are the most abundant rocks in the study area and present gray color, fine to medium granulation, and millimetric to decimetric banding, with separation between the quartz domain and the micaceous minerals domain. They are poor in aluminous minerals and are composed essentially of quartz, biotite and muscovite, with iron oxides, garnet, staurolite and kyanite as varietal minerals. The accessory minerals are titanium oxides (especially ilmenite), sulfides, zircon, monazite and K-feldspar. Chlorite commonly occurs as alteration mineral. The peraluminous mica schists are also gray, with fine to medium granulation, and are remarkably rich in aluminous porphyroblasts, indications of metamorphism (Fig. 5K and 6A-E). They consist mainly of quartz, biotite and muscovite, with varietal minerals such as garnet, staurolite, kyanite and sillimanite. The accessory minerals are iron oxides, sulfides, zircon, tourmaline, allanite, ilmenite, plagioclase and K-feldspar. Chlorite and epidote occur as alteration minerals. The graphite schists (Fig. 5B) consist of muscovite, graphite, quartz and kyanite, with the latter, in some cases, reaching more than 60% of the volume of the rock. The accessory minerals found in these rocks are zircon, sulfides, tourmaline and plagioclase. Still in Unit A, there is also presence of monomictic metabreccia, with mica schist clasts with garnet, full of venules and inserted in a matrix of the same composition (Fig. 5D). The clasts, in general, exhibit a certain orientation, with their major axes subparallel to the schistosity. However, it is noted that many clasts are sinuous and have sigmoidal contours.

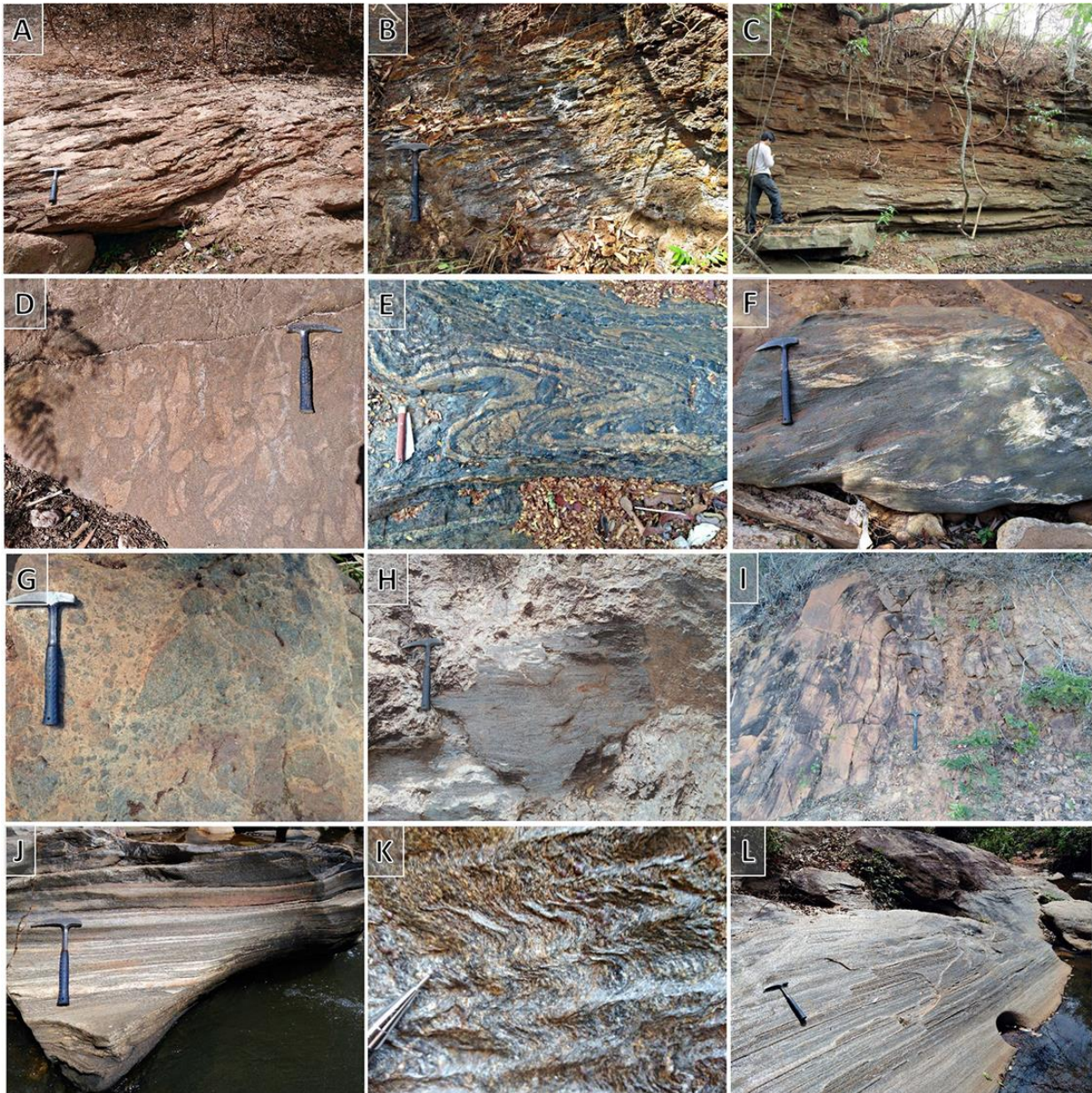


Figure 5. Lithologies and tectonic structures of the Ribeirão da Folha metasedimentary sequence. (A) Typical outcrop of quartz-mica schists along the Ribeirão da Folha Creek riverbed. (B) Graphite schist outcrop. (C) Sandy-pelitic turbidite sequence. (D) Monomictic metabreccia with mica schist matrix and clasts. (E) Banded iron formation with folded rhythmic banding. (F) Orthoamphibolite block with meta-plagiogranite venules. (G) Ultramafic metabreccia block. (H) Mica schist xenolith in granite pegmatite. (I) Fold in quartzite. (J) Ultramylonite zone in mica schist. (K)  $S_{n+1}$  crenulation cleavage in peraluminous mica schists. (L) Mineral stretching lineation in quartz-mica schist.

Unit B (Fig. 4) possesses quartzites as the typical rocks of its predominantly psamitic sedimentation. The quartzites (Fig. 5I) have fine to medium granulation, incipient foliation, and can be divided into two types: micaceous quartzite and hematite quartzite. The first is the predominant rock of Unit B, which occurs at the highest elevations of the study area. Its mineralogy is composed mainly by

quartz, with accessory mineralogy represented by biotite, muscovite, zircon and opaques. The hematite quartzites are positioned at levels close to or intercalated with the banded iron formations of Unit B, and are thus characterized by a remarkable hematite concentration.

#### **4.1.1.2. Chemical sequences**

The chemical sequences correspond to banded iron formations, sulphide-rich metacherts and diopsidites, and calc-silicatic. They occur in an intercalated manner to the siliciclastic sequences and in smaller quantity.

The banded iron formations can be observed both in Units A and B. The best exposure can be found in Unit A (Fig. 5E), in the Ribeirão da Folha Creek riverbed, and occurs in abrupt contact with the mica schists, with colors that vary from black to gray, with or without reddish tones, due to the presence of garnets. They possess distinct rhythmic banding, usually folded, with alternation of quartz rich bands and iron oxides rich bands. In Unit A, three types were recognized: oxide, with high content of magnetite in the oxide rich band; silicate, in which the quartz rich band presents millimetric to centimetric garnet crystals and acicular amphiboles; and sulfide, in which pyrite rich bands and other sulfides can be recognized, interspersed with the quartz rich bands. In Unit B, the exposures are greatly altered and fractured, and only the oxide type can be recognized.

The metacherts consist of metric to decametric intercalations associated to the quartz-mica schist, the peraluminous mica schist, the sulfated diopsidites and the banded iron formations of Unit A. They exhibit fine granulation, gray color with light to dark shades, are massive or with incipient foliation, and commonly possess quartz venules. They are composed essentially of quartz, and contain impurities of various nature and quantities, represented by biotite, muscovite, garnet, amphiboles, plagioclase, ilmenite, titanite, carbonate, with chlorite and epidote as alteration minerals, and zircon as accessory. Sulfides which are disseminated or oriented according to foliation are usually accessories, though, in some cases, they occur as essential minerals. The best exposures can also be found in the Ribeirão da Folha Creek riverbed, and its identification is facilitated in the field by the efflorescence of yellow, white and of greenish tones iron sulfates, resultant of chemical alterations of the sulfated portions.

The diopsidites are observed in Unit A and are rarely found. They are lenticular bodies with irregular edges, greenish colors, decimetric to metric dimensions, and are involved in metachert or associated with quartz-mica schist and graphite schist. They present coarse granulation, and are basically



composed of diopside mega crystals, as well as quartz, amphibole and sulfides, with accessory minerals such as titanite and carbonate. They possess discrete banding, with bands constituted of diopside, amphibole, sulfides, with disseminated titanite and carbonate, and quartz rich bands of fine to medium granulation, with subordinate sulfides.

Calc-silicatic rocks are restricted in the study area, and occur as lenticular bodies of centimetric to decimetric thicknesses, of a few meters in length, usually associated with the quartz-mica schists of Unit A. They are gray and of light shade, with dark green stains, massive, or with incipient foliation. They consist of quartz, plagioclase and amphibole, with accessory minerals such as garnet, biotite and muscovite, with carbonate, epidote and chlorite as secondary minerals.

#### **4.1.2. The meta-mafic and meta-ultramafic ophiolitic section and the meta-plagiogranite of Ribeirão da Folha**

The meta-mafic section of the Ribeirão da Folha ophiolitic complex is tectonically encased in Unit A (Fig. 3, 4 and 5F). The representative rocks of the meta-mafic section are orthoamphibolites of variable granulation, which are associated to the gabbroic, doleritic and basaltic sections of the oceanic crust (Pedrosa-Soares et al., 1992, 1998, 2001). The essential mineralogy is composed of plagioclase, amphibole and clinopyroxene (Fig. 6F), with titanite, sulfides, zircon, rutile and magnetite as accessory minerals. Biotite, sericite, plagioclase, epidote, clinozoisite, chlorite, carbonate and hydroxides are secondary minerals. The gabbroic portion is represented by coarse grained, massive and homogeneous orthoamphibolites. The banded orthoamphibolites, with variable granulation, coarse within the bands and fine at the edges, may be sheeted dikes, characteristic of the intermediate or doleritic portion of the oceanic crust. In this portion, important meta-plagiogranite venules are inserted, from which the zircon grains used to determine the magmatic crystallization age of the Ribeirão da Folha ophiolite and the Macaúbas Basin opening age (Queiroga et al., 2007; Queiroga, 2010) were extracted. The venules are leucocratic and irregular (Fig. 5F), essentially composed of plagioclase, quartz, amphibole and epidote, with accessory minerals such as titanite, chlorite, sulfide, apatite and zircon (Queiroga, 2010). The volcanic basalt portion is represented by orthoamphibolites of predominantly fine granulation, banded or massive, having disseminated sulfides, with possible metachert intercalations.

In the eastern portion of the study area, the meta-ultramafic section of the Ribeirão da Folha ophiolite (Fig. 3) stands out, which corresponds to the greatest tectonic splinter of this nature in the Araçuaí Orogen, with rare good exposures, due to an extensive weathering mantle. In map view, the meta-ultramafic body has an elongated outline in the NE-SW direction and its contact with the encasing metavolcano-sedimentary rocks of Unit A occurs in a dextral shear zone, from top to southwest. The rocks which constitute the meta-ultramafic body are tremolite schist, anthophyllite-dolomite schist and ultramafic metabreccia with clasts and matrix of similar composition. In all cases, disseminated chromite corresponds to the only remaining primary mineral. The tremolite schist is the most abundant rock, presents dark green color, medium to fine granulation and mineralogy dominated by tremolite and chlorite, in variable quantities, with subordinate ilmenite, sulfides, carbonate and chromite. Fibrous serpentine venules occur locally, filling fractures. The anthophyllite-dolomite schist has restricted occurrence, presents predominantly medium granulation, and tectonic banding with alternation of carbonate rich bands and amphibole rich bands. The mineralogy is represented by dolomite, anthophyllite, chlorite and talc, in decreasing order of abundance, with chromite, ilmenite and sulfides as accessory minerals. Both the chlorite and the carbonate occur with varying degrees of hydrothermal alteration. The ultramafic metabreccia can be observed in blocks of metric dimensions, exhibiting angular clasts of millimetric to decimetric dimensions (Fig. 5G). The clasts are basically composed of tremolitites, whereas the matrix is foliated and is characterized as tremolite schist.

#### **4.1.3. Late- to post-collisional intrusions**

In the study area, granites and pegmatoid granite occur in isolated masses of hundreds of meters in diameter, and are both correlated to the Mangabeiras Suite, of post-collisional origin (Fig. 3 and 4). The metasedimentary rocks of Units A and B intrude, which generally causes the disorganization and verticalization of the schistosity. These rocks do not register the regional schistosity, and possess xenoliths of metric dimensions with tectonic structures preserved from the encasing rocks, immersed in granitic material (Fig. 5H). The granites present white to beige color, fine to medium granulation, equigranular texture and incipient igneous flow orientation, defined by the orientation of the biotite and of phenocrystals of potassium feldspar. Microcline, plagioclase and quartz make up about 90% of the total rock composition. Biotite and muscovite are varietal minerals, and zircon, apatite and opaques occur as accessory minerals. The pegmatoid granite receive this name because of their coarse granulation. They

are beige and locally rosy, with an inequigranular texture, and occurrences of fine grains on the edges of the bodies, indicative of rapid cooling. They consist essentially of perthitic K-feldspar and quartz, with often graphic intergrowth of varying granulation from centimeters to decimeters. Muscovite, biotite and black tourmaline are accessory minerals, with centimetric to decimetric dimensions, and are widespreadly found in the rock, whereas the red garnet, in millimetric euhedral crystals, is an accessory which tends to concentrate in the proximity of the contacts. Small and rare apatite also occur.

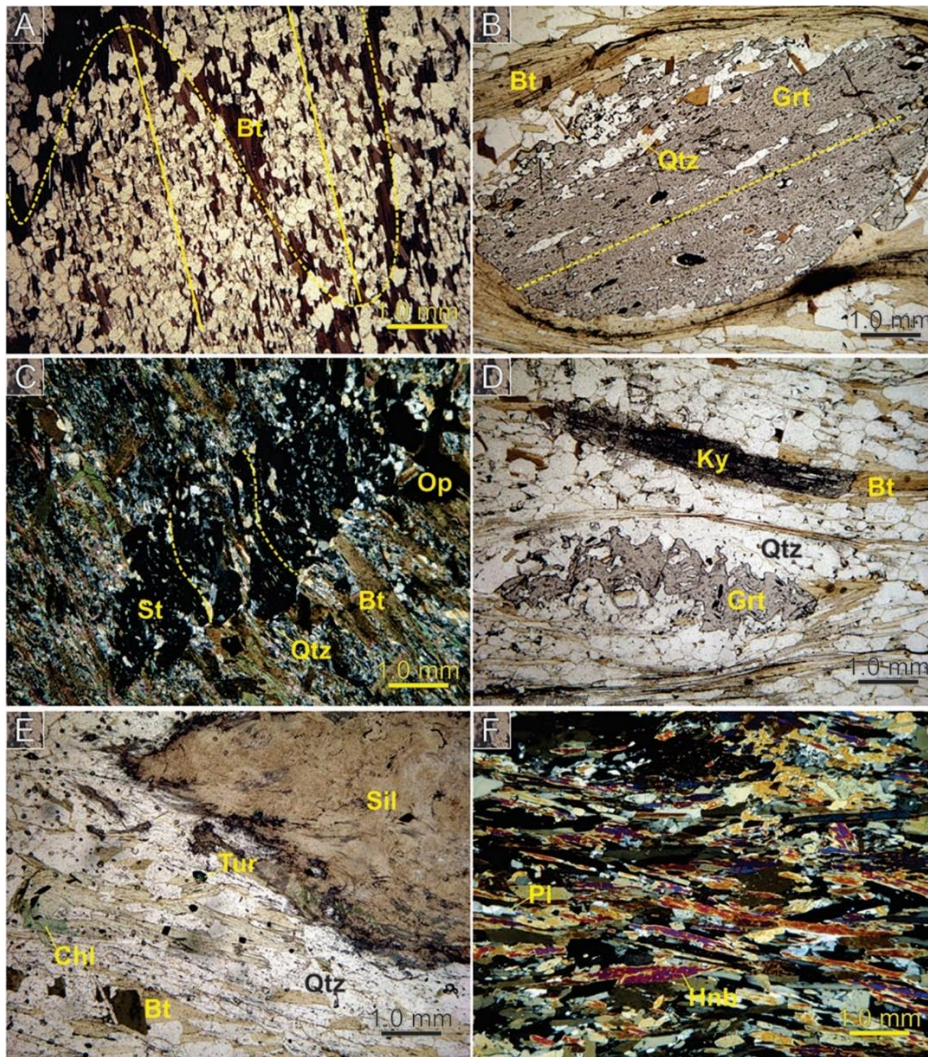


Figure 6. Photomicrographs of the Ribeirão da Folha peraluminous mica schists and orthoamphibolite. (A) Overlapping relation of the  $S_n$  schistosity over  $S_{n-1}$  in mica schist. (B) Inter-tectonic garnet porphyroblast in relation to  $S_{n-1}$  and  $S_n$  with straight pattern of inclusions. (C) Syn-tectonic staurolite porphyroblast with sigmoidal pattern of inclusions. (D) Sinuous garnet porphyroblast involved by  $S_n$  schistosity, and mimetic growth of kyanite on biotite. (E) Sillimanite porphyroblasts and retro-metamorphic chlorite lamellae. (F) Alignment of hornblende needles in orthoamphibolite. All images have magnification of 25x. Figures A, B, D and E are under parallel polarizers, and C and F under crossed polarizers. Bt = biotite, Qtz = quartz, Grt = garnet, St = staurolite, Ky = kyanite, Sil = sillimanite, Op = opaque mineral, Chl = chlorite, Tur = tourmaline, Pl = plagioclase and Hnb = hornblende.

## 4.2. Tectonic structures

The tectonic structures imprinted on the rocks of the study area are well registered in the turbidite sequences of the metavolcano-sedimentary ophiolitic section, especially in the mica schists (Fig. 5K). The main and most recurrent observed structures were nucleated in the  $D_n$  deformation phase, which is related to the collisional event of the Araçuaí Orogen uplifting, and pervasively affected all the Ribeirão da Folha ophiolitic complex. In the field, situations in which primary or secondary structures pre-existent to the  $D_n$  phase can be observed are rare, which, in the latter's case, can be better recognized in micro structures of thin sections, assisting in the interpretation of the deformation history (Fig. 6).

$F_n$  folds are open to isoclinal, usually with rounded or ptigmatic hinge lines. The  $B_n$  fold axes are not regularly observed, however, when present, they occur mainly in the quartz venules present in the mica schists, and exhibit dips usually between  $10^\circ$  and  $30^\circ$  towards ENE-NE, which coincide with the attitude of the physical lineations  $L_n$  (Fig. 7). Banded iron formations exhibit great abundance and variation in the morphology of their folds, with greater frequency of ptigmatic folds.

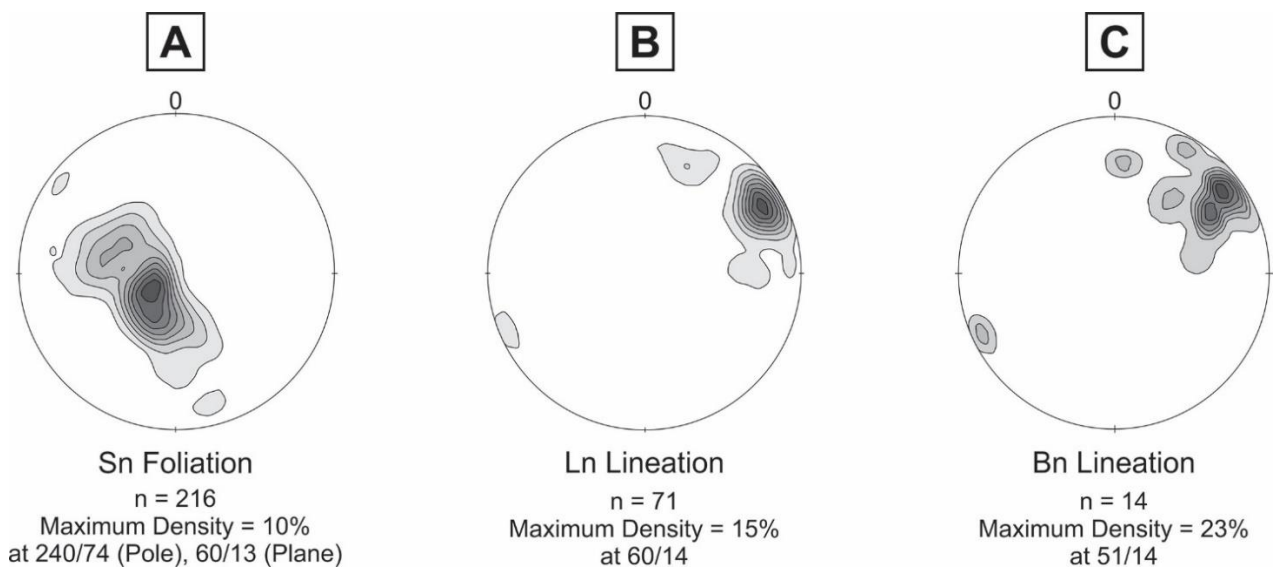


Figure 7. Stereograms with plots and densities contours (equal-area) for the main tectonic structures observed. (A)  $S_n$  schistosity. (B)  $L_n$  Lineation. (C)  $B_n$  Folding axes.

The  $S_n$  foliation is the most regularly observed structure in the study area, and is a spaced schistosity. It presents, generally, dips between  $15^\circ$  and  $30^\circ$  to ENE-NE (Fig. 7), located in the axial plane of the  $F_n$  folds. However,  $S_n$  considerably varies its orientation, with dips also to ESE. Commonly,  $S_n$  progresses to a milonitic foliation ( $S_m$ ), with the presence of S-C structures, verging folds, delta type

porphyroclasts, and asymmetric boudins. In the proximities of the contacts of the metasedimentary sequences with the post-collisional granite and pegmatoid granite,  $S_n$  tends to present more irregular attitudes, and we can observe the occurrence of  $S_{n+1}$  crenulation cleavage (Fig. 5K), relative to the  $D_{n+1}$  deformation, related to the fitting of the intrusive bodies. .

Lineations  $L_n$  are also recurrent structures and can be easily recognized in the  $S_n$  schistosity planes, as stretching lineations in quartz and micaceous minerals. The  $L_n$  lineation presents, in general, dips between  $15^\circ$  and  $25^\circ$  to ENE-NE (Fig. 7), generally down-dip within  $S_n$ , however, there are cases where it occurs parallel to the direction of the  $S_n$  planes (Fig. 5L). The  $L_n$  lineations attest to a general tectonic transportation towards SSW to SW, related to the  $D_n$  deformation phase.

### 4.3. Deformation and metamorphism phases

Analyzes of mica schists in thin sections allowed to recognize three phases of deformation in the study area, each one materialized by a schistosity generation (Fig. 8). In addition, the patterns of inclusions preserved in the aluminous porphyroblasts revealed important evidence concerning the temporal genesis of these minerals, based on their relationships with the identified deformation phases.

The  $D_n$  deformation phase manifests itself in the main  $S_n$  schistosity, which is pervasive and widely distributed in the study area. It is constituted mainly by lamellae of biotite and muscovite, by the garnet aluminous porphyroblasts, staurolite and kyanite, when present, in addition to quartz and plagioclase (Fig. 6A-D). Opaques which are elongated or arranged in parallel trails to  $S_n$  are commonly observed, especially in the mica schists closely related to the banded iron formations and to the meta-ultramafics. The mineral association composed of quartz + biotite + muscovite + garnet + aluminous mineral in varying proportions (in this case, staurolite, kyanite and possibly sillimanite)  $\pm$  opaques is diagnostic of metamorphism in the amphibolite facies (kyanite-staurolite zone), in metapelitic protoliths (Bucher and Grapes, 2010), which might be related to the regional metamorphic event of the Araçuaí Orogen uplifting (Fig. 8). The chlorite also occurs in the  $S_n$  schistosity context, though in a restricted way, replacing biotite, garnet and staurolite, relating to the regressive metamorphism. The quantitative characterization of metamorphism indicates for  $S_n$ , a temperature and pressure interval of  $530$  to  $600^\circ$  and  $4,9$  to  $5,3$  kbar, respectively (Queiroga, 2006).

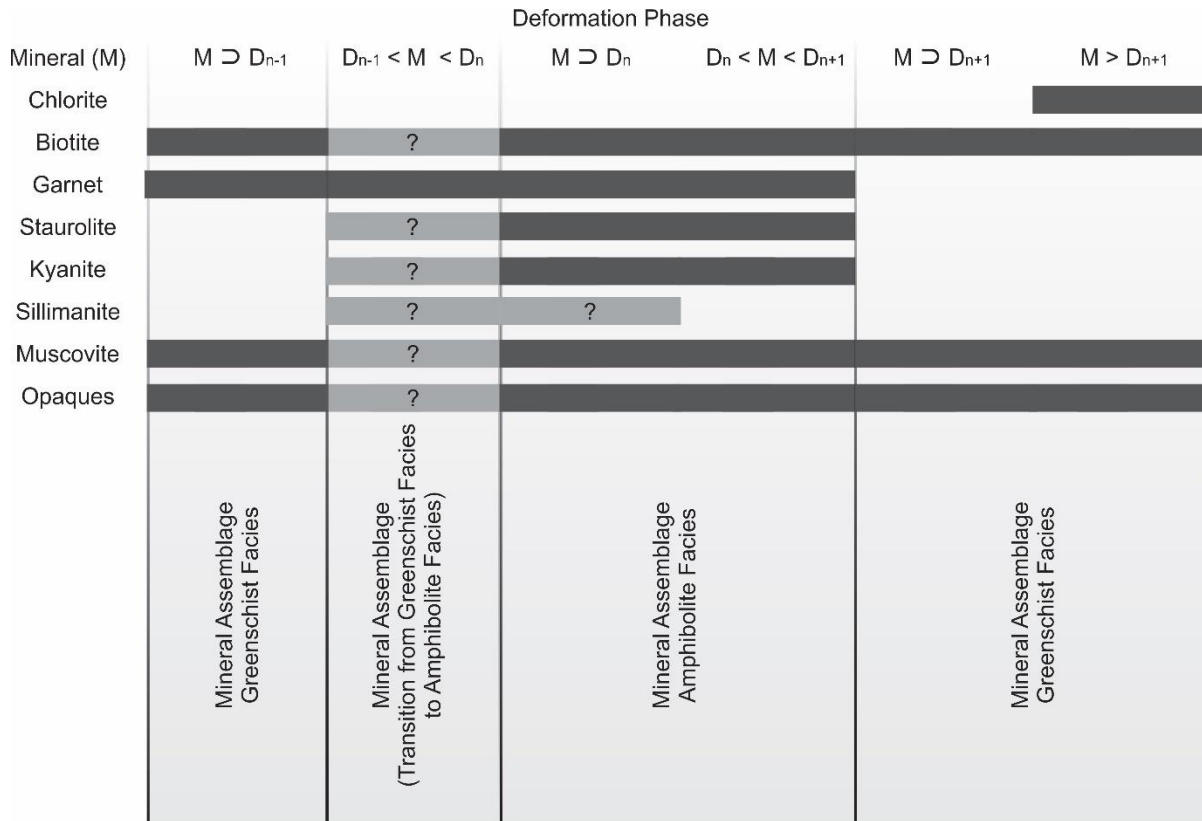


Figure 8. Diagram of relative ages of the commonly found minerals in the Ribeirão da Folha peraluminous mica schists in relation to the deformation phases. The dark gray bands represent, by means of direct (presence in the schistosity) or indirect (inclusion patterns) evidence, that the mineral originated in the associated deformation phase. The light gray bands with a question mark represent the deformation phases of uncertain origin. The fields without bands represent the deformation phases in which the minerals certainly did not originate. Metamorphic facies of mineral associations:  $D_{n-1}$ : greenschist facies;  $D_{n-1} < M < D_n$ : transition from greenschist facies to amphibolite facies;  $M \supset D$  and  $D_n < M < D_{n+1}$ : amphibolite facies;  $M \supset D_{n+1}$  and  $M > D_{n+1}$ : greenschist facies.

In rare cases, overlapping relationships of the  $S_n$  schistosity with other planes of schistosity can be noted, characterizing the crenulation cleavage ( $S_{n+1}$ ), which is incipient and consists of lamellae of biotite and muscovite, leaving open to what metamorphic facies its genesis would have occurred. This schistosity represents the deformation and the mineral transformations imposed by the  $D_{n+1}$  deformation phase, related to the fitting of the post-collisional plutonic bodies. Relicts of previous schistositities ( $S_{n-1}$ ) are evidenced by quartz, biotite, muscovite and opaques included in crystals of garnet, as well as by biotite, muscovite and quartz observed in rare dimmed and transposed fold limbs, where  $S_n$  intercepts them as axial plane (Fig. 6A), or in rare folded crystals of garnet, which are surrounded by the  $S_n$  schistosity (Fig. 6D). These relicts materialize the  $D_{n-1}$  deformation phase, which might have occurred under low-grade greenschist facies conditions (Fig. 8).

Garnet crystals commonly occur as anhedral to subhedral poikiloblasts, with quartz and more rarely biotite, plagioclase, sericite, zircon and/or monazite and opaques inclusions (Fig. 6B, D). The  $S_n$  schistosity surrounds the garnet crystals, which served as a shield for its regular development, in most observed cases. The quartz recrystallization tails originated in the zones of pressure shadows are usually asymmetrical in comparison to a reference line, suggesting non-coaxial deformation. The inclusion patterns in the garnet poikiloblasts present variations, though in most of the observed cases they exhibit sinuous patterns of inclusions, approximately sigmoidal, with obliquity between the internal schistosity ( $S_i$ ), within the crystals, and the external one ( $S_e$ ), characterized by  $S_n$ . Subtle "spiral" inclusion patterns, with rounded garnet crystals, are rarely noticed and suggest rotation during deformation. In some cases, garnet crystals settled on the schistosity occur, with little or no deviation in their surrounding. Thereby, it is understood that most of the observed garnet crystals had their genesis syn-tectonically to  $S_n$ , with small post-tectonic increments in relation to  $D_n$ . Orientated and rectilinear inclusion patterns can also be observed, with marked obliquities, ranging from  $35^\circ$  to  $50^\circ$ , between  $S_i$  and  $S_e$ . These rectilinear patterns are interpreted as indications that the genesis of at least one generation of garnets occurred between the  $D_{n-1}$  and  $D_n$  deformation stages, since the crystals inherit the patterns of the past schistosity  $S_{n-1}$ , with growth on them, being, therefore, post-tectonic to the  $D_{n-1}$  deformation phase, though clearly surrounded by  $S_n$ , which places them in an inter-tectonic stage of development (Fig. 6B).

Porphyroblasts of staurolite are subhedral to anhedral, and possess a large amount of quartz inclusions, evidencing a "sieve" texture. In general, they present their largest axis oriented subparallel way to  $S_n$ , with deviations of this schistosity in their surroundings, and development of pressure shadows. However, cases in which the staurolite porphyroblasts are obliquely oriented, or even perpendicular to  $S_n$ , with no schistosity deviations in their surroundings nor pressure shadows, are not uncommon. Inclusion patterns can rarely be observed, though they present signs of being sinuous to sigmoidal (Fig. 6). These observations allow us to state that the staurolite crystals, as well as the garnet ones, have also had syn-tectonic genesis relative to the  $S_n$ , nevertheless, they present their genesis more clearly evidenced in post-tectonic stages in relation to  $D_n$  deformation phase.

The kyanite also occur as porphyroblasts, with inclusion patterns even less evident than those observed in the staurolites. When they occur, they consist predominantly of quartz, with small occurrences of biotite and muscovite. The kyanite slats occur more commonly parallel to  $S_n$ , which does not deviate from their contours. In these cases, they are interpreted as mimetic crystals, which grew after the development of  $S_n$  and inherited the shapes of the existing micaceous minerals (Fig. 6D). However, cases in which they are contoured by  $S_n$ , with the presence of pressure shadows, are also observed. Their

inclusion patterns are usually rectilinear; though, since in most cases they are parallel to the schistosity, no further conclusions can be drawn as to whether they are inter-tectonic with significant rotation during their development, or post-tectonic to  $D_n$  deformation phase. Sinuous patterns also occur in some crystals. It is understood from the analyzed thin sections that the kyanite genesis, as well as that of the garnet and the staurolite, is mainly syn-tectonic, nevertheless they suggest post-tectonic increments in relation to the  $D_n$ , even more evident than the other aluminous porphyroblasts found.

The fibrous sillimanite porphyroblasts are contoured by  $S_n$ , in which no type of inclusion can be observed (Fig. 6E). In this case, therefore, it is only possible to conclude that they have no post-tectonic genesis in relation do  $D_n$ .

#### 4.4. Mineral chemistry

Four samples of peraluminous mica schists from Unit A (LC-004, LC-022B, LC-030 and LC-039) were selected for mineral chemistry analyzes in garnet porphyroblasts. Cross sections were performed passing through their nuclei, with varying amounts of spots, according to grain sizes, with the objective of recognizing their mineral compositions and chemical zoning, in order to investigate the progression of the metamorphism.

##### 4.4.1. Garnet zoning

Garnet crystals in the samples commonly occur as poikiloblasts, with inclusions of quartz and more rarely of biotite, plagioclase, sericite, zircon and/or monazite and opaques. The sizes of the crystals vary significantly, ranging from submillimetric dimensions to larger than 6.0 mm. In general, the crystals are subhedral, with subrounded to rounded contours. In samples LC-030 and LC-039, the crystals also occur as trails arranged parallel to  $S_n$ , skeletal, or with sinuous contours. They also tend to occur as submillimetric crystals, which can be found in granular aggregates or scattered dots amid the schistosity.

In general, samples LC-004, LC-022B and LC-030 present similar compositions and chemical distribution patterns (Fig. 9). The analyzes of these crystals show almandine rich garnets (Alm 72-62%), with lower concentrations of spessartine (Sps 18-6%), pyrope (Prp 16-8%) and grossular (Grs 11-3%). The three samples present nuclei with a higher concentration of spessartine, which decreases towards the



boundaries, unlike what happens to the contents of almandine and pyrope, which increase their concentration from the nucleus towards the boundaries. This replacement of spessartine by almandine and pyrope from the nucleus characterizes a normal zoning pattern, typical of progressive metamorphism.

Sample LC-039 also displays higher contents of almandine (Alm 53-50%), however, its spessartine (Sps 31-25%) and grossular (Grs 13-7%) contents are generally higher in relation to the pyrope (Prp 11-9%). The garnet crystals found in this sample are uniquely anhedral and show, in general, constant chemical distribution patterns, with no evidence of zoning, which suggests chemical homogenization.

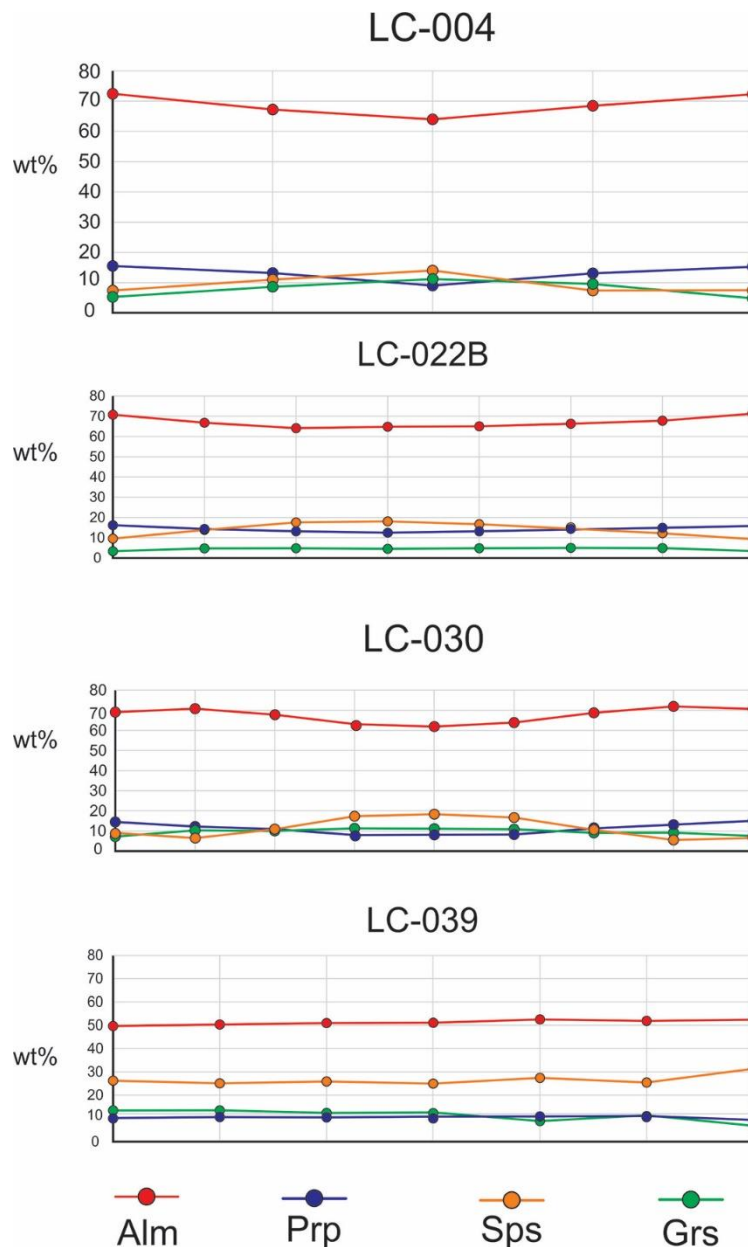


Figure 9. Chemical profiles along garnet porphyroblasts of the peraluminous mica schists. Alm: Almandine. Prp: Pyrope. Sps: Spessartine. Grs: Grossular.

#### 4.5. Whole rock geochemistry

Ten samples of mica schists from the metavolcano-sedimentary section of the Ribeirão da Folha ophiolitic complex were selected for chemical analyzes of their major, minor and trace elements (Table 1). A better chemical characterization of the rock is sought with these analyzes, so to better understand its protolith and its sedimentary history, with greater clarification about its provenance and depositional environment.

Sample	LC-004	LC-006	LC-012	LC-022B	LC-030	LC-039	LC-053	LC-071	LC-073B	LC-088
<b>Major Elements (%)</b>										
<b>SiO<sub>2</sub></b>	65.8	61.9	49.0	66.5	56.0	51.8	62.5	60.9	66.4	60.6
<b>TiO<sub>2</sub></b>	1.00	0.23	1.61	0.89	1.25	0.36	1.10	0.87	0.84	0.98
<b>Al<sub>2</sub>O<sub>3</sub></b>	17.1	18.5	25.9	15.7	20.9	17.7	16.5	17.1	14.4	19.4
<b>Fe<sub>2</sub>O<sub>3</sub></b>	8.14	7.94	11.5	7.32	9.68	6.29	9.00	6.80	8.39	6.31
<b>MnO</b>	0.16	0.04	0.18	0.17	0.15	0.12	0.19	0.10	0.10	0.05
<b>MgO</b>	3.14	4.26	4.83	3.23	3.84	8.00	3.86	3.37	2.22	1.98
<b>CaO</b>	1.13	0.43	0.41	0.74	0.57	11.8	1.53	3.53	0.28	0.20
<b>Na<sub>2</sub>O</b>	2.78	3.54	0.48	1.53	0.81	3.09	2.17	3.21	0.43	0.64
<b>K<sub>2</sub>O</b>	2.95	2.75	4.29	4.91	3.47	0.22	3.46	2.83	6.03	5.91
<b>Cr<sub>2</sub>O<sub>3</sub></b>	0.02	<0.01	0.02	0.01	0.02	0.03	0.02	0.01	<0.01	0.02
<b>P<sub>2</sub>O<sub>5</sub></b>	0.12	0.13	0.12	0.10	0.09	<0.01	0.11	0.15	0.11	0.15
<b>LOI</b>	1.52	1.23	1.09	1.72	1.39	0.88	1.03	1.31	1.90	3.77
<b>TOTAL</b>	104	101	99.4	103	98.2	100	101	100	101	100
<b>Trace Elements (ppm)</b>										
<b>Sc</b>	19.7	4.60	28.6	19.0	257	47.3	24.4	20.6	16.4	18.7
<b>V</b>	122	30.0	184	128	139	177	139	102	92.0	63.0
<b>Cr</b>	65.0	11.0	81.0	46.0	67.0	56.0	54.0	56.0	36.0	72.0
<b>Co</b>	19.1	1.80	24.9	16.8	21.5	32.1	21.0	9.60	46.6	4.50
<b>Ni</b>	45.0	20.0	44.0	36.0	46.0	91.0	51.0	22.0	88.0	12.0
<b>Cu</b>	20.8	6.90	32.1	17.4	59.9	27.5	36.0	29.6	19.0	12.5
<b>Zn</b>	126	642	460	108	276	22.0	101	136	122	81.0
<b>Rb</b>	137	88.7	153.0	168	135	1.80	111	124	215	205
<b>Sr</b>	114	202	12.0	81.0	46.0	300	144	345	23.0	59.0
<b>Y</b>	32.7	167	38.1	26.3	35.3	4.73	25.0	24.0	27.3	32.0
<b>Zr</b>	123.7	136	235.1	137.2	181.1	19.7	149.9	137.1	127.3	104.8
<b>Nb</b>	14.9	540	36.3	17.3	21.7	0.94	23.8	11.7	18.1	31.2
<b>Mo</b>	0.33	0.32	1.06	0.65	1.30	0.45	0.62	0.91	0.37	0.86
<b>Cs</b>	8.12	2.97	9.03	10.8	7.81	0.11	5.28	8.38	4.24	5.43
<b>Sn</b>	3.10	23.5	3.20	3.70	3.10	0.40	2.70	12.7	2.60	4.80
<b>Ba</b>	531	817	870	784	742	134	836	536	941	1488
<b>Hf</b>	4.34	4.47	8.56	5.38	6.81	0.70	5.34	5.21	4.36	4.01

<b>Ta</b>	1.32	32.3	1.68	1.53	0.92	0.40	1.11	1.12	1.37	2.08
<b>W</b>	2.20	2.60	1.40	3.20	1.40	0.10	0.90	2.00	2.70	2.70
<b>Tl</b>	0.79	0.34	0.73	0.92	0.70	<0.02	0.52	0.70	0.74	1.13
<b>Pb</b>	22.6	58.4	8.80	18.9	13.1	1.70	23.4	42.8	14.1	22.7
<b>Bi</b>	0.23	0.18	0.58	0.18	0.48	<0.04	0.27	0.30	0.10	0.21
<b>Th</b>	13.9	96.6	20.5	15.2	15.6	0.40	12.8	12.3	11.2	23.0
<b>U</b>	3.20	7.79	4.06	2.73	3.47	0.07	2.52	2.87	1.43	4.26
<b>La</b>	30.4	354	31.9	26.6	40.2	1.50	37.9	23.7	33.1	54.7
<b>Ce</b>	76.6	824	99.3	75.4	86.9	3.30	78.4	68.5	68.3	127
<b>Pr</b>	8.90	79.6	11.6	8.47	10.1	0.40	9.10	8.19	8.02	14.6
<b>Nd</b>	32.8	256	41.9	30.9	37.2	1.10	33.0	31.5	30.2	51.7
<b>Sm</b>	7.00	43.8	8.00	6.30	7.00	0.50	6.30	6.60	6.10	9.50
<b>Eu</b>	1.39	2.97	1.07	1.12	1.06	0.37	1.48	1.27	1.21	1.64
<b>Gd</b>	6.14	35.0	6.97	5.18	5.83	0.74	4.89	4.87	5.41	6.98
<b>Tb</b>	0.95	5.93	1.06	0.83	0.95	0.14	0.81	0.72	0.82	1.04
<b>Dy</b>	6.23	34.9	6.71	4.90	6.15	0.94	4.91	4.69	5.05	6.29
<b>Ho</b>	1.28	6.50	1.45	0.99	1.29	0.20	0.96	0.89	1.00	1.20
<b>Er</b>	3.44	17.4	4.20	3.01	3.83	0.51	2.77	2.67	2.97	3.41
<b>Tm</b>	0.48	2.43	0.58	0.44	0.57	0.08	0.41	0.36	0.44	0.49
<b>Yb</b>	3.20	14.7	4.10	2.90	3.70	0.50	2.60	2.40	2.90	3.10
<b>Lu</b>	0.40	1.58	0.33	0.35	0.32	0.08	0.35	0.18	0.17	0.15
<b>CIA</b>	71.3	73.3	83.3	68.7	81.2	54.0	69.7	64.2	68.1	74.2
<b>Nb/Ta</b>	11.3	16.7	21.6	11.3	23.6	37.6	21.5	10.5	13.2	15.0
<b>Rb/Sr</b>	1.20	0.44	12.8	2.07	2.94	0.01	0.77	0.36	9.34	3.48
<b>Th/Sc</b>	0.71	21.0	0.72	0.80	0.61	0.01	0.52	0.60	0.68	1.23
<b>Th/U</b>	4.34	12.4	5.05	5.57	4.50	5.71	5.08	4.29	7.83	5.39
<b>Zr/Hf</b>	28.5	30.3	27.5	25.5	26.6	28.1	28.1	26.3	29.2	26.1
<b>Zr/Sc</b>	6.28	29.5	8.22	7.22	7.05	0.42	6.14	6.66	7.76	5.60
<b>(La/Yb)<sub>N</sub></b>	6.42	16.3	5.26	6.20	7.34	2.03	9.85	6.67	7.71	11.9
<b>(Gd/Yb)<sub>N</sub></b>	1.56	1.93	1.38	1.45	1.28	1.20	1.52	1.64	1.51	1.82
<b>(Eu/Eu*)<sub>N</sub></b>	0.65	0.23	0.44	0.60	0.51	1.86	0.81	0.68	0.64	0.62

Table 1. Geochemical data of the mica schists of Ribeirão da Folha. CIA: chemical index of alteration.  $Eu/Eu^* = [Eu/(Sm + Nd)^{1/2}]_N$ .

#### 4.5.1. Nature of the protolith and general geochemical characteristics

The  $\log (SiO_2/Al_2O_3)$  vs.  $\log (Fe_2O_3^t/K_2O)$  Herron diagram (1988) for chemical discrimination of siliciclastic sediments indicates that seven samples plot in the shale region, two samples in the graywacke region, and one sample in the Fe-Shale region (sample LC-039) (Fig. 10). In order to simplify, when referring to the protoliths of the analyzed mica schists, they will be solely called shale-graywackes.

The contents obtained from the mica schists analyzes display, in eight out of ten samples, similar trace and rare earth elements (REE) contents, with some small variations in their major elements, which can be associated with the chemical heterogeneities in the sedimentation which originated the turbidite protoliths (Table 1 and Fig. 11). Expressive variations occur especially in the trace element contents, especially in the HFSE (High Field Strength Elements) of samples LC-006 and LC-039, which will have their considerations made separately from the others.

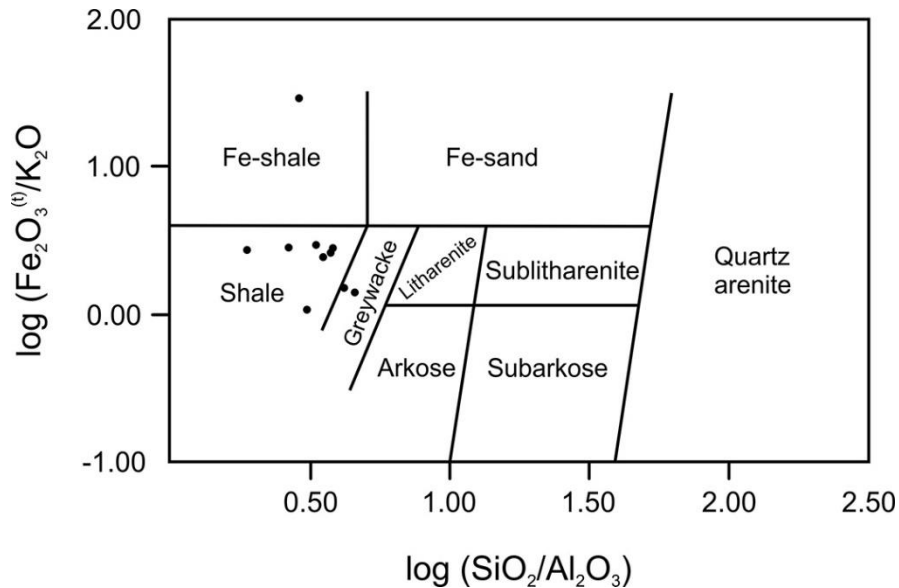


Figure 10. Classification of the pelitic rocks of Ribeirão da Folha according to the Herron  $\log (\text{SiO}_2/\text{Al}_2\text{O}_3)$  vs.  $\log (\text{Fe}_2\text{O}_3^{(t)}/\text{K}_2\text{O})$  diagram (1988).

The group of the eight mica schists samples present moderate to high levels of  $\text{SiO}_2$  (49.0 - 66.5%) and high levels of  $\text{Al}_2\text{O}_3$  (14.4 - 25.9%), characteristic for pelitic sediments. The  $\text{Na}_2\text{O}$  (0.4 - 3.1%),  $\text{K}_2\text{O}$  (2.8 - 6.0%) and  $\text{MgO}$  (1.8 - 4.8%) contents are variable and controlled by the presence and/or quantity of muscovite, biotite or chlorite. The  $\text{CaO}$  contents are variable, though low in most samples (0.2 - 3.5%), due to the essentially sodic nature of the plagioclase ( $\text{Ab}_{94-75}$ ) and to the scarcity of carbonatic material in the mica schists during the sedimentation. The REE (Rare Earth Elements) chondrite-normalized patterns (Taylor and McLennan, 1985) exhibit enrichment in light rare earth elements (LREE) ( $[\text{La} / \text{Yb} = 11.9 - 5.4]_N$ ), negative Eu anomaly [ $\text{Eu}/\text{Eu}^* = 0.8 - 0.4]_N$ ) and a relatively flat distribution pattern for the heavy rare earth elements (HREE) ( $[\text{Gd} / \text{Yb} = 1.8 - 1.3]_N$ ) (Fig. 11).

The LC-039 sample plots in the Fe-shale field of the Herron diagram (Fig. 10), and its REE contents are well below the other samples analyzed (Fig. 11). It is enriched in LREE ( $[\text{La} / \text{Yb} = 2.0]_N$ ),

with positive Eu anomaly ( $[Eu / Eu^* = 1.9]_N$ ), and a relatively flat distribution pattern for the HREE ( $[Gd / Yb = 1.2]_N$ ). Whereas the LC-006 sample shows much higher REE contents than the others (Fig. 11), with a great enrichment in LREE ( $[La / Yb = 16.3]_N$ ), negative Eu anomaly ( $[Eu / Eu^* = 0.2]_N$ ), and a relatively flat distribution pattern for the HREE ( $[Gd / Yb = 1.9]_N$ ).

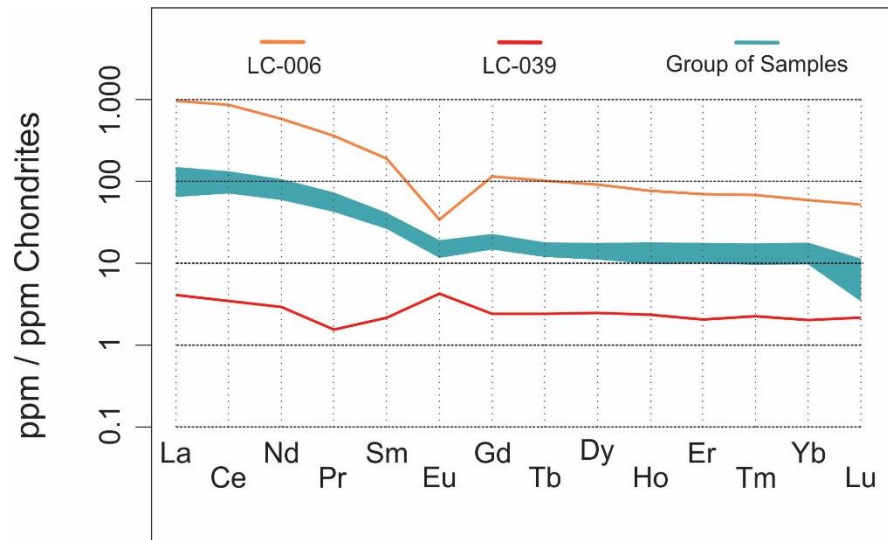


Figure 11. Chondrite-normalized REE diagram (Taylor and McLennan, 1985) for ten samples of selected mica schists.

#### 4.6. U-Pb geochronology and Lu-Hf isotopic analysis in detrital zircons

Three samples (LC-004, LC-019 and LC-037) were selected for studies on detrital zircons using geochronological U-Pb and isotopic Lu-Hf analyzes, with the purpose of characterizing the sedimentary provenances and of restricting deposition ages of the metavolcano-sedimentary ophiolitic section of Ribeirão da Folha. Samples LC-019 and LC-037 correspond to medium to fine granulation micaceous quartzites, with accessory minerals such as biotite, muscovite, zircon and opaques. Sample LC-004 is a staurolite-garnet-muscovite-biotite schist of medium granulation with zircon, chlorite, tourmaline and opaques as accessory minerals.

#### 4.6.1. Sample LC-004 (staurolite-garnet-muscovite-biotite schist): U-Pb and Lu-Hf in detrital zircons

Thirty-two grains of the LC-004 sample were analyzed, which corresponds to a peraluminous mica schist with staurolite and garnet. The grains are mostly subhedral to anhedral, prismatic, little to very elongated and with irregular to rounded boundaries (Fig. 12). Rounded shapes occur in some cases. The sizes barely vary, from 50 to 100  $\mu\text{m}$ , with the largest grain having approximately 200  $\mu\text{m}$ . Recrystallized boundaries occur in some cases, and oscillatory zoning with varied patterns appear in grains of all ages.

For the U-Pb analyzes, after the data reduction, all collected grains were used. The histogram (Fig. 13) shows that the most significant statistical peak occurs in the spectrum of Paleoproterozoic ages, in ages between 2,000 Ma and 2,200 Ma. The second greatest sedimentary contribution occurs in the zircon grains of Mesoproterozoic ages between 1,200 Ma and 1,300 Ma. Grains with Neoproterozoic ages, of about 600 Ma to 700 Ma, are expressive in the data set and contain the youngest grain found in the study area, with an age of  $599 \pm 7$  Ma. Grains of Archean ages, of approximately 2,900 Ma, are also found.

In the Lu-Hf isotopic analyzes, 22 zircon grains were used (Fig. 14). In comparison to the values of the depleted mantle, most of the grains are evolved. Only one of the analyzed zircons is Archean, dated 2,921 Ma and possesses  $\epsilon_{\text{Hf}(t)}$  of -4.2, and a  $T_{\text{DM}}$  model age of 3,293 Ma. Nine analyzed grains are Paleoproterozoic, aged from 2,114 Ma to 1,783 Ma, and present  $\epsilon_{\text{Hf}(t)}$  from -13.5 to +2.37, with  $T_{\text{DM}}$  model ages of 2,938 Ma to 2,085 Ma. The Mesoproterozoic contributions are represented by eight grains, with ages from 1,365 Ma to 1,099 Ma,  $\epsilon_{\text{Hf}(t)}$  values from -13.5 to +3.0 (with only one of those having a positive value), and  $T_{\text{DM}}$  model ages from 2,222 Ma to 1,557 Ma. Four grains are of Neoproterozoic contribution, aged from 971 Ma to 599 Ma, exhibiting  $\epsilon_{\text{Hf}(t)}$  from -17.6 to +3.1, with  $T_{\text{DM}}$  model ages from 2,158 Ma to 1,430 Ma, while the youngest grain found for the sample and also for the study area is of 599 Ma, with  $\epsilon_{\text{Hf}(t)}$  signature of -6.3.

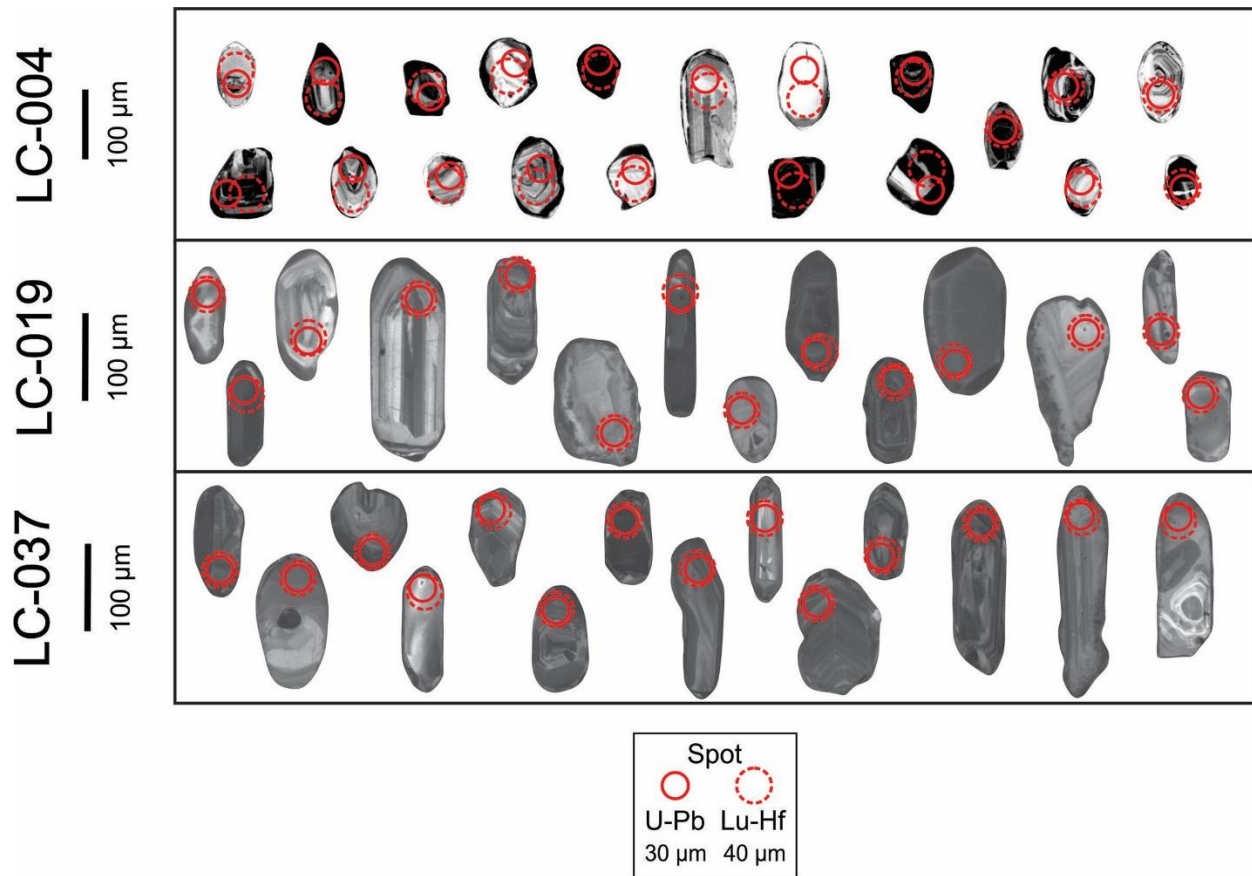


Figure 12. Cathodoluminescence (CL) images of the detrital zircons of samples LC-004 (Salinas Formation, Salinas Basin), LC-019 (Unit B, Ribeirão da Folha Formation, Macaúbas Basin) and LC-037 (Unit A, Ribeirão da Folha Formation, Macaúbas Basin).

#### 4.6.2. Sample LC-019 (quartzite): U-Pb and Lu-Hf in detrital zircons

There were analyzed 117 detrital zircon grains from sample LC-019, which corresponds to an impure quartzite with accessory minerals such as biotite, muscovite, zircon and opaques. The zircon grains are mostly subhedral, prismatic, elongated and irregularly shaped (Fig. 12). Rounded shapes and fractures occur in some cases. Most grains range from 100 to 200  $\mu\text{m}$ , with rare grains under or over these sizes. Recrystallized boundaries are common and, regarding their internal characteristics, the majority of them have oscillatory zoning, among which varying patterns are observed and distributed throughout the age spectrum.

From its histogram (Fig. 13), it is observed that the highest concentration of the grains occurs in a Mesoproterozoic statistical peak, from about 1,100 Ma to 1,300 Ma, though presenting expressive

contributions from as old as 1,500 Ga, approximately. An expressive set of grains present Paleoproterozoic ages, in the approximate range of 1,700 Ma to 2,200 Ma, with the most expressive concentration from approximately 2,100 Ma. A statistical peak of Neoproterozoic age occurs near 900 Ma to 1,000 Ma, despite the youngest dated grain for the sample being of  $672 \pm 10$  Ma. Other contributions are of Paleoproterozoic to Archean ages, ranging from 2,400 Ma to 2,700 Ma.

For the Lu-Hf isotopic analyzes, 24 zircon grains were used (Fig. 14). In comparison to the values of the depleted mantle, the grains were, in their majority, evolved, with only three of them plotting in the moderately juvenile field. Two grains exhibit Archean crystallization ages, of 2,795 Ma and 2,612 Ma, with negative  $\epsilon_{\text{Hf}(t)}$  values of -2.6 and -9.5, and  $T_{\text{DM}}$  model ages of 3,083 Ma and 3,244 Ma, respectively. The group of 11 Paleoproterozoic grains aged between 2,173 Ma and 1,719 Ma exhibit  $\epsilon_{\text{Hf}(t)}$  values of -5.9 to +2.3 (of which only two possess positive values), with  $T_{\text{DM}}$  model ages from 2,590 Ma to 2,139 Ma. Four analyzed zircons are Mesoproterozoic, with ages from 1,296 Ma to 1,202 Ma,  $\epsilon_{\text{Hf}(t)}$  values of -16.9 to +3.7, and  $T_{\text{DM}}$  model ages from 2,349 to 1,592 Ma. Seven analyzed grains are Neoproterozoic, aged from 977 Ma to 690 Ma, all having negative values of  $\epsilon_{\text{Hf}(t)}$ , ranging from -27.0 to -4.0,  $T_{\text{DM}}$  model ages from 2,386 Ma to 1,620 Ma, with the sample's youngest dated grain being the representative of the  $\epsilon_{\text{Hf}(t)}$  value of -27.0.



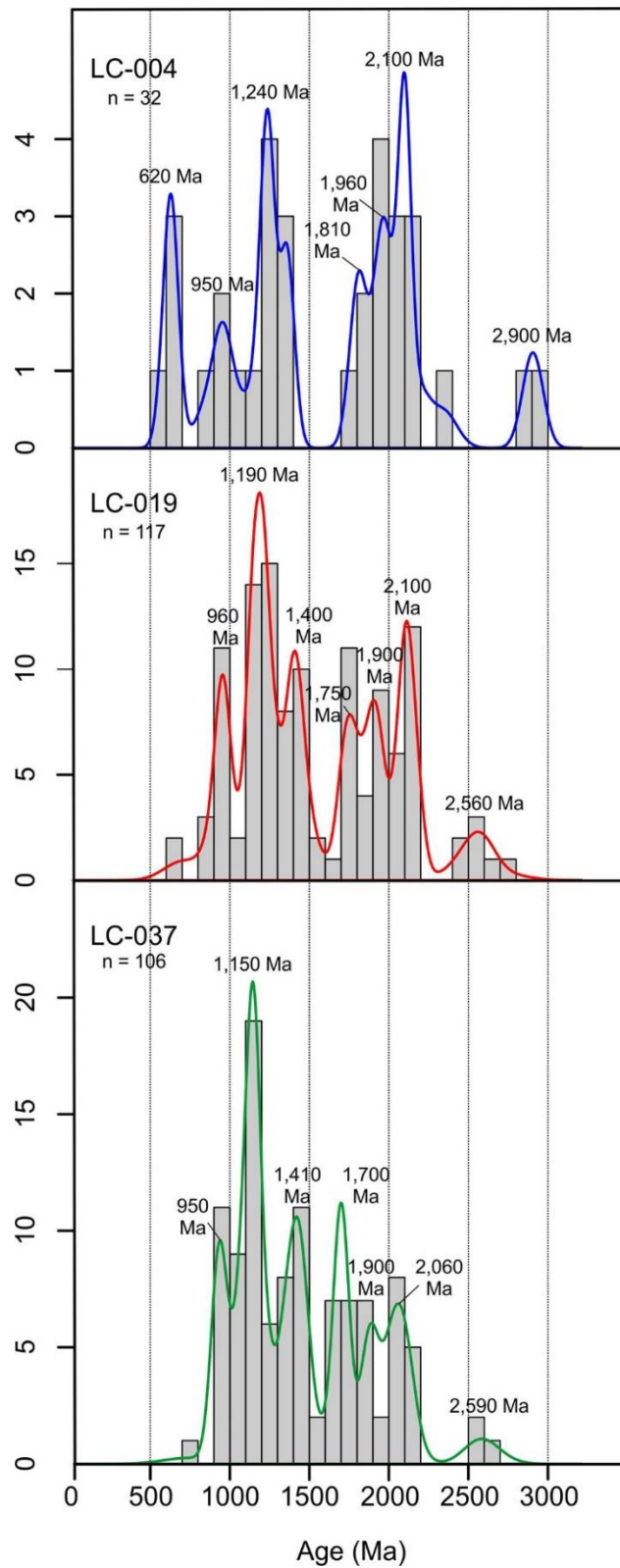


Figure 13. Frequency and probability curves histograms of the U-Pb geochronological analyzes for samples LC-004, LC-019 and LC-037.

#### 4.6.3. Sample LC-037 (quartzite): U-Pb and Lu-Hf in detrital zircons

For the micaceous quartzite with accessory minerals represented by biotite, muscovite, zircon and opaques, 106 grains were analyzed. The grains are subhedral to euhedral, prismatic, little to very elongated, with irregular or rounded boundaries (Fig. 12). More than half of the grains range from 120 to 200  $\mu\text{m}$ , though the largest analyzed grain exceeds 650  $\mu\text{m}$ . After the data reduction, all 106 grains could be used to calculate the ages. Rounded grains occur only in two cases, and internal fractures are rare. It is observed that the zircons which are representative of the more recent ages tend to present more irregular boundaries, whereas the older ones tend to be more rounded. Recrystallized boundaries are also common and most grains present oscillatory zoning with varying patterns throughout the entire spectrum of ages.

Based on the histogram (Fig. 13), the greatest sedimentary contribution comes from grains of Mesoproterozoic ages, ranging from 1,100 Ma to 1,200 Ma. However, significant contributions around this Mesoproterozoic peak reach ages close to 1,500 Ma, as well as Neoproterozoic ages of approximately 900 Ma. Another important spectrum of contribution occurs between Paleoproterozoic ages, from 1,600 Ma to 2,200 Ma. The Archean contribution is of lower expression, with ages between 2,500 Ma and 2,700 Ma. The youngest sample grain exhibits Neoproterozoic age of  $741 \pm 9$  Ma.

For the Lu-Hf isotopic analyzes, 25 grains were used (Fig. 14). In comparison to the values of the depleted mantle, the grains are predominately evolved, though the amount of Mesoproterozoic grains which plot in the field of moderately juvenile is significant. Only one analyzed zircon grain is Archean, aged 2,635 Ma, and presents  $\epsilon_{\text{Hf}(t)}$  of -5.4 and  $T_{\text{DM}}$  model age of 3,108 Ma. Nine zircons are representative of the Paleoproterozoic group, aging from 1,908 Ma to 1,688 Ma, all presenting negative values of  $\epsilon_{\text{Hf}(t)}$ , which range from -16.7 to -0.3, with  $T_{\text{DM}}$  model ages from 2,882 to 2,121 Ma. Six analyzed grains are Mesoproterozoic, aging from 1,172 Ma to 1,114 Ma, and present, with the exception of the oldest grain of the set, positive values of  $\epsilon_{\text{Hf}(t)}$  which vary from +2.3 to +0.5, with  $T_{\text{DM}}$  model ages from 1,633 Ma to 1,523 Ma. Nine analyzed zircons are Neoproterozoic, with ages ranging from 958 Ma to 741 Ma, all with negative  $\epsilon_{\text{Hf}(t)}$  values of -16.2 to -4.5, and  $T_{\text{DM}}$  model ages of 2,065 Ma to 1,508 Ma. The sample's youngest dated grain ( $741 \pm 9$  Ma) presents a value of  $\epsilon_{\text{Hf}(t)}$  value of -5.6.

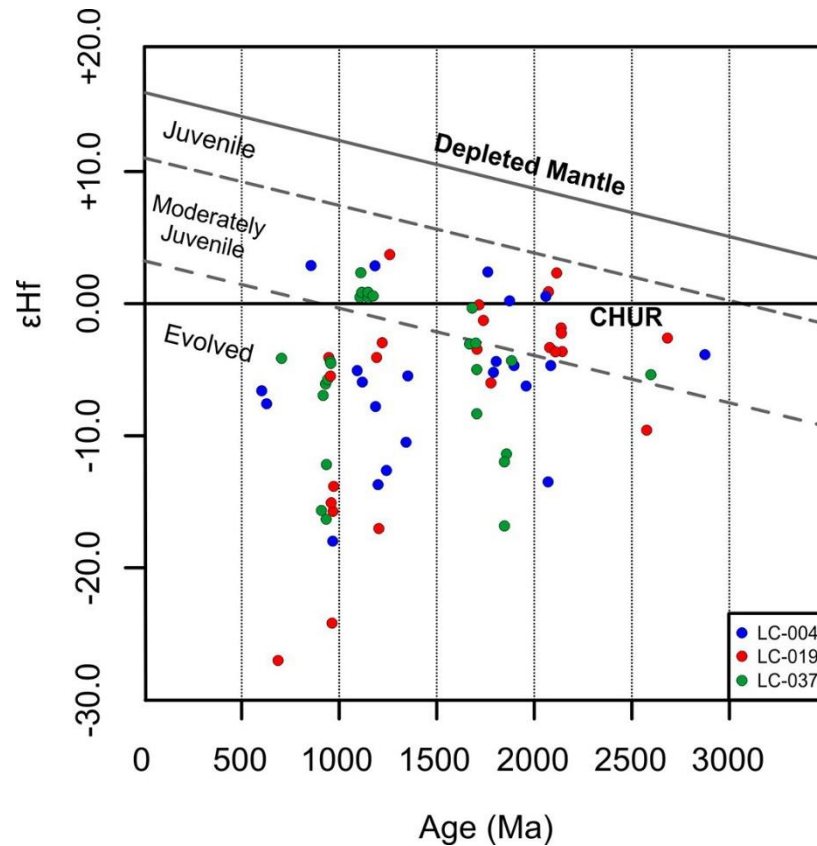


Figure 14. Hf isotopic diagram for samples LC-004, LC-019 and LC-037. The reference lines in the Hf plots are: CHUR chondritic uniform reservoir (Bouvier et al., 2008). Gray dashed lines classify fields of juvenile (0-5  $\epsilon$ -units below DM), moderately juvenile (5-12  $\epsilon$ -units below DM) and evolved (> 12  $\epsilon$ -units below DM); Bahlburg et al., 2011).

## 5. DISCUSSIONS

### 5.1. REE geochemical signature

Sample LC-039 plots in the Fe-Shale field, and its contents (Table 1), especially its REE distribution (Fig. 11), suggest a sedimentary contribution distinct from the other samples. When compared to the chemical analyzes of the Ribeirão da Folha amphibolites (Pedrosa-Soares et al., 1998), their major elements contents are similar and there is similarity in the REE distribution patterns (Fig. 15). The use of major and trace elements for the geotectonic discrimination of the amphibolites indicates that they are constituents of the ocean floor, originated from an ocean ridge. Its REE signatures suggest a succession of mafic rocks of mid-ocean ridge, with the presence of the enriched (E-MORB), transitional (T-MORB) and normal (N-MORB) MORB types. When chondrite-normalized, and in comparison to

each other, sample LC-039 shows a REE distribution trend with great approximations to the N-MORB and T-MORB. In all cases, there is enrichment in LREE in relation to the HREE ( $[La/Yb = 2.0]_{LC-039/N}$ ;  $[La/Yb = 12.5]_{E-MORB/N}$ ;  $[La/Yb = 2.4]_{T-MORB/N}$ ;  $[La/Yb = 1.0]_{N-MORB/N}$ ), and positive europium anomalies ( $[Eu/Eu^* = 1.9]_{LC-039/N}$ ;  $[Eu/Eu^* = 1.0]_{E-MORB/N}$ ;  $[Eu/Eu^* = 1.5]_{T-MORB/N}$ ;  $[Eu/Eu^* = 1.4]_{N-MORB/N}$ ). The Eu enrichment and the Nd negative anomaly in sample LC-039 are the main contrasts in its distributions, which can be explained by the sedimentary contribution of crustal material at the moment of sedimentation, with the presence of plagioclase originated from chemically evolved crustal rocks. Considering these evidences, there are mica schists closely associated to the amphibolites, which indicates a presence of basic volcanic sediments, such as clastic or tuffaceous debris, at the time of sedimentation.

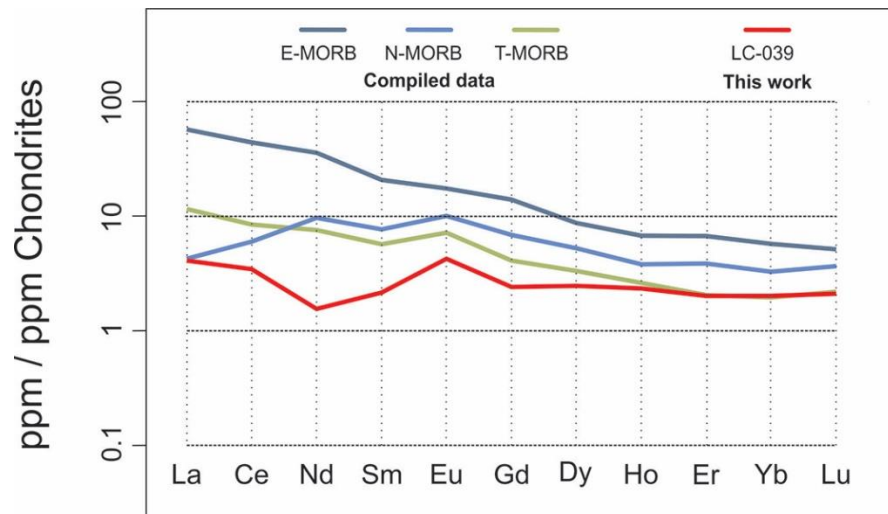


Figure 15. Chondrite-normalized REE diagram, comparing sample LC-039 with data compiled from Pedrosa-Soares et al. (1998).

Sample LC-006 presents very superior REE contents to the others, and by virtue of this, it was initially considered that it could be a rock which had undergone secondary processes of hydrothermal alterations and/or metassomatism. However, these processes cause large fractionations in the Nb/Ta and Zr/Hf ratios (Bau, 1996), and produce changes in the behavior of other trace elements (e.g. Kerrich and King, 1993; Bau, 1996). The Nb/Ta and Zr/Hf ratios for the sample are of 16.7 and 30.3, respectively, which are very similar to the analyzes obtained in the other samples (Table 1). This indicates that the LC-006 sample probably did not endure these processes and that, although it is a single collected sample, attention is drawn to its occurrence, which may denote a sedimentary contribution not yet recognized in the setting of the region.

## 5.2. Intensity of weathering and sediment recycling

The chemical indexes of weathering (or alteration indexes) are commonly used to interpret the intensity of the weathering experienced by rocks and sediments, considering the mobility of some major elements during the process (e.g. Nesbitt et al., 1990; Condie, 1993; Fedo et al., 1996; Gao et al., 1999; Young, 1999; Bolhar et al., 2005). It is also known that metasedimentary rocks may have their chemical signatures altered by their pre-metamorphic weathering history, erosion and chemical maturation from their source area (Price and Velbel, 2003). Thus, the Chemical Index of Alteration ( $CIA = [Al_2O_3 / (Al_2O_3 + K_2O + Na_2O + CaO^*)] \times 100$ , Nesbitt and Young, 1982) was used, where  $CaO^*$  simply represents the content in the silicates. The indexes for each of the analyzed samples are displayed in Table 1. Non-weathered igneous rocks present values close to or lower than 50, and typical shales present an average of 70 to 75 (McLennan et al., 1993). The CIA values for the group of eight samples with similar composition range from 64.2 to 83.3, with an average of 72.6. The CIA values for samples LC-006 and LC-039 are of 73.3 and 54.0, respectively.

In order to analyze the sediment recycling experienced by the mica schists, the Th/U ratio was used, at first. Under oxidizing conditions, the sediment recycling promotes a distinct Th and U concentration, due to the oxidation of the  $U^{+4}$  cation to  $U^{+6}$ , which forms several highly soluble acid salts that can be easily removed by weathering, whereas the Th, under the same conditions, maintains its oxidation state and remains relatively insoluble (McLennan and Taylor, 1980). As a consequence, the Th/U ratio progressively increases with the weathering and deposition cycles. The Th/U ratio for the eight samples group range from 4.3 to 7.8, which are higher values than the 3.8 found for the average of the upper continental crust by Taylor and McLennan (1985), suggesting that the sediments which originated the shale-graywackes protoliths underwent a significant sediment recycling process. Another way to evaluate this is by the Rb/Sr ratio, due to the intemperic and diagenetic processes that lead to the increase in the Rb/Sr ratio. Rb/Sr ratios  $> 0.5$  have been interpreted as indicators of weathering and sediment recycling (McLennan et al., 1993). The values found for the eight samples group are greater than this reference, with the exception of one sample, which presents a value of 0.4.

Considering the important sediment recycling experienced by the analyzed rocks, the enrichment in heavy minerals through reworking and selection during the sediments transportation is plausible. Nevertheless, the monazite is a heavy mineral which commonly occurs as accessory in the analyzed mica

schists, and concentrates LREE, which may be responsible for the concentration of these elements in the REE diagrams (Fig. 11).

### 5.3. Sedimentary provenance and tectonic ambience: geochemical perspective

Besides the REE and HFSE, elements such as Th, Sc, Cr and Ti exhibit low remobilization in post-depositional processes (e.g. Taylor and McLennan 1985; Taylor et al., 1986; McLennan et al. 1993), which can also be considered suitable for the sedimentary provenance analysis. The Th/Sc and Zr/Sc ratios involve incompatible and compatible elements, and are useful for indicating processes of magmatic differentiation, since Th and Zr are considered incompatible, and Sc compatible in the igneous system (McLennan, 1989; McLennan et al., 1993). The analyzed samples display Th/Sc and Zr/Sc ratios of 0.5 to 1.2, and 5.6 to 8.2, respectively, which are considered high and therefore indicate sedimentary provenance originated mainly from evolved igneous rocks.

Considering the plate tectonics so to perform a broader analysis on the sedimentary provenance of the Ribeirão da Folha mica schists, the Verma and Armstrong-Altrin (2013) multi-dimensional diagrams, which involve major elements, were used. These diagrams are very useful for the analyzes of the provenance of metasedimentary rocks, because they are robust to great chemical alteration due to analytical errors, weathering, sediment recycling and post-depositional processes. In the diagrams, the ten major elements (SiO<sub>2</sub> to P<sub>2</sub>O<sub>5</sub>) are considered so to discriminate between tectonic arc (presence of active, continental or oceanic volcanism), continental rift (extension) and continental collision (compression) settings. The samples are separated into high and low silica levels ( $[\text{SiO}_2]_{\text{adj}} = 63 - 95\%$  and  $[\text{SiO}_2]_{\text{adj}} = 35 - 63\%$ , respectively), in which  $[\text{SiO}_2]_{\text{adj}}$  are the SiO<sub>2</sub> values obtained after the adjustments to 100% on an anhydrous basis. Further details on the construction of the diagrams can be found in the authors' work.

By using the TecSand software (Verma et al., 2016), it is observed that six samples plot in the continental collision field, two in the arc field, and two in the continental rift field (Fig. 16). Thus, the sedimentary sources that originated the analyzed mica schists are mainly derived from rocks that had its origins in collisional environments, though, rocks from the setting of active magmatic arc and continental rift also contributed to the sedimentation of the Macaúbas Basin, in the Ribeirão da Folha region. Some considerations for the plotting are worth mentioning: sample LC-004 is in the arc field, which is in accordance with the U-Pb geochronological analyzes obtained in this work (chapter 6.4.2), having an

important contribution of zircon grains from the Rio Doce Magmatic Arc. Sample LC-006 plots in the rift field and presents anomalous REE patterns in relation to the other samples (Fig. 11). Sample LC-039 plots in the arc region, though, as observed (chapter 6.1), it presents a significant basic contribution and is chemically associated to the amphibolites. However, the used diagrams are not able to determine the ambiance of oceanic opening, so it can be disregarded or considered with reservations.

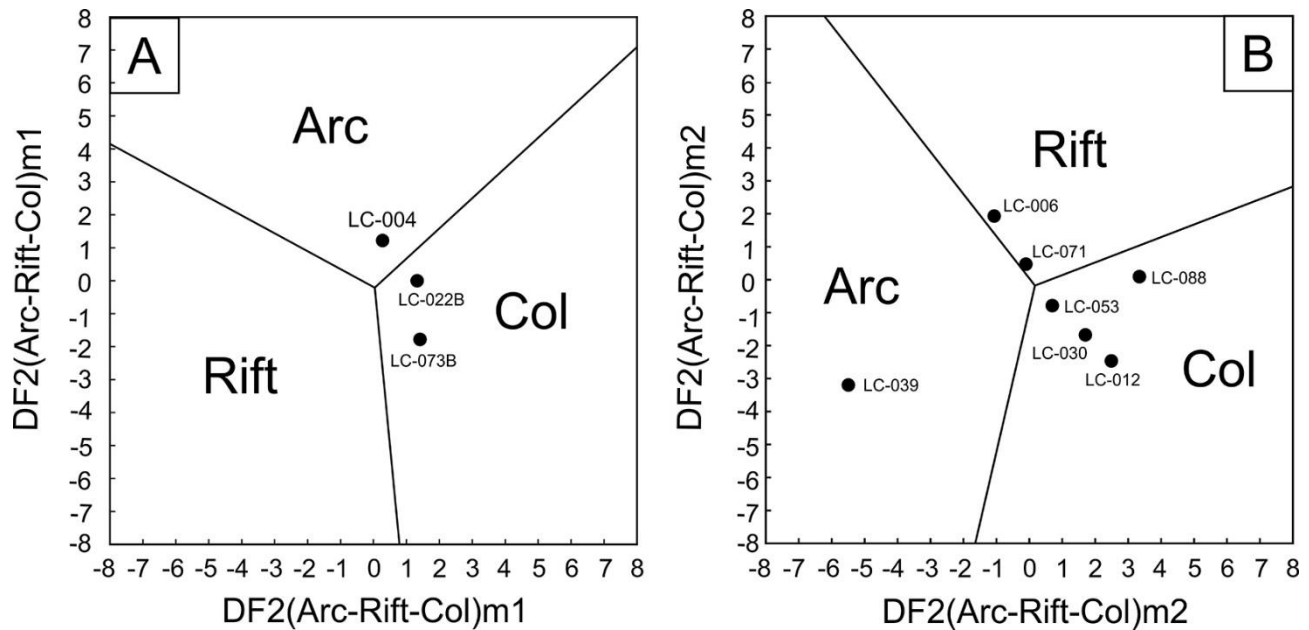


Figure 16. Verma and Armstrong-Altrin multi-dimensional diagram (2013) for tectonic discrimination of siliciclastic sediments. (A) High silica ( $[\text{SiO}_2]_{\text{adj}} = 63 - 95\%$ ). (B) Low silica ( $[\text{SiO}_2]_{\text{adj}} = 35 - 63\%$ ).

#### 5.4. Sedimentary provenance: U-Pb and Lu-Hf analyzes

The discussions concerning the sedimentary provenances of the metavolcano-sedimentary section of the Ribeirão da Folha ophiolitic complex are mainly based on the U-Pb geochronological and Lu-Hf isotopic analyzes of the detrital zircons collected from three samples (LC-004, LC-019 and LC-037). In order to investigate the provenances, the various units of the cratonic and orogenic domain of the setting will be considered. The ages distribution in the geological time observed in the three samples is broad and ranges from Archean to Neoproterozoic (Fig. 13). The Meso-Paleoproterozoic sedimentary contributions are the most numerous in all three histograms, with a common Calimian valley from

approximately 1,500 Ma to 1,600 Ma. Nevertheless, sample LC-004 differs from the other two due to its important Neoproterozoic contribution, so it will be discussed separately.

#### 5.4.1. Samples LC-019 and LC-037

Samples LC-019 and LC-037 exhibit the same geochronological pattern, with an important sedimentary contribution of Meso and Paleoproterozoic ages, as well as a relative scarcity of Archean and younger than 900 Ma Neoproterozoic grains (Fig 13).

The most important contributions are those of Mesoproterozoic ages, which represent approximately 44% of the analyzed grains of sample LC-019, and approximately 52% of sample LC-037. The  $\epsilon_{\text{Hf}}(t)$  signatures (Fig. 14) for the Mesoproterozoic grains of sample LC-019 exhibit wide distributions, ranging from very negative to positive (-16.9 to +3.7), whereas the LC-037 sample shows concentrated and positive values in the performed analyzes (+2.3 to +0.4). The variation in the  $\epsilon_{\text{Hf}}(t)$  signatures for sample LC-019 occurs even for detrital zircons with similar ages, which suggests a mixture from different sedimentary sources. For the Mesoproterozoic grains with negative  $\epsilon_{\text{Hf}}(t)$  signatures, the most likely candidate is the Espinhaço Supergroup and its correlated units, which is a relatively close sediment source, and exhibits a broad spectrum of detrital zircon ages, ranging from 1,100 Ma to 3,600 Ma (Chemale et al., 2012; Lopes, 2012; Kuchenbecker 2014). For the grains with positive signature, considering the two samples, the candidates are the volcanic rocks of the Bomba Formation (c. 1,500-1,600 Ma), of the Espinhaço Supergroup (Danderfer et al., 2009), for which Hf results are not available, or the Karagwe-Ankole-Kibarian belt, which registers positive  $\epsilon_{\text{Hf}}(t)$  values (+6.2 to +0.2) for its granitic rocks (Tack et al., 2010). Despite abundant Mesoproterozoic contributions being typically associated with the Tonian stage of the Macaúbas Basin rift (Kuchenbecker et al., 2015), Ectasian zircons, dated from 1,200 Ma to 1,300 Ma, are also found in sedimentary units linked to the passive margin stage of the Araçuaí Orogen itself, as in the Jequitinhonha Complex (Gonçalves-Dias et al., 2016), as well as in the Brasília Orogen, in the Andrelândia (Valeriano et al., 2004; Valladares et al., 2004), Vazante (Rodrigues et al., 2012), Canastra and Ibiá (Rodrigues et al., 2010, Gonçalves-Dias et al., 2016) groups, and, in part, in the Araxá Group (Falci et al., 2018), besides the Canabravinha Formation of the Rio Preto Belt (Caxito et al. al., 2013).

The Paleoproterozoic contributions are represented by 37% of sample LC-019, and 34% of sample LC-037, both exhibiting essentially negative Hf (t) signatures, despite a significant variation (-



5.9 to +2.3, and -16.7 to -0.3, for samples LC-019 and LC-037, respectively), with the occurrence of only two grains of the LC-019 sample with positive signatures. For the grains aged from 2,300 Ma to 1,800 Ma, of negative or positive signatures, the probable candidates are the Rhyacian-Orosirian cratonic basement complexes (Teixeira et al., 2000; Noce et al., 2007; Novo, 2013; Caxito et al., 2015), with the negative ones being contemplated by the Mantiqueira Complex, and the positive ones by the Juiz de Fora and Pocrane complexes. Staterian contributions may be related to the Espinhaço Supergroup and its related units. Archean contributions correspond to approximately 6% of the LC-019 sample population, and to 3% of sample LC-037, all of which exhibit negative signatures. The candidates in this case are the Archean basement complexes, with several occurrences in the São Francisco and Congo cratons (Teixeira et al., 2000; Noce et al., 2007).

The Neoproterozoic contributions correspond to 14% of sample LC-019, 11% of sample LC-037, and are essentially of Tonian ages, from 900 Ma to 1,000 Ma. Considering both samples, Neoproterozoic grains exhibit negative  $\epsilon_{\text{Hf}}(t)$  signatures, though with distinct concentrations, one of them with very negative values (-24.0 and -12.1), and the other with moderately negative values (-6.9 and -4.5). The Tonian grains have as main candidates the bimodal magmatism found in the São Francisco Craton and in the Araçuaí Orogen, represented by the Salto da Divisa Suite (Silva et al., 2008; Menezes et al., 2012), with secondary contributions possibly related to the anorogenic granites of the West Congo belt, associated to the Zadinian-Mayumbian volcanic pile (Tack et al., 2001). In effect, the 900-1000 Ma interval is marked by widespread rifting of the São Francisco Craton, with intrusion of mafic dyke swarms and large mafic-ultramafic complexes (e.g. Salgado et al., 2016; Girardi et al., 2017). Although located further north in the northern São Francisco Craton margin, rocks of the Cariris Velhos Belt (960 Ma to 1,000 Ma; Santos et al., 2010; Caxito et al., 2014) could also provide some of those zircon grains, specially through reworking in cratonic basins.

From the distribution spectrum of the two samples (Fig. 13), it is understood that they are related to the passive margin units of the Macaúbas Group (e.g. Kuchenbecker et al., 2015; Peixoto et al., 2015; Gonçalves-Dias et al., 2016). In addition, samples LC-037 (maximum sedimentation age of 741 Ma) and LC-019 (maximum sedimentation age of 673 Ma) correspond to Units A and B, respectively. Both are representative of the oceanic turbidite sedimentation, with the occurrence of suboceanic and oceanic splinters (Fig. 3 and 4), as well as the presence of meta-plagiogranite – of ages related to the oceanic opening of the Macaúbas Basin (Queiroga et al., 2007; Queiroga, 2010) – which attests that they belong to the top unit of the Macaúbas Group, the Ribeirão da Folha Formation.

### 5.4.2. Sample LC-004

Sample LC-004, despite its general similarity to the geochronological patterns of samples LC-019 and LC-037, presents a more expressive Neoproterozoic contribution – 22% of the zircon grains of this sample date to this era – and provides the youngest zircon grain found in the study area, of Ediacaran age of 599 Ma (Fig. 13). It should be noted that it was possible to extract only 32 zircons from this sample, in spite of the recurrent attempts to obtain more grains of the mica schists of the study area. As for the distribution of the  $\epsilon\text{Hf}(t)$  (Fig. 14) signatures for its Neoproterozoic grains, a variation from -17.6 to +3.1 occurs. Two of the analyzed grains are of Tonian age, with divergent  $\epsilon\text{Hf}(t)$  values, one of them being very negative (-17.6), and the other, positive (+3.1), suggesting a mixture of sedimentary sources. The best candidates for the evolved grain are the Salto da Divisa Suite, with occurrences of bimodal magmatism in the Araçuaí Orogen, whereas for the moderately juvenile grain, the main candidates are the mafic dikes found in the South Bahia Alkaline Province (Rosa et al., 2007), and the dikes of the Pedro Lessa Suite (Machado et al., 1989, Dussin and Chemale, 2012). The two youngest analyzed grains, Ediacaran, are notably negative (-6.3 and -7.2), and are possibly related to the Rio Doce Magmatic Arc (Gonçalves et al., 2016; Tedeschi et al., 2016).

28% of the analyzed grains in the sample are of Mesoproterozoic ages, and exhibit a very wide  $\epsilon\text{Hf}(t)$  distribution (-13.5 to +3.0), which also suggests distinct sedimentary sources. The best candidates for its negative contributions are the Espinhaço Supergroup and its related units, while its only positive grain might be related to the volcanic Bomba Formation, or the Karagwe-Ankole-Kibarian belt. Its Paleoproterozoic contributions represent approximately 44% of the obtained grains, and show mostly evolved  $\epsilon\text{Hf}(t)$  data (-13.5 to +2.4). Both negative and positive grains have as most probable candidates the Rhyacian-Orosirian cratonic basement complexes. From the sample's Archean detrital zircons, which represent approximately 6% of the grains, Lu-Hf isotopic analysis was performed in only one, the oldest grain found in the study area, of 2,921 Ma. This grain possess a  $\epsilon\text{Hf}(t)$  signature of -4.2, and may be related to the Archean basement complexes.

Due to its significant Neoproterozoic sedimentary contribution, with Ediacaran zircon crystals, it is understood that sample LC-004 received a significant contribution from the Rio Doce Magmatic Arc, and may therefore be related to the syn-orogenic Salinas Basin, in the Ribeirão da Folha region.

Furthermore, in the multi-dimensional diagrams (Fig. 15), the sample unquestionably plots in the arc field (unlike LC-039, discussed in Chapter 6.3), which also supports its syn-orogenic nature.

## 6. CONCLUSION AND TECTONIC MODEL

The stratigraphy of the region was divided into Units A and B (Fig. 3 and 4), taking into account their lithological associations and geochronological and isotopic contributions. Unit A corresponds to the inferior unit, with predominance of metapelitic sequences (mica schists of varied composition) over metapsamitic ones (micaceous and hematite quartzites), with recurrent presence of chemical sedimentation (banded iron formations, sulfated metacherts, sulfated diopsidites, and calc-silicatic), besides the meta-mafic and meta-ultramafic section, and maximum sedimentation age around 740 Ma. Unit B, superior, has a predominance of metapsamitic siliciclastic sequences over metapelitic ones, with scarce chemical sedimentation, and maximum sedimentation age around 670 Ma.

Based on the layout of the units on the map, the proposed stratigraphic column for the study area (Fig. 4), and the whole rock geochemistry analyzes, it is interpreted that the region's sedimentary ambiance may correspond to a distal passive margin environment, of oceanic sedimentation, with relative proximity to the continental slope. The shale-graywackes protoliths (Fig. 10 and Table 1) may correspond to sedimentary deposits of turbidite gravitational fluxes, while the presence of monomictic breccia (Fig. 5D) denotes the occurrence of debris flow. From the REE analyzes, it is worth noting that there was also the contribution of basic volcanic sediments, such as clastic or tuffaceous debris, during the sedimentation of Unit A, as attested by the comparative diagrams with chemical analyzes of amphibolites (Fig. 15).

The two Units exhibit great geochronological similarity, relatable to the top unit of the Macaúbas Group, the Ribeirão da Folha Formation (Fig. 13). However, their sedimentary provenance comes greatly from distinct sources, as evidenced by the  $\epsilon_{\text{Hf}}(t)$  signatures (Fig. 14). The signatures of the Mesoproterozoic grains of Unit A are positive (+2.3 to +0.4), while the Paleoproterozoic are very to slightly negative (-16.7 to -0.3). Unit B has very variable  $\epsilon_{\text{Hf}}(t)$  signatures in its Mesoproterozoic grains (-17.0 to +3.7), and negative to slightly positive in the Paleoproterozoic contributions (-5.9 to +2.3).

Considerations regarding the sedimentary provenances for these Units, based on the geochemical data, show that most of the analyzed samples present an important history of sediment recycling (Th/U: 4.3 to 7.8, and Rb/Sr > 0.5), which is in agreement with the significant Paleo and Mesoproterozoic and

Archean observed contributions, with several sedimentary contributions originating from reworked complexes. Moreover, from the plotting in the multi-elementary diagrams (Fig. 16), it is observed that most of the studied samples fall in the collisional field, which endorses their complex sedimentary histories.

The structural framework of the study area involves all the present units and may be related to the collisional event of the Araçuaí Orogen uplifting. The structures, as well as the stereograms of the  $D_n$  phase (Fig. 7), suggest a shear zone dominated by dextral transpression, with general tectonic transport towards SSW-SW, which may have led to the positioning of oceanic and suboceanic splinters – correspondents to the mafic-ultramafic section – in the midst of the marine sequences. This mechanism is in agreement with the late to post-collisional stages of the Araçuaí Orogen (Pedrosa-Soares et al., 2001; Alkmim et al., 2006, Pedrosa-Soares et al., 2007), which involve lateral escaping of blocks and the positioning of the late plutonic bodies. A similar process may also have acted in the region of the accretionary wedge of the Araçuaí Orogen, to the southeast of the study area, in the São José da Safira region (see Peixoto et al., 2015), where the Guanhães Block may have served as a shield in the shortening of the basin, resulting in the transportation of rocks from northeast to southwest.

Three deformation phases were recognized in the metavolcano-sedimentary section, each characterized by an associated schistosity, which occurred in progressive conditions of the schist facies to the amphibolite facies (Fig. 8). The compressional nature with progressive metamorphism is also evidenced by the mineral chemistry analyzes in garnets (Fig. 9), which exhibit chemical zoning characteristic of progressive path.

In the Ribeirão da Folha region, there is an extensive lithological diversity in a reduced area, with rocks representative of oceanic and suboceanic sections, and siliciclastic and chemical metasedimentary sequences with sedimentary contributions of varied ages and sources, as well as late to post-collisional plutonic intrusions, which suggests that the site, besides corresponding to the ophiolitic complex of the Araçuaí Orogen, is also the region of possible tectonic *mélange* (Fig. 17). This idea is supported, initially, by the presence of discontinuous suboceanic and oceanic splinters, tectonically encased by shear zones in the oceanic passive margin, correspondent to the Ribeirão da Folha Formation, the top unit of the Macaúbas Basin. In addition, the geochronological, isotopic and geochemical analyzes demonstrate the broad and complex nature of its sedimentary sources, which would have involved contributions of diverse environments and tectonic units, with the participation of two temporarily distinct sedimentary basins, Macaúbas and Salinas, in the process of amalgamation, a typical scenario of regions located in the

vicinity of suture zones. Recently, very similar interpretations suggesting an important shift in sedimentary provenance involving the orogenic fronts were presented for the Brasília Belt in the western São Francisco Craton margin (Falci et al., 2018) and for the Riacho do Pontal Belt in the northern cratonic margin (Caxito et al., 2016). Thus, this seems to be a fairly common process in the orogenic belts that surround the São Francisco Craton in the central portion of Western Gondwana.

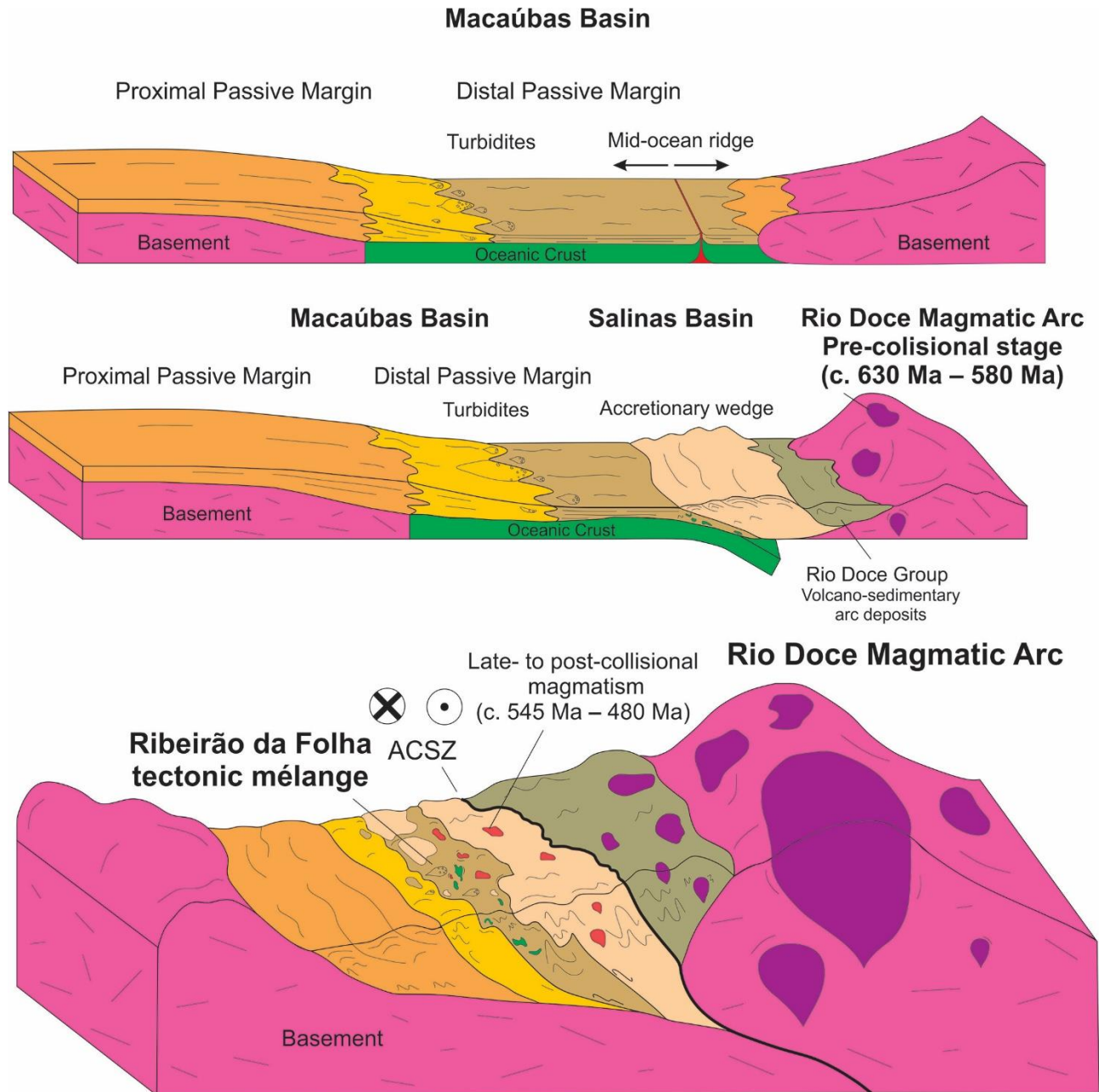


Figure 17. Evolutionary model illustrating the development of the tectonic mélangé of Ribeirão da Folha (without scale). (A) Opening of the Macaúbas Basin. (B) Accretionary orogeny stage of the Araçuaí Orogen with start of subduction. (C) Orogenic stage of continental collision between the São Francisco Craton and the Congo Craton, with establishment of the Abre Campo shear zone as suture zone and rock mixture characterizing the tectonic mélangé of Ribeirão da Folha.

## **Acknowledgments**

This work was supported by CNPq (grant number – 446483/2014-1), FAPESP and by the Laboratório de Geotectônica of the Centro de Pesquisa Manoel Teixeira da Costa, IGC-UFMG. Special thanks to the Microanalysis Laboratory of the Universidade Federal de Ouro Preto, a member of the Microscopy and Microanalysis Network of Minas Gerais State/Brazil/FAPEMIG, for the mineral chemistry analyses. We also thank Bruno Alcântara for field support. All of the co-authors are Research Fellows of the CNPq (Brazilian Research Council) and acknowledge for the support received.

## REFERÊNCIAS BIBLIOGRÁFICAS

- Aguilar, C., Alkmim, F.F., Lana, C., Farina, F. 2017. Palaeoproterozoic assembly of the São Francisco craton, SE Brazil: New insights from U–Pb titanite and monazite dating. *Precambrian Research*, **289**:95-115.
- Alkmim, F., Marshak, S., Pedrosa-Soares, A.C., Peres, G.G., Cruz, S.C.P., Whittington, A. 2006. Kinematic evolution of the Araçuaí-West Congo orogen in Brazil and Africa: Nutcracker tectonics during the Neoproterozoic assembly of Gondwana. *Precambrian Research*, **149**:43-64.
- Alkmim, F.F., Pedrosa-Soares, A.C., Noce, C.M., Cruz, S.C.P. 2007. Sobre a evolução tectônica do Orógeno Araçuaí-Congo Ocidental. *Geonomos*, **15**:25–43.
- Andersen, T., Andersson, U.B., Graham, S., Aberg, G., Simonsen, S.L. 2009. Granitic magmatism by melting of juvenile continental crust: new constraints on the source of Palaeoproterozoic granitoids in Fennoscandia from Hf isotopes in zircon. *J. Geological Society of London*, **166**:233-247.
- Aracema, L.W., Neves, A.C., Cristina, J., Ferreira, H., Pedrosa-Soares, A.C., Lobato, L.M., Noce, C.M. 2000. Novas evidências de remanescentes oceânicos na Faixa Araçuaí: as rochas meta-ultramáficas de São José da Safira. *Geonomos*, **8**:55-61.
- Babinski, M., Pedrosa-Soares, A.C., Trindade, R.I.F., Martins, M., Noce, C.M., Liu, D. 2012. Neoproterozoic glacial deposits from the Araçuaí orogen, Brazil: Age, provenance and correlations with the São Francisco craton and West Congo belt. *Gondwana Research*, **21**:451-465.
- Bahlburg, H., Vervoort, J.D., Dufrane, S.A., Carlotto, V., Reimann, C., Cárdenas, J. 2011. The U–Pb and Hf isotope evidence of detrital zircons of the Ordovician Ollantaytambo Formation, southern Peru, and the Ordovician provenance and paleogeography of southern Peru and northern Bolivia. *Journal of South American Earth Sciences*, **32**:196-209.
- Bau, M. 1996. Controls on the fractionation of isovalent trace elements in magmatic and aqueous systems: evidence from Y/Ho, Zr/ Hf, and lanthanide tetrad effect. *Contributions to Mineralogy and Petrology*, **123**:323-333.
- Bolhar, R., Kamber, B.S., Moor bath, S., Whitehouse, M.J., Collerson, K. 2005. Chemical characterization of earth's most ancient clastic metasediments from the Isua Greenstone Belt, southern West Greenland. *Geochimica et Cosmochimica Acta*, **69**:1555-1573.

- Bouvier, A., Vervoort, J.D., Patchett, P.J. 2008. The Lu-Hf and Sm-Nd isotopic composition of CHUR: Constraints from unequilibrated chondrites and implications for the bulk composition of terrestrial planets. *Earth Planet Science Letters*, **273**:48-57.
- Brandani, D.B. and Costa, L.P. 2004. Geologia da região de Baixa Quente, sudeste de Minas Novas (MG). BS Dissertation, Instituto de Geociências, Universidade Federal de Minas Gerais, Belo Horizonte, 50 p.
- Brito Neves, B.B. and Cordani, U.G. 1991. Tectonic evolution of South America during the late Proterozoic. *Precambrian Research*, **53**:23-40.
- Bucher, K. and Grapes, R. (eds.) 2011. *Petrogenesis of Metamorphic Rocks*, 8th ed. Springer Science and Business Media, p. 428.
- Castro, M.P. 2014. Caracterização geológica da Formação Capelinha como uma unidade basal do Grupo Macaúbas em sua área tipo, Minas Gerais. MS Dissertation, Escola de Minas, Departamento de Geologia, Universidade Federal de Ouro Preto, Belo Horizonte, p. 114.
- Caxito, F.A., Halverson, G.P., Uhlein, A., Stevenson, R., Uhlein, G.J. 2012. Marinoan glaciation in east central Brazil. *Precambrian Research*, **203**:38-58.
- Caxito, F.A., Dantas, E.L., Ross, S., Uhlein, A. 2013. Detrital zircon (U–Pb) and Sm–Nd isotope studies of the provenance and tectonic setting of basins related to collisional orogens: The case of the Rio Preto fold belt on the northwest São Francisco Craton margin, NE Brazil. *Gondwana Research*, **26**:741-754.
- Caxito, F.A., Uhlein, A., Dantas, E.L. 2014. The Afeição augen-gneiss Suite and the record of the Cariris Velhos Orogeny (1000–960 Ma) within the Riacho do Pontal fold belt, NE Brazil. *Journal of South American Earth Sciences*. **51**:12-27.
- Caxito, F.A., Uhlein, A., Dantas, E.L., Stevenson, R. 2015. Orosirian (ca. 1.96 Ga) mafic crust of the northwestern São Francisco Craton margin: Petrography, geochemistry and geochronology of amphibolites from the Rio Preto fold belt basement, NE Brazil. *Journal of South American Earth Sciences*. **59**:95-111.
- Chemale, F., Dussin, I.A., Alkmim, F.F., Martins, M.S., Queiroga, G., Armstrong, R., Santos, M.N. 2012. Unravelling a Proterozoic basin history through detrital zircon geochronology: The case of the Espinhaço Supergroup, Minas Gerais, Brazil. *Gondwana Research*, **22**:200-206.



- Condie, K.C. 1993. Chemical composition and evolution of the upper continental crust: Contrasting results from surface samples and shales. *Chemical Geology*, **104**:1-37.
- Cunningham, W.D., Marshak, S., Alkmim, F.F. 1996. Structural style of basin inversion at mid-crustal levels: two transects in the internal zone of the Brasiliano Araçuaí Belt, Minas Gerais, Brazil. *Precambrian Research*, **77**:1-15.
- Cunningham, D., Alkmim, F.F., Marshak, S. 1998. A structural transect across the coastal mobile belt in the Brazilian Highlands (latitude 20°S): The roots of a Precambrian transpressional orogen. *Precambrian Research*, **92**:251-275.
- Danderfer, A., Waele, B. De, Pedreira, A.J., Nalini, H.A. 2009. New geochronological constraints on the geological evolution of Espinhaço basin within the São Francisco Craton—Brazil. *Precambrian Research*, **170**:116-128.
- De Campos, C.P., Mendes, J.C., Ludka, I.P., de Medeiros, S.R., de Moura, J.C., Wallfuss, C. 2004. A review of the Brasiliano magmatism in Southern Espírito Santo, Brazil, with emphasis on post-collisional magmatism. *Journal of Virtual Explorer*, **17**:1-39.
- Degler, R., Pedrosa-Soares, A., Novo, T., Tedeschi, M., Silva, L.C., Dussin, I., Lana, C. 2018. Rhyacian-Orosirian isotopic records from the basement of the Araçuaí-Ribeira orogenic system (SE Brazil): Links in the Congo-São Francisco palaeocontinent. *Precambrian Research*, **317**:179-195.
- Dussin, I.A. and Chemale, F. 2012. *Geologia estrutural e estratigrafia do sistema Espinhaço – Chapada Diamantina e sua aplicação nas bacias mesocenozóicas da margem passiva brasileira, 1th ed.* Particular, Belo Horizonte, p. 218.
- Falci, A., Caxito, F.A., Seer, H.J., Valeriano, C. de M., Dias, P.H.A., Pedrosa-Soares, A.C. 2018. Provenance shift from a continental margin to a syn-orogenic basin in the Neoproterozoic Araxá nappe system, southern Brasília belt, Brazil. *Precambrian Research*, **306**:209-219.
- Fedo, C.M., Eriksson, K.A., Krogstad, E.J. 1996. Geochemistry of shales from the Archean (~3.0 Ga) Buhwa Greenstone Belt, Zimbabwe: Implications for provenance and source-area weathering. *Geochimica et Cosmochimica Acta*, **60**: 1751-1763.
- Ferrari, P.G. 1985. Aspectos metalogenéticos do Pré-Cambriano de Minas Gerais. In: Sociedade Brasileira de Geologia Núcleo Minas Gerais, Anais do 3º Simpósio de Geologia de Minas Gerais. Belo Horizonte, *Boletim* n° 5, p. 348-353.

- Festa, A., Pini, G.A., Dilek, Y., Codegone, G. 2010a. Mélanges and mélange-forming processes: a historical overview and new concepts. *International Geology Review*, **52**:1040-1105.
- Festa, A., Pini, G.A., Dilek, Y., Codegone, G., Vezzani, L., Ghisetti, F., Lucente, C.C., Ogata, K. 2010b. Peri-Adriatic mélanges and their evolution in the Tethyan realm. *International Geology Review*, **52**:369-403.
- Festa, A., Dilek, Y., Pini, G.A., Codegone, G., Ogata, K. 2012. Mechanisms and processes of stratal disruption and mixing in the development of mélanges and broken formations: Redefining and classifying mélanges. *Tectonophysics*, **568-569**:7-24.
- Fontes, C.A., Ferrari P.G., Pereira A.P.C., Neto C., Pereira A.S., Lima J.R.P.Q., Costa M.R.A., Baltazar O.F., Silva S.L., Vieira V.S., Ramalho R. 1978. *Projeto Jequitinhonha*. Escala 1:250.000. Belo Horizonte, DNPM/CPRM, Relatório Final, p. 368.
- Freitas-Silva, F.H. and Pereira, L.A. 1987. A geologia da região de Ribeirão da Folha, nordeste de Capelinha, MG (subárea norte). BS Dissertation, Instituto de Geociências, Universidade Federal de Minas Gerais, Belo Horizonte, p. 156.
- Gao, S., Ling, W., Qiu, Y., Lian, Z., Hartmann, G., Simon, K. 1999. Contrasting geochemical and Sm-Nd isotopic compositions of Archean metasediments from the Kongling high-grade terrain of the Yangtze craton: Evidence for cratonic evolution and redistribution of REE during crustal anatexis. *Geochimica et Cosmochimica Acta*, **63**:2071-2088.
- Girardi, V.A. V, Teixeira, W., Mazzucchelli, M., Oliveira, E.P., Costa, P.C.C. 2017. Mafic Dykes: Petrogenesis and Tectonic Inferences. In: Heilbron, M., Cordani, U.G., Alkmim, F.F. (eds.). *São Francisco Craton, Eastern Brazil*. Regional Geology Reviews, Springer, p. 145-169.
- Gonçalves-Dias, T., Caxito, F.A., Pedrosa-Soares, A.C., Stevenson, R., Dussin, I., Silva, L.C., Alkmim, F., Pimentel, M. 2016. Age, provenance and tectonic setting of the high-grade Jequitinhonha Complex, Araçuaí orogen, eastern Brazil. *Brazilian Journal of Geology*, **46**:199-219.
- Gonçalves, L., Farina, F., Lana, C., Pedrosa-Soares, A.C., Alkmim, F., Nalini Jr., H.A. 2014. New U-Pb ages and lithochemical attributes of the Ediacaran Rio Doce magmatic arc, Araçuaí confined orogen, southeastern Brazil. *Journal of South American Earth Sciences*, **52**:129-148.
- Gonçalves, L., Alkmim, F.F., Pedrosa-Soares, A.C., Dussin, I.A., Valeriano, C. de M., Lana, C., Tedeschi, M. 2016. Granites of the intracontinental termination of a magmatic arc: an example from the Ediacaran Araçuaí orogen, southeastern Brazil. *Gondwana Research*, **36**:439-458.

- Gonçalves, L., Alkmim, F.F., Pedrosa-Soares, A., Gonçalves, C.C., Vieira, V. 2017. From the plutonic root to the volcanic roof of a continental magmatic arc: a review of the Neoproterozoic Araçuaí orogen, southeastern Brazil. *International Journal of Earth Sciences*, **107**:337-358.
- Gradim, C., Roncato, J., Pedrosa-Soares, A.C., Cordani, U., Dussin, I., Alkmim, F.F., Queiroga, G., Jacobsohn, T., Silva, L.C., Babinski, M. 2014. The hot back-arc zone of the Araçuaí orogen, Eastern Brazil: from sedimentation to granite generation. *Brazilian Journal of Geology*, **44**:155-180.
- Griffin, W.L., Pearson, N.J., Belousova, E., Jackson, S.E., Van Acherbergh, E., O'Reilly, S.Y., Shee, S.R. 2000. The Hf isotope composition of cratonic mantle: LAM-MC-ICPMS analysis of zircon megacrysts in kimberlites. *Geochimica et Cosmochimica Acta*, **64**:133-147.
- Grossi-Sad, J.H. and Motta, E.G.M. 1991. Geologia e prospecção geoquímica na área Capelinha-Turmalina-Minas Novas, MG. Relatório Inédito, ACESITA-GEOSOL. Belo Horizonte, 129 p.
- Grossi-Sad, J.H., Motta, E.G.M., Baars, F.J. 1993. Formação Capelinha: uma nova entidade litoestratigráfica do Grupo Macaúbas Superior. In: Sociedade Brasileira de Geologia, Anais do VII Simpósio de Geologia de Minas Gerais. Belo Horizonte, *Boletim* n° 12. 30-33.
- Guadagnin, F., Chemale, F., Magalhães, A.J.C., Santana, A., Dussin, I., Takehara, L. 2015. Age constraints on crystal-tuff from the Espinhaço Supergroup – Insight into the Paleoproterozoic to Mesoproterozoic intracratonic basin cycles of the Congo – São Francisco Craton. *Gondwana Research*, **27**:363–376.
- Herron, M.M. 1988. Geochemical classification of terrigenous sands and shales from core or log data. *Journal of Sedimentary Petrology*, **58**:820-829.
- Jackson, S.E., Pearson, N.J., Griffin, W.L., Belousova, E.A. 2004. The application of laser ablation-inductively coupled plasma-mass spectrometry to in situ U–Pb zircon geochronology. *Chemical Geology*, **211**:47-69.
- Kerrick, R. and King, R. 1993. Hydrothermal zircon and baddeleyite in Val-d'Or Archean mesothermal gold deposits: characteristics, compositions, and fluid-inclusion properties, with implications for timing of primary gold mineralization. *Canadian Journal of Earth Sciences*, **30**:2334-2351.
- Kuchenbecker, M. 2014. Relações entre coberturas do Cráton do São Francisco e bacias situadas em orógenos marginais: o registro de datações U-Pb de grãos detríticos de zircão e suas implicações geotectônicas. PhD Thesis, Instituto de Geociências, Universidade Federal de Minas Gerais, Belo Horizonte, 163 p.

- Kuchenbecker, M., Pedrosa-Soares, A.C., Babinski, M., Fanning, M. 2015. Detrital zircon age patterns and provenance assessment for pre-glacial to post-glacial successions of the Neoproterozoic Macaúbas Group, Araçuaí Orogen, Brazil. *Precambrian Research*, **266**:12-26.
- Lagoeiro, L.E. and Menegasse, L.M. 1987. Geologia da região de Ribeirão da Folha, município de Minas Novas, Minas Gerais (área sul). BS Dissertation, Instituto de Geociências, Universidade Federal de Minas Gerais, Belo Horizonte, 91 p.
- Lima, S. de A., Martins-Neto, M., Pedrosa-Soares, A.C., Cordani, U., Nutman, A. 2002. A Formação Salinas na área-tipo, NE de Minas Gerais: uma proposta de revisão da estratigrafia da Faixa Araçuaí com base em evidências sedimentares, metamórficas e idades U-Pb SHRIMP. *Revista Brasileira de Geociências*, **32**:491-500.
- Lopes, T.C. 2012. O Supergrupo Espinhaço na Serra do Cabral, Minas Gerais: contribuição ao estudo de proveniência sedimentar. MS Dissertation, Instituto de Geociências, Universidade Federal de Minas Gerais, Belo Horizonte, 116 p.
- Machado, N., Schrank, A., Abreu, F.R., Knauer, L.G., Almeida-Abreu, P.A. 1989. Resultados preliminares da geocronologia U-Pb na Serra do Espinhaço Meridional. In: Sociedade Brasileira de Geologia Núcleo Minas Gerais, Anais 5º Simpósio de Geologia. Belo Horizonte, *Boletim* n° 10, 171-174.
- Martins, V.T. de S., Teixeira, W., Noce, C.M., Pedrosa-Soares, A.C. 2004. Sr and Nd characteristics of Brasiliano/Pan-African granitoid plutons of the Araçuaí orogen, southeastern Brazil: tectonic implications. *Gondwana Research*, **7**:75-89.
- McLennan, S.M. 1989. Rare earth elements in sedimentary rocks: influence of provenance and sedimentary processes. *Reviews of Mineralogy*, **21**:169-200.
- McLennan, S.M., Taylor, S.R. 1980. Th and U in sedimentary rocks: crustal evolution and sedimentary recycling. *Nature* **285**:621-624.
- McLennan, S.M., Hemming, S., McDaniel, D.K., Hanson, G.N. 1993. Geochemical approaches to sedimentation, provenance, and tectonics. In: GSA, Geological Society of America. *Special Papers*, **284**:21-40.
- Menezes, R.C.L., Conceição, H., Rosa, M.L.S., Macambira, M.J., Galarza, M.A., Rios, D.C., 2012. Geoquímica e geocronologia de granitos anorogênicos tonianos (ca. 914–899 Ma) da Faixa Araçuaí no sul do estado da Bahia. *Geonomos*, **20**:1-13.

- Morel, M.L.A., Nebel, O., Nebel-Jacobsen, Y.J., Miller, J.S., Vroon, P.Z. 2008. Hafnium isotope characterization of the GJ-1 zircon reference material by solution and laser-ablation MC-ICPMS. *Chemical Geology*, **255**:231-235.
- Nalini Jr., H.A., Machado, R., Bilal, E. 2005. Geoquímica e petrogênese da Suíte Galiléia: exemplo de magmatismo tipo-I metaluminoso pré-colisional neoproterozóico da região do Médio Vale do Rio Doce (MG). *Revista Brasileira de Geociências*, **35** (4 – **Suplemento**):23-34.
- Nesbitt, H.W. and Young, G.M. 1982. Early Proterozoic climates and plate motions inferred from major element chemistry of lutites. *Nature*, **299**:715-717.
- Nesbitt, H.W., MacRae, N.D., Kronberg, B.I. 1990. Amazon deep-sea fan muds: light REE enriched products of extreme chemical weathering. *Earth Planet Science. Letters*, **100**:118-123.
- Noce, C.M., Pedrosa-Soares, A.C., Piuzana, D., Armstrong, R., Laux, J.H., de Campos, C.M., de Medeiros, S.R. 2004. Ages of sedimentation of the kinzigitic complex and a late orogenic thermal episode in the Aracuaí orogen, northern Espírito Santo state, Brazil: zircon and monazite U-Pb SHRIMP and ID-TIMS data. *Revista Brasileira de Geociências*, **34**:587-592.
- Noce, C.M., Pedrosa-Soares, A.C., Silva, L.C.S., Alkmim, F.F. 2007. O embasamento arqueano e paleoproterozóico do Orógeno Araçuaí. *Geonomos*, **15**:17-23.
- Novo, T.A. 2013. Caracterização do Complexo Pocrane, magmatismo básico mesoproterozóico e unidades neoproterozóicas do sistema Araçuaí-Ribeira, com ênfase em geocronologia U-Pb (SHRIMP e LA-ICP-MS). PhD Thesis, Instituto de Geociências, Universidade Federal de Minas Gerais, Belo Horizonte, 193 p.
- Novo, T.A., Pedrosa-Soares, A.C., Vieira, V.S., Dussin, I., Silva, L.C. 2018. The Rio Doce Group revisited: an ediacaran arc-related volcano-sedimentary basin, Araçuaí orogen (SE Brazil). *Journal of South American Earth Sciences*, **85**:345-361.
- Pedrosa-Soares, A.C. 1995. Potencial aurífero do Vale do Araçuaí, Minas Gerais: história da exploração, geologia e controle tectonometamórfico. PhD Thesis, Instituto de Geociências, Universidade de Brasília, 177 p.
- Pedrosa-Soares, A.C. 1997. Geologia da Folha Jenipapo, In: J.H. Grossi-Sad, L.M. Lobato, A.C. Pedrosa-Soares, B.S. Soares-Filho (eds). Projeto Espinhaço em CD-Rom. Belo Horizonte.

- Pedrosa-Soares, A.C. and Alkmim, F.F. 2011. How many rifting events preceded the development of the Araçuaí-West Congo orogen? *Geonomos*, **19**:244-251.
- Pedrosa-Soares, A.C., Meira, L.P., Fogaça, A.C.C., Teixeira, L.E., Schettino, A. 1986. Sequência sulfetada no Ribeirão da Folha, Minas Novas, MG. In: SBG, Sociedade Brasileira de Geologia, Anais do XXXIV Congresso Brasileiro de Geologia. Goiânia, *Boletim de Resumos*, 119.
- Pedrosa-Soares, A.C., Noce, C.M., Monteiro, R.L.B.P., Mourão, M.A.A., Lima, A.J. 1990a. A evolução monocíclica da Faixa Araçuaí no Médio Jequitinhonha: evidências estratigráficas, estruturais e metamórficas. In: SBG, Sociedade Brasileira de Geologia, Anais do XXXVI Congresso Brasileiro de Geologia. Natal, *Boletim de Resumos*, 292.
- Pedrosa-Soares, A.C., Monteiro, R.L.B.P., Noce, C.M., Freitas-Silva, F.H., Oliveira, M.J.R., Schettino, A. 1990b. Caracterização de uma sequência vulcano-sedimentar distal na Faixa Araçuaí, MG: bacia oceânica restrita? In: SBG, Sociedade Brasileira de Geologia, XXXVI Congresso Brasileiro de Geologia. Natal, *Boletim de Resumos*, 308.
- Pedrosa-Soares, A.C., Noce, C.M., Vidal, P., Monteiro, R.L.B.P., Leonardos, O.H. 1992. Toward a new tectonic model for the Late Proterozoic Araçuaí (SE Brazil)-West Congolian (SW Africa) Belt. *Journal of South American Earth Sciences*, **6**:33-47.
- Pedrosa-Soares, A.C., Vidal, P., Leonardos, O.H., De Brito-Neves, B.B. 1998. Neoproterozoic oceanic remnants in eastern Brazil: further evidence and refutation of an exclusively ensialic evolution for the Aracuai–West Congo orogen. *Geology*, **26**:519-522.
- Pedrosa-Soares, A.C. and Wiedemann, C. M. 2000. Evolution of the Araçuaí Belt and its connection to the Ribeira Belt, Eastern Brazil. In: Cordani, U.G., Milani, E.J., Thomaz-Filho, A., Campos, D.A. (eds). *Tectonic evolution of South America*, p. 265-285.
- Pedrosa-Soares, A.C., Noce, C.M., Wiedemann, C.M., Pinto, C.P. 2001. The Aracuai–West-Congo Orogen in Brazil: an overview of a confined orogen formed during Gondwanaland assembly. *Precambrian Research*, **110**:307-323.
- Pedrosa-Soares, A.C., Noce, C.M., Alkmim, F.F., da Silva, L.C., Babinski, M., Cordani, U., Castañeda, C. 2007. Orógeno Araçuaí: Síntese do conhecimento 30 anos após Almeida 1977. *Geonomos*, **15**:1-16.
- Pedrosa-Soares, A.C., Alkmim, F.F., Tack, L., Noce, C.M., Babinski, M., Silva, L.C., Martins-Neto, M.A. 2008. Similarities and differences between the Brazilian and African counterparts of the Neoproterozoic Araçuaí-West Congo orogen. In: Pankhurst, R. J., Trouw. R. A. J., Brito Neves, B. B,

- De Wit, M. J. (eds.) West Gondwana Pre-Cenozoic Correlations Across the South Atlantic Region. Geological Society of London, *Special Publications*, **294**:153-172.
- Pedrosa-Soares, A.C., Babinski, M., Noce, C.M., Martins, M. de S., Queiroga, G.N., Vilela, F. 2011a. The Neoproterozoic Macaúbas Group (Araçuaí orogen, SE Brazil) with emphasis on the diamictite formations. In: Arnaud, E., Halverson, G. P. Shield. G (eds). The Geological Records of Neoproterozoic Glaciations. Geological Society of London, *Memoirs*, **36**:523-534.
- Pedrosa-Soares, A.C., Campos, C.P.C., Noce, C., Silva, L.C., Novo, T., Roncato, J., Medeiros, S., Castañeda, C., Queiroga, G., Dantas, E., Dussin, I., Alkmim, F. 2011b. Late Neoproterozoic–Cambrian granitic magmatism in the Araçuaí orogen (Brazil), the Eastern Brazilian Pegmatite Province and related mineral resources. In: Sial, A. N., Bettencourt, J. S., Campos, C. P., Ferreira, V. P. Granite-Related Ore Deposits. Geological Society of London, *Special Publications*, **350**: 25-51.
- Peixoto, E., Pedrosa-Soares, A.C., Alkmim, F.F., Dussin, I.A. 2015. A suture-related accretionary wedge formed in the Neoproterozoic Aracuai orogen (SE Brazil) during Western Gondwanaland assembly. *Gondwana Research*, **27**:878-896.
- Peres, G.G., Alkmim, F.F., Jordt-Evangelista, H. 2004. The southern Araçuaí belt and the Dom Silvério Group: Geologic architecture and tectonic significance. *Annals of the Brazilian Academy of Sciences*, **76**:771-790.
- Pietranik, A.B., Hawkesworth, C.J., Storey, C.D., Kemp, A.I.S., Sircombe, K.N., Whitehouse, M.J., Bleeker, W. 2008. Episodic, mafic crust formation from 4.5 to 2.8 Ga: New evidence from detrital zircons, Slave craton, Canada. *Geology*, **36**:875-878.
- Pinto, C.P., Drumond, J.B.V., Féboli, W.L. 2001. Projeto Leste (CD-ROM). CPRM/CODEMIG, Belo Horizonte.
- Porada, H. 1989. Pan-African rifting and orogenesis in southern to equatorial Africa and eastern Brazil. *Precambrian Research*, **44**:103-136.
- Price, J.R., Velbel, M.A. 2003. Chemical weathering indices applied to weathering profiles developed on heterogeneous felsic metamorphic parent rocks. *Chemical Geology*, **202**:397-416.
- Queiroga, G.N. 2006. A seção sedimentar sulfetada do ofiolito de Ribeirão da Folha e seu potencial metalogenético, Orógeno Araçuaí, MG. MS Dissertation, Instituto de Geociências, Universidade Federal de Minas Gerais, Belo Horizonte, 130 p.

- Queiroga, G.N. 2010. Caracterização de restos de litosfera oceânica do Orógeno Araçuaí entre os paralelos 17° e 21°S. PhD Thesis, Instituto de Geociências, Universidade Federal de Minas Gerais, Belo Horizonte, 180 p.
- Queiroga, G., Pedrosa-Soares, A.C., Quéméneur, J., Castañeda, C. 2006. A unidade metassedimentar do ofiolito de Ribeirão da Folha, Orógeno Araçuaí, Minas Gerais: petrografia, geotermobarometria e calcografia. *Geonomos*, **14**:25-35.
- Queiroga, G.N., Pedrosa-Soares, A.C., Noce, C.M., de Alkmim, F.F., Martins Pimentel, M., Dantas, E., Martins, M., Castañeda, C., Suita, M.T.F., Prichard, H.M. 2007. Age of the Ribeirão da Folha ophiolite, Araçuaí orogen: the U-Pb zircon (LA-ICPMS) dating of a plagiogranite. *Geonomos*, **15**:61-65.
- Richter, F., Lana, C., Stevens, G., Buick, I., Pedrosa-Soares, A.C., Alkmim, F.F., Cutts, K. 2016. Sedimentation, metamorphism and granite generation in a back-arc region: Records from the Ediacaran Nova Venécia Complex (Araçuaí Orogen, Southeastern Brazil). *Precambrian Research*, **272**:78-100.
- Rodrigues, J.B., Pimentel, M.M., Dardenne, M.A., Armstrong, R.A. 2010. Age, provenance and tectonic setting of the Canastra and Ibiá Groups (Brasília Belt, Brazil): Implications for the age of a Neoproterozoic glacial event in central Brazil. *Journal of South American Earth Sciences*, **29**:512-521.
- Rodrigues, J.B., Pimentel, M.M., Buhn, B., Matteini, M., Dardenne, M.A., Alvarenga, C.J.S., Armstrong, R.A. 2012. Provenance of the Vazante Group: New U–Pb, Sm–Nd, Lu–Hf isotopic data and implications for the tectonic evolution of the Neoproterozoic Brasília Belt. *Gondwana Research*, **21**:439-450.
- Rosa, M.L.S., Conceição, H., Macambira, M.J., Galarza, M.A., Cunha, M.P., Menezes, R.C.L., Marinho, M.M., Filho, B.E.C., Rios, D.C. 2007. Neoproterozoic anorogenic magmatism in the Southern Bahia Alkaline Province of NE Brazil: U–Pb and Pb–Pb ages of the blue sodalite syenites. *Lithos*, **97**:88-97.
- Salgado, S.S., Filho, C.F.F., Caxito, F.A., Uhlein, A., Dantas, E.L., Stevenson, R. 2016. The Ni-Cu-PGE mineralized Brejo Seco mafic-ultramafic layered intrusion, Riacho do Pontal Orogen: Onset of Tonian (ca. 900 Ma) continental rifting in Northeast Brazil. *Journal South American Earth Sciences*, **70**, 324-339.
- Santos, E.J., Schmus, W.R. Van, Kozuch, M., Brito Neves, B.B. 2010. The Cariris Velhos tectonic event in Northeast Brazil. *Journal of South American Earth Sciences*, **29**:61-76.
- Santos, M.M., Lana, C., Scholz, R., Kamo, S.L., Gerdes, A., Corfu, F., Tapster, S. 2017. A new appraisal of Sri Lankan BB Zircon as reference material for LA- ICP-MS U-Pb geochronology and Lu-Hf isotope tracing. *Geostandards and Geoanalytical Research*, **41**:335-358.



- Santos, R.F., Alkmim, F.F., Pedrosa-Soares, A.C. 2009. A Formação Salinas, Orógeno Araçuaí (MG): história deformacional e significado tectônico. *Revista Brasileira de Geociências*, **39**:81-100.
- Serrano, P., Pedrosa-Soares, A.C., Medeiros-Júnior, E., Fonte-boa, T., Araujo, C., Dussin, I., Queiroga, G., Lana, C. 2018. A-type Medina batholith and post-collisional anatexis in the Araçuaí orogen (SE Brazil). *Lithos*, **320**:515-536.
- Silva, C.M.A., Gomes, J.B., Caldeira, S.M.B. 1987. Geologia da região de Ribeirão da Folha, município de Minas Novas, MG (área central). BS Dissertation, Instituto de Geociências, Universidade Federal de Minas Gerais, Belo Horizonte, 71 p.
- Silva, L.C., Pedrosa-Soares, A.C., Teixeira, L.R., Armstrong, R. 2008. Tonian rift-related, A-type continental plutonism in the Araçuaí Orogen, eastern Brazil: New evidence for the breakup stage of the São Francisco–Congo Palecontinent. *Gondwana Research*, **13**:527-537.
- Sláma, J., Košler, J., Condon, D.J., Crowley, J.L., Gerdes, A., Hanchar, J.M., Horstwood, M.S.A., Morris, G.A., Nasdala, L., Norberg, N., Schaltegger, U., Schoene, B., Tubrett, M.N., Whitehouse, M.J. 2008. Plešovice zircon — A new natural reference material for U–Pb and Hf isotopic microanalysis. *Chemical Geology*, **249**:1-35.
- Söderlund, U., Patchett, P.J., Vervoort, J.D., Isachsen, C.E. 2004. The  $^{176}\text{Lu}$  decay constant determined by Lu–Hf and U–Pb isotope systematics of Precambrian mafic intrusions. *Earth Planet Science Letters*, **219**:311-324.
- Suita, M.T.F., Pedrosa-Soares, A.C., Leite, A.S., Nilson, A.A., Prichard, H.M. 2004. Complexos ofiolíticos do Brasil e a metalogenia comparada das faixas Araçuaí e Brasília. In: E. Pereira., R. Castroviejo., F. Ortiz. (eds). *Complejos Ofiolíticos em Iberoamérica: guías de prospección para metales preciosos*, 101-132.
- Tack, L., Wingate, M.T.D., Liégeois, J., Fernandez-Alonso, M., Deblond, A. 2001. Early Neoproterozoic magmatism (1000 – 910 Ma) of the Zadinian and Mayumbian Groups (Bas-Congo): onset of Rodinia rifting at the western edge of the Congo craton. *Precambrian Research*, **110**:277-306.
- Tack, L., Wingate, M.T.D., De Waele, B., Meert, J., Belousova, E., Griffin, B., Tahon, A., Fernandez-Alonso, M. 2010. The 1375 Ma “Kibaran event” in Central Africa: Prominent emplacement of bimodal magmatism under extensional regime. *Precambrian Research*, **180**:63-84.

- Taylor, S.R., McLennan, S.M. 1985. *The Continental Crust: Its Composition and Evolution*. Blackwell Scientific, 312 p.
- Taylor, S.R., Rudnick, R.L., McLennan, S.M., Kenneth, A.E. 1986. Rare earth element patterns in Archean high-grade metasediments and their tectonic significance. *Geochimica et Cosmochimica Acta*, **50**:2267-2279.
- Tedeschi, M., Novo, T., Pedrosa-Soares, A., Dussin, I., Tassinari, C., Silva, L.C., Gonçalves, L., Alkmim, F., Lana, C., Figueiredo, C., Dantas, E., Medeiros, S., De Campos, C., Corrales, F., Heilbron, M. 2016. The Ediacaran Rio Doce magmatic arc revisited (Araçuaí-Ribeira orogenic system, SE Brazil). *Journal of South American Earth Sciences*, **68**: 167-186.
- Teixeira, W., Sabaté, P., Barbosa, J., Noce, C. M., Carneiro, M. A. 2000. Archean and Paleoproterozoic tectonic evolution of the São Francisco Craton. In: Cordani, U.G., Milani, E. J., Thomaz-Filho, D. A., Campos, D. A. (eds.) *Tectonic Evolution of South America*. SBG, Sociedade Brasileira de Geologia, Rio de Janeiro, p. 101-137.
- Teixeira, W., Oliveira, E.P., Marques, L.S. 2017. Nature and evolution of the Archean Crust of the São Francisco craton. In: Heilbron, M., Cordani, U.G., Alkmim, F.F. (eds.). *São Francisco Craton, Eastern Brazil*. Springer, 29-56 p.
- Trompette, R., 1997. Neoproterozoic (~600 Ma) aggregation of Western Gondwana: a tentative scenario. *Precambrian Research*, **82**:101-112.
- Uhlein, A. 1991. Transição cráton-faixa dobrada: exemplo do Cráton do São Francisco e da Faixa Araçuaí (Ciclo Brasileiro) no Estado de Minas Gerais (aspectos estratigráficos e estruturais). PhD Thesis, Instituto de Geociências, Universidade de São Paulo, São Paulo, 295 p.
- Valeriano, C.M., Machado, N., Simonetti, A., Valladares, C.S., Seer, H.J., Sergio, L., Simões, A. 2004. U–Pb geochronology of the southern Brasília belt (SE-Brazil) sedimentary provenance, Neoproterozoic orogeny and assembly of West Gondwana. *Precambrian Research*, **130**:27-55.
- Valladares, C.S., Machado, N., Heilbron, M., Gauthier, G. 2004. Ages of detrital zircon from siliciclastic successions south of the Proterozoic basins. *Gondwana Research*, **7**:913-921.
- van Achterbergh, E., Ryan, C.G., Jackson, S.E., Griffin, W. 2001. Data reduction software for LA-ICP-MS. In: Sylvester, P. J. (ed.). *Laser Ablation ICP-Mass Spectrometry in the Earth Sciences: Principles and Applications*. MAC, *Mineralogical Association of Canada*, **29**:239-243.

- Verma, S.P., Armstrong-Altrin, J.S. 2013. New multi-dimensional diagrams for tectonic discrimination of siliciclastic sediments and their application to Precambrian basins. *Chemical Geology*, **355**:117-133.
- Verma, S.P., Díaz-González, L., Armstrong-Altrin, J.S. 2016. Application of a new computer program for tectonic discrimination of Cambrian to Holocene clastic sediments. *Earth Sciences Informatics*, **9**:151-165.
- Vermeesch, P. 2018. IsoplotR: a free and open toolbox for geochronology. *Geoscience Frontier*, **9**:1479-1493.
- Vieira, V.S. 2007. Significado do Grupo Rio Doce no contexto do Orógeno Araçuaí. PhD Thesis, Instituto de Geociências, Universidade Federal de Minas Gerais, Belo Horizonte, 117 p.
- Woodhead, J.D., Hergt, J.M. 2005. A preliminary appraisal of seven natural zircon reference materials for In Situ Hf isotope determination. *Geostandards and Geoanalytical Research*, **29**:183-195.
- Young, G.M. 1999. Some aspects of the geochemistry, provenance and palaeoclimatology of the Torridonian of NW Scotland. *Journal of the Geological Society of London*, **156**:1097-1111.

## **ANEXOS**











U-Pb data produced by LA-ICP-MS dating of zircon from sample LC-019 (LOPAG-DEGEO-UFOP)																								
Grain/Spot	<sup>207</sup> Pb	<sup>206</sup> Pb	<sup>206</sup> Pb/ <sup>204</sup> Pb	f-206	U	Th/U	204 corrected ratios								204 corrected ages								RHO	Conc.
							<sup>207</sup> Pb/ <sup>206</sup> Pb	±2s	<sup>206</sup> Pb/ <sup>238</sup> U	±2s	<sup>207</sup> Pb/ <sup>235</sup> U	±2s	Pb- <sup>206</sup> /Th- <sup>232</sup>	±2s	<sup>207</sup> Pb/ <sup>206</sup> Pb	±2s	<sup>206</sup> Pb/ <sup>238</sup> U	±2s	<sup>207</sup> Pb/ <sup>235</sup> U	±2s	<sup>206</sup> Pb/ <sup>232</sup> Th	±2s		
					(ppm)		(%)	(%)	(%)	(%)	(%)	(%)	(%)	(Ma)	(Ma)	(Ma)	(Ma)	(Ma)	(Ma)	(%)	(%)			
5.sSMPABC143	163451	14496	0,00	0,0000	173,92	0,55	0,0887	1,15	0,2534	1,37	3,0981	1,79	0,0600	2,57	1397	22	1456	18	1432	14	1177	29	0,77	102
5.sSMPABC144	20637	1514	0,00	0,0000	34,31	3,08	0,0734	1,34	0,1622	1,59	1,6402	2,08	0,0475	2,06	1024	27	969	14	986	13	939	19	0,77	98
5.sSMPABC145	96792	11485	0,00	0,0000	71,03	1,58	0,1187	1,12	0,3674	1,45	6,0102	1,83	0,1048	2,12	1936	20	2017	25	1977	16	2014	41	0,79	102
5.sSMPABC146	203376	19014	0,00	0,0000	203,10	0,60	0,0935	1,12	0,2700	1,35	3,4798	1,75	0,0765	2,28	1498	21	1541	19	1523	14	1489	33	0,77	101
5.sSMPABC147	68721	5120	0,00	0,0000	116,34	0,55	0,0745	1,13	0,1592	1,38	1,6359	1,78	0,0551	2,25	1055	23	953	12	984	11	1083	24	0,77	97
5.sSMPABC148	64870	5637	0,00	0,0000	69,73	0,79	0,0869	1,21	0,2508	1,46	3,0049	1,89	0,0758	2,61	1358	23	1443	19	1409	15	1476	37	0,77	102
5.sSMPABC149	139567	12247	1292,25	0,2261	148,94	0,50	0,0878	1,17	0,2526	1,36	3,0565	1,79	0,0758	1,95	1377	22	1452	18	1422	14	1477	28	0,76	102
5.sSMPABC150	209685	16917	0,00	0,0000	263,63	0,57	0,0807	1,18	0,2144	1,57	2,3852	1,96	0,0296	3,32	1214	23	1252	18	1238	14	589	19	0,80	101
5.sSMPABC151	98949	13427	0,00	0,0000	69,27	0,77	0,1357	1,21	0,3851	1,53	7,2052	1,95	0,1132	2,88	2173	21	2100	28	2137	18	2168	59	0,79	98
5.sSMPABC152	36601	2954	0,00	0,0000	46,34	0,79	0,0807	1,20	0,2129	1,54	2,3695	1,95	0,0540	2,78	1214	24	1244	17	1233	14	1062	29	0,79	101
5.sSMPABC153	59067	5027	0,00	0,0000	68,52	0,83	0,0851	1,35	0,2324	1,75	2,7272	2,21	0,0680	3,38	1318	26	1347	21	1336	17	1330	44	0,79	101
5.sSMPABC154	51245	4169	0,00	0,0000	65,06	0,87	0,0814	1,11	0,2123	1,41	2,3816	1,79	0,0645	2,14	1230	22	1241	16	1237	13	1262	26	0,79	100
5.sSMPABC155	50264	3623	0,00	0,0000	84,18	1,79	0,0721	1,25	0,1610	1,53	1,5996	1,97	0,0476	2,31	988	25	962	14	970	12	940	21	0,77	99

U-Pb data produced by LA-ICP-MS dating of zircon from sample LC-037 (LOPAG-DEGEO-UFOP)																								
Grain/Spot	<sup>207</sup> Pb	<sup>206</sup> Pb	<sup>206</sup> Pb/ <sup>204</sup> Pb	f-206	U	Th/U	204 corrected ratios							204 corrected ages						RHO	Conc.			
							<sup>207</sup> Pb/ <sup>206</sup> Pb	±2s	<sup>206</sup> Pb/ <sup>238</sup> U	±2s	<sup>207</sup> Pb/ <sup>235</sup> U	±2s	Pb <sup>208</sup> /Th <sup>232</sup>	±2s	<sup>207</sup> Pb/ <sup>206</sup> Pb	±2s	<sup>206</sup> Pb/ <sup>238</sup> U	±2s	<sup>207</sup> Pb/ <sup>235</sup> U			±2s	<sup>208</sup> Pb/ <sup>232</sup> Th	±2s
							(%)	(%)	(%)	(%)	(%)	(%)	(Ma)	(Ma)	(Ma)	(Ma)	(Ma)	(Ma)	(%)					
5.sSMPABC005	67338	5179	0,00	0,0000	141,22	0,91	0,0769	1,03	0,1801	1,27	1,9094	1,63	0,0560	1,89	1119	20	1067	12	1084	11	1100	20	0,78	98
5.sSMPABC006	190978	16730	0,00	0,0000	316,36	0,89	0,0876	1,10	0,2280	1,25	2,7534	1,66	0,0696	2,38	1374	21	1324	15	1343	12	1360	31	0,75	99
5.sSMPABC007	373663	28477	0,00	0,0000	686,47	0,69	0,0762	0,96	0,2056	1,19	2,1599	1,53	0,0580	1,41	1101	19	1205	13	1168	11	1140	16	0,78	103
5.sSMPABC008	213954	16417	0,00	0,0000	437,60	0,63	0,0767	1,08	0,1846	1,22	1,9533	1,63	0,0579	2,31	1114	22	1092	12	1100	11	1138	26	0,75	99
5.sSMPABC009	125352	11480	0,00	0,0000	184,11	1,29	0,0916	0,99	0,2571	1,23	3,2465	1,58	0,0724	1,55	1459	19	1475	16	1468	12	1414	21	0,78	100
5.sSMPABC010	166583	14654	0,00	0,0000	262,50	1,03	0,0880	0,98	0,2396	1,22	2,9067	1,56	0,0687	1,49	1382	19	1385	15	1384	12	1342	19	0,78	100
5.sSMPABC011	125363	8851	0,00	0,0000	300,65	1,19	0,0706	1,01	0,1575	1,27	1,5328	1,62	0,0439	1,64	946	21	943	11	944	10	867	14	0,78	100
5.sSMPABC012	113285	8230	3492,50	0,0802	276,85	0,72	0,0727	1,06	0,1545	1,23	1,5479	1,62	0,0462	1,86	1004	21	926	11	950	10	913	17	0,76	98
5.sSMPABC013	268717	35188	0,00	0,0000	262,05	1,10	0,1310	0,98	0,3872	1,20	6,9916	1,55	0,1083	1,48	2111	17	2110	22	2110	14	2078	29	0,78	100
5.sSMPABC014	61366	5081	0,00	0,0000	106,16	1,69	0,0828	1,14	0,2183	1,31	2,4920	1,73	0,0651	2,06	1265	22	1273	15	1270	13	1274	25	0,76	100
5.sSMPABC019	128086	10153	0,00	0,0000	282,30	0,67	0,0793	0,98	0,1713	1,23	1,8727	1,57	0,0644	1,65	1179	19	1019	12	1071	10	1261	20	0,78	95
5.sSMPABC020	66861	4894	0,00	0,0000	163,10	1,09	0,0732	1,09	0,1548	1,25	1,5622	1,66	0,0497	1,97	1019	22	928	11	955	10	980	19	0,75	97
5.sSMPABC021	172045	13063	0,00	0,0000	321,88	1,14	0,0759	0,97	0,2018	1,28	2,1131	1,61	0,0549	1,60	1093	20	1185	14	1153	11	1081	17	0,80	103
5.sSMPABC022	229695	18599	1018,62	0,2814	420,59	0,90	0,0810	1,23	0,2062	1,20	2,3024	1,72	0,0611	1,60	1221	24	1209	13	1213	12	1199	19	0,70	100
5.sSMPABC023	392959	41508	15062,71	0,0198	479,27	1,02	0,1056	0,94	0,3096	1,41	4,5093	1,70	0,0600	2,03	1725	17	1739	22	1733	14	1177	23	0,83	100
5.sSMPABC024	272404	21501	0,00	0,0000	578,72	0,78	0,0789	0,99	0,1778	1,18	1,9344	1,54	0,0625	1,50	1170	20	1055	12	1093	10	1225	18	0,77	96
5.sSMPABC025	382762	26831	4617,08	0,0607	941,39	0,50	0,0701	0,97	0,1535	1,24	1,4840	1,58	0,0374	1,60	931	20	921	11	924	10	742	12	0,79	100
5.sSMPABC026	187728	15131	0,00	0,0000	324,22	1,56	0,0806	0,98	0,2187	1,35	2,4299	1,67	0,0487	1,73	1212	19	1275	16	1251	12	961	16	0,81	102
5.sSMPABC027	585629	104295	0,00	0,0000	438,76	0,90	0,1781	0,94	0,5040	1,19	12,3765	1,52	0,1258	1,34	2635	16	2631	26	2633	14	2395	30	0,78	100
5.sSMPABC028	516599	50751	0,00	0,0000	956,37	1,27	0,0982	0,93	0,2040	1,38	2,7630	1,66	0,0293	1,91	1591	17	1197	15	1346	12	585	11	0,83	89
5.sSMPABC029	244831	18316	4320,24	0,0655	527,68	1,09	0,0748	0,98	0,1752	1,30	1,8073	1,63	0,0441	1,63	1063	20	1041	13	1048	11	872	14	0,80	99
5.sSMPABC034	77939	6576	0,00	0,0000	136,31	1,39	0,0844	1,03	0,2159	1,34	2,5121	1,69	0,0573	1,88	1301	20	1260	15	1276	12	1127	21	0,79	99
5.sSMPABC035	334407	26836	0,00	0,0000	617,27	1,03	0,0803	0,95	0,2046	1,20	2,2637	1,53	0,0459	1,39	1203	19	1200	13	1201	11	907	12	0,79	100
5.sSMPABC036	332905	37956	7537,08	0,0400	372,23	1,37	0,1140	0,96	0,3377	1,27	5,3092	1,59	0,0717	1,53	1864	17	1876	21	1870	14	1400	21	0,80	100
5.sSMPABC037	40879	2832	1753,52	0,1600	98,61	1,44	0,0693	1,36	0,1566	1,57	1,4956	2,08	0,0444	2,66	907	28	938	14	929	13	877	23	0,76	101
5.sSMPABC038	156651	19286	47181,23	0,0065	162,02	1,24	0,1231	0,97	0,3651	1,23	6,1976	1,57	0,0968	1,53	2002	17	2006	21	2004	14	1867	27	0,79	100
5.sSMPABC039	166348	15307	0,00	0,0000	243,10	1,14	0,0920	1,02	0,2584	1,28	3,2785	1,64	0,0716	1,82	1468	19	1482	17	1476	13	1397	25	0,78	100
5.sSMPABC040	195272	33309	0,00	0,0000	151,58	2,44	0,1706	0,99	0,4865	1,23	11,4413	1,58	0,1282	1,47	2563	17	2555	26	2560	15	2437	34	0,78	100
5.sSMPABC041	125097	13003	0,00	0,0000	153,43	2,49	0,1039	1,03	0,3079	1,33	4,4124	1,68	0,0852	1,71	1696	19	1730	20	1715	14	1652	27	0,79	101
5.sSMPABC042	331180	38086	0,00	0,0000	376,99	0,12	0,1150	0,97	0,3317	1,21	5,2601	1,55	0,1105	2,61	1880	18	1847	19	1862	13	2119	52	0,78	99
5.sSMPABC043	374268	46821	0,00	0,0000	395,96	0,74	0,1251	0,98	0,3569	1,27	6,1568	1,60	0,0955	1,72	2030	17	1968	22	1998	14	1844	30	0,79	98
5.sSMPABC048	42530	3909	0,00	0,0000	62,86	0,32	0,0919	1,12	0,2555	1,36	3,2380	1,76	0,0984	4,63	1466	21	1467	18	1466	14	1897	84	0,77	100
5.sSMPABC049	346290	43395	14439,47	0,0211	347,15	1,50	0,1253	0,96	0,3767	1,21	6,5085	1,54	0,0932	1,37	2033	17	2061	21	2047	14	1801	24	0,78	101
5.sSMPABC050	126087	9866	0,00	0,0000	234,54	1,14	0,0783	1,00	0,2030	1,28	2,1903	1,62	0,0556	1,73	1153	20	1191	14	1178	11	1094	18	0,79	101
5.sSMPABC051	236208	24889	0,00	0,0000	290,16	1,38	0,1054	1,07	0,3074	1,36	4,4662	1,73	0,0863	2,20	1721	20	1728	21	1725	14	1674	35	0,79	100
5.sSMPABC052	45684	6154	0,00	0,0000	45,44	0,94	0,1347	1,07	0,3797	1,50	7,0510	1,84	0,1425	2,81	2160	19	2075	27	2118	17	2692	71	0,81	98







Lu-Hf data produced by LA-ICP-MS dating of zircon from sample LC-019 (LOPAG-DEGEO-UFOP)														
Grain/Spot	U-Pb Age (Ma)	Sample (present-day ratios)				CHUR	DM	Sample (initial ratios)				Crust Model Ages		TDM (Hf)
		$^{176}\text{Hf}/^{177}\text{Hf}$	$\pm 2\text{SE}$	$^{176}\text{Lu}/^{177}\text{Hf}$	$\pm 2\text{SE}$	$^{176}\text{Hf}/^{177}\text{Hf}$	$^{176}\text{Hf}/^{177}\text{Hf}$	$^{176}\text{Hf}/^{177}\text{Hf}$	$\epsilon\text{Hf}$	$\pm 2\text{SE}$	Mafic source (Ma)	Felsic source (Ma)	(Ma)	
5.sSMPABC009	2122	0,281346	17,586376	0,000374	2,258115	0,281427	0,281682	0,281330	-3,4	20867,7	3230	2772	2591	
5.sSMPABC017	2117	0,281361	14,861278	0,000622	3,752673	0,281430	0,281686	0,281336	-3,3	20344,6	3220	2763	2586	
5.sSMPABC028	2100	0,281496	18,200498	0,000759	4,554034	0,281441	0,281698	0,281466	0,9	5204,1	2838	2532	2415	
5.sSMPABC031	973	0,281740	16,584527	0,000585	3,508676	0,282169	0,282539	0,281729	-15,6	94464,2	3494	2458	2076	
5.sSMPABC032	1737	0,281697	16,141415	0,000684	4,985176	0,281677	0,281971	0,281674	-0,1	744,8	2674	2286	2139	
5.sSMPABC047	1202	0,281947	28,522543	0,001657	9,968803	0,282023	0,282370	0,281909	-4,0	24614,2	2650	2051	1847	
5.sSMPABC056	1760	0,281659	15,879320	0,000958	5,782161	0,281662	0,281954	0,281627	-1,3	7660,3	2792	2364	2206	
5.sSMPABC084	1269	0,282101	17,979830	0,000734	4,437297	0,281980	0,282320	0,282083	3,7	22442,4	2018	1707	1593	
5.sSMPABC091	977	0,281794	20,279101	0,000749	4,637963	0,282167	0,282536	0,281780	-13,7	85755,4	3334	2364	2011	
5.sSMPABC101	951	0,282083	17,284569	0,000808	4,850722	0,282183	0,282555	0,282069	-4,0	24554,2	2479	1848	1620	
5.sSMPABC107	2144	0,281494	18,226366	0,000405	2,430284	0,281413	0,281666	0,281478	2,3	14007,9	2739	2492	2395	
5.sSMPABC108	2612	0,280886	19,199161	0,000942	5,652622	0,281106	0,281311	0,280839	-9,5	57615,7	4096	3482	3244	
5.sSMPABC110	1727	0,281627	13,648507	0,001203	7,243997	0,281684	0,281978	0,281587	-3,4	20822,2	2960	2450	2264	
5.sSMPABC113	2167	0,281361	15,093705	0,000348	2,089243	0,281398	0,281648	0,281346	-1,8	11072,3	3121	2725	2569	
5.sSMPABC114	958	0,282040	19,745943	0,000916	5,498912	0,282178	0,282550	0,282023	-5,5	33354,2	2610	1928	1684	
5.sSMPABC121	2170	0,281355	24,344851	0,000499	3,027300	0,281396	0,281646	0,281335	-2,2	13378,8	3153	2746	2586	
5.sSMPABC128	1800	0,281498	24,683369	0,000824	4,989558	0,281637	0,281924	0,281470	-5,9	36474,8	3229	2638	2416	
5.sSMPABC134	690	0,281598	26,390718	0,000824	4,978537	0,282350	0,282747	0,281588	-27,0	165551,4	4264	2804	2280	
5.sSMPABC141	2725	0,281012	19,088516	0,001036	6,216817	0,281031	0,281225	0,280958	-2,6	15768,0	3568	3218	3083	
5.sSMPABC144	969	0,281518	20,920932	0,000783	4,703217	0,282172	0,282542	0,281504	-23,7	143937,4	4181	2866	2387	
5.sSMPABC150	1214	0,281569	17,231562	0,001327	7,971426	0,282015	0,282361	0,281539	-16,9	102407,1	3772	2721	2350	
5.sSMPABC151	2173	0,281324	15,991055	0,000746	4,498949	0,281394	0,281644	0,281293	-3,6	21868,6	3280	2821	2645	
5.sSMPABC154	1230	0,281936	26,059381	0,000636	3,851603	0,282005	0,282349	0,281922	-2,9	18073,2	2575	2018	1813	
5.sSMPABC155	962	0,281769	18,019769	0,000803	4,820521	0,282176	0,282547	0,281754	-14,9	90648,2	3431	2416	2048	
$^{176}\text{Lu}$ decay constant ( $1.867 \times 10^{-11}/\text{yr}$ ) of Söderlund et al. (2004)										Constants				
Chondritic values of $^{176}\text{Hf}/^{177}\text{Hf}=0.0336$ and $^{176}\text{Lu}/^{177}\text{Hf}=0.282785$ (Bouvier et al., 2008)									$^{176}\text{Lu}/^{177}\text{Hf}=0,022$	$^{176}\text{Lu}/^{177}\text{Hf}=0,010$				
Model depleted mantle with present day $^{176}\text{Hf}/^{177}\text{Hf}$ ratio of 0.28325 and $^{176}\text{Lu}/^{177}\text{Hf}$ ratio of 0.0388 (Griffin et al., 2000; updated by Andersen et al., 2009)														
$^{176}\text{Lu}/^{177}\text{Hf}$ ratios of mafic and felsic crust from Pietranik et al. (2008)														

Lu-Hf data produced by LA-ICP-MS dating of zircon from sample LC-037 (LOPAG-DEGEO-UFOP)														
Grain/Spot	U-Pb Age (Ma)	Sample (present-day ratios)				CHUR	DM	Sample (initial ratios)				Crust Model Ages		TDM (Hf)
		$^{176}\text{Hf}/^{177}\text{Hf}$	$\pm 2\text{SE}$	$^{176}\text{Lu}/^{177}\text{Hf}$	$\pm 2\text{SE}$	$^{176}\text{Hf}/^{177}\text{Hf}$	$^{176}\text{Hf}/^{177}\text{Hf}$	$^{176}\text{Hf}/^{177}\text{Hf}$	$^{176}\text{Hf}/^{177}\text{Hf}$	$\epsilon\text{Hf}$	$\pm 2\text{SE}$	Mafic source (Ma)	Felsic source (Ma)	(Ga)
5.sSMPABC005	1119	0,282167	26,961436	0,001252	8,340499	0,282076	0,282431	0,282141	2,3	15601,7	2036	1656	1523	
5.sSMPABC008	1114	0,282105	15,743734	0,000584	5,156860	0,282079	0,282434	0,282092	0,5	4321,4	2194	1746	1582	
5.sSMPABC011	943	0,282040	17,570246	0,000816	6,307680	0,282188	0,282561	0,282026	-5,8	44966,1	2623	1929	1680	
5.sSMPABC023	1725	0,281500	26,664164	0,001448	9,036022	0,281685	0,281980	0,281452	-8,3	52340,0	3381	2697	2453	
5.sSMPABC025	921	0,282037	13,956138	0,001677	16,192773	0,282202	0,282577	0,282008	-6,9	66883,5	2706	1969	1722	
5.sSMPABC027	2635	0,280982	21,564581	0,000831	5,499596	0,281091	0,281293	0,280940	-5,4	35881,7	3750	3288	3108	
5.sSMPABC037	938	0,281744	19,182848	0,000490	5,869285	0,282192	0,282565	0,281735	-16,2	194850,5	3519	2458	2065	
5.sSMPABC050	1153	0,282077	14,799569	0,000505	4,966255	0,282054	0,282406	0,282066	0,4	4349,3	2225	1781	1616	
5.sSMPABC051	1721	0,281623	17,555368	0,000567	5,033838	0,281688	0,281983	0,281605	-3,0	26478,0	2915	2420	2232	
5.sSMPABC053	1882	0,281302	21,344705	0,001012	7,206777	0,281583	0,281863	0,281266	-11,3	81272,6	3752	2981	2693	
5.sSMPABC065	939	0,281875	19,965395	0,001390	10,203595	0,282191	0,282564	0,281851	-12,1	89412,3	3166	2249	1933	
5.sSMPABC077	1701	0,281725	13,293616	0,001052	6,973418	0,281701	0,281998	0,281692	-0,3	2239,8	2670	2268	2121	
5.sSMPABC093	741	0,282178	16,747499	0,001263	8,960323	0,282317	0,282710	0,282160	-5,6	39749,9	2464	1753	1508	
5.sSMPABC104	934	0,282032	22,026251	0,000459	5,814333	0,282194	0,282568	0,282024	-6,0	76667,7	2639	1935	1674	
5.sSMPABC108	1871	0,281289	17,749143	0,000932	15,698292	0,281590	0,281871	0,281256	-11,9	200855,5	3796	3002	2704	
5.sSMPABC110	1172	0,282081	31,859548	0,001057	8,809589	0,282042	0,282392	0,282058	0,6	4835,7	2226	1789	1633	
5.sSMPABC113	911	0,281778	14,898075	0,000451	3,322755	0,282208	0,282584	0,281770	-15,5	115296,5	3445	2404	2017	
5.sSMPABC120	1725	0,281595	16,432912	0,001497	9,546383	0,281685	0,281980	0,281546	-5,0	31931,9	3093	2527	2326	
5.sSMPABC124	944	0,282041	34,343463	0,000851	5,243348	0,282187	0,282560	0,282026	-5,7	36007,6	2621	1929	1680	
5.sSMPABC133	1125	0,282121	18,133330	0,001182	10,769875	0,282072	0,282427	0,282096	0,8	7735,1	2169	1736	1584	
5.sSMPABC139	1908	0,281475	26,594451	0,000824	6,835599	0,281567	0,281843	0,281445	-4,3	36107,0	3161	2642	2446	
5.sSMPABC140	958	0,282068	15,359731	0,000905	6,937057	0,282179	0,282550	0,282051	-4,5	34839,5	2524	1877	1646	
5.sSMPABC142	1869	0,281150	26,472096	0,000812	5,578546	0,281592	0,281872	0,281121	-16,7	116307,5	4211	3248	2882	
5.sSMPABC147	1688	0,281645	20,680389	0,000696	4,657988	0,281709	0,282007	0,281623	-3,0	20627,1	2900	2398	2209	
5.sSMPABC149	1156	0,282087	23,688681	0,000619	3,943424	0,282052	0,282403	0,282074	0,8	4946,1	2198	1766	1607	
$^{176}\text{Lu}$ decay constant ( $1.867 \times 10^{-11}$ /yr) of Söderlund et al. (2004)										Constants				
Chondritic values of $^{176}\text{Hf}/^{177}\text{Hf}=0.0336$ and $^{176}\text{Lu}/^{177}\text{Hf}=0.282785$ (Bouvier et al., 2008)										$^{176}\text{Lu}/^{177}\text{Hf} = 0,022$	$^{176}\text{Lu}/^{177}\text{Hf} = 0,010$			
Model depleted mantle with present day $^{176}\text{Hf}/^{177}\text{Hf}$ ratio of 0.28325 and $^{176}\text{Lu}/^{177}\text{Hf}$ ratio of 0.0388 (Griffin et al., 2000; updated by Andersen et al., 2009)														
$^{176}\text{Lu}/^{177}\text{Hf}$ ratios of mafic and felsic crust from Pietranik et al. (2008)														

Whole rock geochemistry determined by ICP-MS and ICP-OES											
	Analytical reference	LC-004	LC-006	LC-012	LC-022B	LC-030	LC-039	LC-053	LC-071	LC-073B	LC-088
SiO <sub>2</sub>	ICP95A	65,78	61,91	49,00	66,45	56,02	51,80	62,48	60,94	66,43	60,55
TiO <sub>2</sub>	ICP95A	1,00	0,23	1,61	0,89	1,25	0,36	1,10	0,87	0,84	0,98
Al <sub>2</sub> O <sub>3</sub>	ICP95A	17,07	18,48	25,89	15,73	20,92	17,74	16,48	17,13	14,39	19,43
Fe <sub>2</sub> O <sub>3</sub>	ICP95A	8,14	7,94	11,47	7,32	9,68	6,29	9,00	6,80	8,39	6,31
MnO	ICP95A	0,16	0,04	0,18	0,17	0,15	0,12	0,19	0,10	0,10	0,05
MgO	ICP95A	3,14	4,26	4,83	3,23	3,84	8,00	3,86	3,37	2,22	1,98
CaO	ICP95A	1,13	0,43	0,41	0,74	0,57	11,83	1,53	3,53	0,28	0,20
Na <sub>2</sub> O	ICP95A	2,78	3,54	0,48	1,53	0,81	3,09	2,17	3,21	0,43	0,64
K <sub>2</sub> O	ICP95A	2,95	2,75	4,29	4,91	3,47	0,22	3,46	2,83	6,03	5,91
Cr <sub>2</sub> O <sub>3</sub>	ICP95A	0,02	<0,01	0,02	0,01	0,02	0,03	0,02	0,01	<0,01	0,02
P <sub>2</sub> O <sub>5</sub>	ICP95A	0,12	0,13	0,12	0,10	0,09	<0,01	0,11	0,15	0,11	0,15
LOI	PHY01E	1,52	1,23	1,09	1,72	1,39	0,88	1,03	1,31	1,90	3,77
TOTAL		103,79	100,94	99,37	102,79	98,19	100,33	101,41	100,24	101,12	99,97
Sc	ICM40B	19,70	4,60	28,60	19,00	25,70	47,30	24,40	20,60	16,40	18,70
V	ICP95A	122,00	30,00	184,00	128,00	139,00	177,00	139,00	102,00	92,00	63,00
Cr	ICM40B	65,00	11,00	81,00	46,00	67,00	56,00	54,00	56,00	36,00	72,00
Co	IMS95A	19,10	1,80	24,90	16,80	21,50	32,10	21,00	9,60	46,60	4,50
Ni	IMS95A	45,00	20,00	44,00	36,00	46,00	91,00	51,00	22,00	88,00	12,00
Cu	ICM40B	20,80	6,90	32,10	17,40	59,90	27,50	36,00	29,60	19,00	12,50
Zn	ICP95A	126,0	642,0	460,0	108,0	276,0	22,0	101,0	136,0	122,0	81,0
Rb	IMS95A	137,10	88,70	153,00	167,90	135,10	1,80	110,50	123,90	214,90	205,10
Sr	ICP95A	114,0	202,0	12,0	81,0	46,0	300,0	144,0	345,0	23,0	59,0
Y	IMS95A	32,72	166,84	38,14	26,30	35,32	4,73	24,96	23,98	27,33	31,98
Zr	ICM40B	123,7	135,6	235,1	137,2	181,1	19,7	149,9	137,1	127,3	104,8
Nb	IMS95A	14,86	539,88	36,33	17,30	21,73	0,94	23,83	11,71	18,07	31,24
Mo	ICM40B	0,33	0,32	1,06	0,65	1,30	0,45	0,62	0,91	0,37	0,86
Cs	IMS95A	8,12	2,97	9,03	10,75	7,81	0,11	5,28	8,38	4,24	5,43
Sn	ICM40B	3,10	23,50	3,20	3,70	3,10	0,40	2,70	12,70	2,60	4,80
Ba	ICP95A	531,0	817,0	870,0	784,0	742,0	134,0	836,0	536,0	941,0	1488,0
Hf	ICM40B	4,34	4,47	8,56	5,38	6,81	0,70	5,34	5,21	4,36	4,01
Ta	ICM40B	1,32	32,30	1,68	1,53	0,92	0,40	1,11	1,12	1,37	2,08
W	ICM40B	2,20	2,60	1,40	3,20	1,40	0,10	0,90	2,00	2,70	2,70
Tl	ICM40B	0,79	0,34	0,73	0,92	0,70	<0,02	0,52	0,70	0,74	1,13
Pb	ICM40B	22,60	58,40	8,80	18,90	13,10	1,70	23,40	42,80	14,10	22,70
Bi	ICM40B	0,23	0,18	0,58	0,18	0,48	<0,04	0,27	0,30	0,10	0,21
Th	IMS95A	13,90	96,60	20,50	15,20	15,60	0,40	12,80	12,30	11,20	23,00
U	IMS95A	3,20	7,79	4,06	2,73	3,47	0,07	2,52	2,87	1,43	4,26



<b>Whole rock geochemistry determined by ICP-MS and ICP-OES</b>											
	Analytical reference	LC-004	LC-006	LC-012	LC-022B	LC-030	LC-039	LC-053	LC-071	LC-073B	LC-088
La	ICM40B	30,4	353,5	31,9	26,6	40,2	1,5	37,9	23,7	33,1	54,7
Ce	IMS95A	76,6	824,0	99,3	75,4	86,9	3,3	78,4	68,5	68,3	126,9
Pr	IMS95A	8,9	79,6	11,6	8,5	10,1	0,4	9,1	8,2	8,0	14,6
Nd	IMS95A	32,8	256,2	41,9	30,9	37,2	1,1	33	31,5	30,2	51,7
Sm	IMS95A	7,0	43,8	8,0	6,3	7,0	0,5	6,3	6,6	6,1	9,5
Eu	IMS95A	1,39	2,97	1,07	1,12	1,06	0,37	1,48	1,27	1,21	1,64
Gd	IMS95A	6,14	34,97	6,97	5,18	5,83	0,74	4,89	4,87	5,41	6,98
Tb	IMS95A	0,95	5,93	1,06	0,83	0,95	0,14	0,81	0,72	0,82	1,04
Dy	IMS95A	6,23	34,85	6,71	4,9	6,15	0,94	4,91	4,69	5,05	6,29
Ho	IMS95A	1,28	6,5	1,45	0,99	1,29	0,2	0,96	0,89	1	1,2
Er	IMS95A	3,44	17,41	4,2	3,01	3,83	0,51	2,77	2,67	2,97	3,41
Tm	IMS95A	0,48	2,43	0,58	0,44	0,57	0,08	0,41	0,36	0,44	0,49
Yb	IMS95A	3,20	14,70	4,10	2,90	3,70	0,50	2,60	2,40	2,90	3,10
Lu	ICM40B	0,40	1,58	0,33	0,35	0,32	0,08	0,35	0,18	0,17	0,15
Y	IMS95A	32,72	166,84	38,14	26,3	35,32	4,73	24,96	23,98	27,33	31,98
ICM40B: Determination by multi-acid digestion - ICP-OES/ICP-MS											
ICP95A: Melting with lithium metaborate - ICP-OES											
IMS95A: Melting with lithium metaborate - ICP-MS											
PHY01E: LOI (Loss on Ignition) - 450°C - 1000°C											

Mineral Chemistry (LMlc-DEGEO-UFOP)																	
Sample	No.	Na2O	F	SiO2	Al2O3	MgO	BaO	FeO	Cl	Cr2O3	SrO	TiO2	CaO	K2O	MnO	Total	Comment
LC-004	12	0,01	0,00	37,35	21,10	3,88	0,00	32,91	0,01	0,01	0,00	0,01	1,86	0,00	2,97	100,11	LC-004_campo2_01_Grt-1
LC-004	13	0,03	0,00	37,05	20,83	3,27	0,00	30,99	0,00	0,02	0,00	0,02	3,07	0,00	4,69	99,96	LC-004_campo2_01_Grt-2
LC-004	14	0,02	0,00	37,01	20,86	2,61	0,00	29,40	0,00	0,00	0,00	0,04	3,99	0,00	6,12	100,04	LC-004_campo2_01_Grt-3
LC-004	15	0,05	0,02	37,32	20,93	3,27	0,00	31,14	0,01	0,05	0,00	0,03	3,39	0,01	3,84	100,04	LC-004_campo2_01_Grt-4
LC-004	16	0,00	0,04	37,26	21,19	3,81	0,00	33,49	0,00	0,02	0,00	0,00	1,93	0,00	3,07	100,79	LC-004_campo2_01_Grt-5
LC-022B	67	0,03	0,04	37,70	21,21	4,10	0,00	32,40	0,00	0,00	0,00	0,00	1,20	0,00	4,28	100,95	LC-022B_campo3_01_Grt-1
LC-022B	68	0,06	0,00	37,08	20,81	3,57	0,01	31,10	0,00	0,00	0,00	0,04	1,74	0,00	6,07	100,48	LC-022B_campo3_01_Grt-2
LC-022B	69	0,02	0,00	36,86	20,81	3,27	0,03	29,75	0,00	0,03	0,00	0,03	1,74	0,00	7,67	100,21	LC-022B_campo3_01_Grt-3
LC-022B	70	0,05	0,00	37,12	20,72	3,11	0,00	29,44	0,00	0,08	0,00	0,02	1,60	0,00	7,93	100,06	LC-022B_campo3_01_Grt-4
LC-022B	71	0,00	0,08	37,07	20,77	3,29	0,01	29,93	0,00	0,06	0,00	0,02	1,74	0,01	7,30	100,25	LC-022B_campo3_01_Grt-5
LC-022B	72	0,01	0,09	37,21	20,80	3,51	0,00	30,46	0,00	0,05	0,00	0,02	1,80	0,00	6,37	100,28	LC-022B_campo3_01_Grt-6
LC-022B	73	0,02	0,01	37,02	20,81	3,70	0,00	30,97	0,01	0,00	0,00	0,01	1,75	0,00	5,35	99,65	LC-022B_campo3_01_Grt-7
LC-022B	74	0,01	0,00	36,41	20,64	3,86	0,00	32,74	0,01	0,02	0,02	0,00	1,22	0,00	3,98	98,89	LC-022B_campo3_01_Grt-8
LC-030	13	0,02	0,07	37,33	20,98	3,63	0,00	31,43	0,00	0,00	0,00	0,00	2,56	0,00	3,99	99,99	LC-030_campo2_01_Grt-1
LC-030	14	0,03	0,00	36,89	20,59	3,02	0,01	31,88	0,01	0,00	0,00	0,01	3,63	0,01	2,81	98,88	LC-030_campo2_01_Grt-2
LC-030	15	0,00	0,00	36,85	20,67	2,70	0,00	30,93	0,00	0,00	0,04	0,00	3,58	0,01	4,74	99,51	LC-030_campo2_01_Grt-3
LC-030	16	0,04	0,00	36,93	20,56	1,98	0,00	28,50	0,01	0,00	0,04	0,00	3,99	0,00	7,55	99,59	LC-030_campo2_01_Grt-4
LC-030	17	0,05	0,00	36,82	20,73	2,00	0,00	28,48	0,01	0,00	0,01	0,05	4,00	0,00	7,98	100,12	LC-030_campo2_01_Grt-5
LC-030	18	0,03	0,00	36,91	20,71	2,05	0,00	28,97	0,02	0,00	0,00	0,03	3,85	0,01	7,27	99,83	LC-030_campo2_01_Grt-6
LC-030	19	0,03	0,01	37,01	20,81	2,80	0,00	31,19	0,01	0,00	0,07	0,00	3,25	0,00	4,63	99,80	LC-030_campo2_01_Grt-7
LC-030	20	0,05	0,00	36,80	20,89	3,25	0,05	32,44	0,02	0,00	0,00	0,00	3,22	0,02	2,41	99,14	LC-030_campo2_01_Grt-8
LC-030	21	0,05	0,00	37,05	20,84	3,74	0,00	32,20	0,00	0,00	0,00	0,00	2,68	0,00	2,87	99,43	LC-030_campo2_01_Grt-9
LC-039	36	0,11	0,00	37,01	20,82	2,52	0,00	23,36	0,03	0,00	0,00	0,05	4,86	0,00	11,44	100,19	LC-039_campo3_01_Grt-1
LC-039	37	0,03	0,00	37,19	20,80	2,64	0,00	23,61	0,00	0,00	0,00	0,10	4,89	0,01	11,03	100,29	LC-039_campo3_01_Grt-2
LC-039	38	0,03	0,02	37,59	20,98	2,64	0,00	23,81	0,01	0,01	0,00	0,13	4,48	0,00	11,49	101,18	LC-039_campo3_01_Grt-3
LC-039	39	0,04	0,00	37,25	20,79	2,69	0,00	24,14	0,00	0,05	0,00	0,13	4,59	0,01	11,00	100,69	LC-039_campo3_01_Grt-4
LC-039	40	0,01	0,06	37,35	20,65	2,71	0,00	24,75	0,00	0,02	0,00	0,06	3,23	0,00	12,11	100,93	LC-039_campo3_01_Grt-5
LC-039	41	0,05	0,11	37,50	20,89	2,77	0,03	24,18	0,02	0,00	0,00	0,05	4,10	0,01	11,25	100,92	LC-039_campo3_01_Grt-6
LC-039	42	0,02	0,00	37,36	20,56	2,34	0,04	23,94	0,00	0,04	0,00	0,00	2,42	0,01	13,84	100,57	LC-039_campo3_01_Grt-7

Analytical Conditions of Mineral Chemistry (LMIC-DEGEO-UFOF)										
Spot Size = 5 micrometers										
Voltage = 15 kV										
Probe Current = 20 nA										
Measurement										
Condition										
WDS elements										
	Element	X-ray	Crystal	CH	Acc.v	Peak Pos.	(nm)	BG_L	BG_U	(mm)
1	Na	Ka	TAPH	1	15	130,25	1,19	2,59	1,46	
2	F	Ka	TAPH	1	15	199,49	1,83	3,75	2,00	
3	Si	Ka	TAP	2	15	77,45	0,71	2,61	1,34	
4	Al	Ka	TAP	2	15	90,62	0,83	2,40	1,19	
5	Mg	Ka	TAP	2	15	107,47	0,99	2,03	0,83	
6	Ba	La	PETH	3	15	88,75	0,28	1,10	0,88	
7	Fe	Ka	LIFH	3	15	134,65	0,19	0,83	0,78	
8	Cl	Ka	PETH	3	15	151,30	0,47	2,70	1,83	
9	Cr	Ka	LIF	4	15	158,59	0,23	0,57	0,64	
10	Sr	La	PETJ	4	15	219,35	0,69	1,78	0,72	
11	Ti	Ka	PETL	5	15	87,39	0,27	0,89	0,82	
12	Ca	Ka	PETL	5	15	107,02	0,34	2,04	1,30	
13	K	Ka	PETL	5	15	119,28	0,37	1,06	0,53	
14	Mn	Ka	LIFL	5	15	145,60	0,21	0,48	0,68	
	Element	Peak	Back	Pksk	Gain	High.V	Base.L	Window.W	Mode	
1	Na	10	5.0 (s)	2	16	1622	0,7	0 (V)	Int	
2	F	10	5.0 (s)	2	16	1622	0,7	0 (V)	Int	
3	Si	10	5.0 (s)	2	8	1668	0,5	9.4 (V)	Dif	
4	Al	10	5.0 (s)	2	8	1668	0,5	9.4 (V)	Dif	
5	Mg	10	5.0 (s)	2	8	1668	0,5	9.4 (V)	Dif	
6	Ba	10	5.0 (s)	2	32	1686	1,0	0 (V)	Int	
7	Fe	10	5.0 (s)	2	8	1772	1,0	9.0 (V)	Dif	
8	Cl	10	5.0 (s)	2	32	1686	1,0	0 (V)	Int	
9	Cr	10	5.0 (s)	2	32	1642	0,7	0 (V)	Int	
10	Sr	10	5.0 (s)	2	64	1620	0,7	0 (V)	Int	
11	Ti	10	5.0 (s)	2	16	1754	0,4	9.3 (V)	Dif	
12	Ca	10	5.0 (s)	2	16	1754	0,4	9.3 (V)	Dif	
13	K	10	5.0 (s)	2	16	1754	0,4	9.3 (V)	Dif	
14	Mn	10	5.0 (s)	2	8	1754	0,4	9.6 (V)	Dif	

Analytical Conditions of Mineral Chemistry (LMic-DEGEO-UFOP)								
Measurement	Order	of	WDS					
Order	Channel 1	2	3	4	5			
1	Na_1TAPH	Si_2TAP_	Ba_3PETH	Cr_4LIF_	Ti_CH5_P			
2	F_1TAPH_	Al_2TAP_	Fe_3LIFH	Sr_4PETJ	Ca_5LIFL			
3	0	Mg_2TAP_	Cl_3PETH	0	K_5PETL_			
4	0	0	0	0	Mn_5LIFL			
Calc.	Elements :	O	(Anion)					
Standard Data								
	Element	Standard	Mass(%)	ZAF Fac.	Z	A	F	
1	Na2O	Anorthoclase	9,31	5,31	10,74	0,49	1,004	
2	F	CaF2	48,67	5,56	22,06	0,25	1,000	
3	SiO2	Quartz	99,99	3,51	4,36	0,81	1,000	
4	Al2O3	Corundum	99,99	4,43	5,89	0,75	1,000	
5	MgO	Olivine	49,42	4,78	7,88	0,60	1,003	
6	BaO	BaSO4	65,70	0,54	0,57	0,93	1,000	
7	FeO	Magnetite	91,12	0,21	0,22	0,99	1,000	
8	Cl	Scapolite(Meionite)	1,43	1,61	1,99	0,81	1,004	
9	Cr2O3	Chromite	60,50	0,36	0,36	0,98	1,016	
10	SrO	Strontianite	67,67	3,47	4,40	0,79	1,000	
11	TiO2	Rutile	100,00	0,59	0,61	0,98	1,000	
12	CaO	Fluor-Apatite	54,02	0,89	0,95	0,93	1,000	
13	K2O	Microcline	15,14	1,07	1,20	0,89	1,000	
14	MnO	MnO2	81,60	0,28	0,28	0,99	1,000	
Standard Intensity of WDS								
	Element	Curr.(A)	Net(cps)	Bg-(cps)	Bg+(cps)	S.D.(%)	Date	
1	Na	2,00E-08	1592,50	60,80	43,60	1,00	3/2/2017	13:25:46
2	F	2,01E-08	1436,90	36,80	46,10	1,05	11/16/2017	11:40:03
3	Si	2,01E-08	17853,50	273,20	129,30	0,29	11/16/2017	11:45:11
4	Al	2,00E-08	19103,80	253,90	159,00	0,28	11/13/2017	10:31:59
5	Mg	2,01E-08	6157,10	150,40	144,80	0,51	11/16/2017	11:50:11
6	Ba	2,01E-08	14052,30	515,80	433,70	0,29	11/16/2017	11:56:31
7	Fe	2,01E-08	9866,40	208,00	260,60	0,40	11/16/2017	12:01:53
8	Cl	2,01E-08	570,40	18,30	17,70	0,97	3/13/2017	14:56:30
9	Cr	2,01E-08	1462,00	25,00	27,70	1,03	4/3/2017	15:00:07
10	Sr	2,00E-08	551,80	17,60	15,70	1,70	11/16/2017	12:20:52
11	Ti	2,01E-08	37217,10	252,80	257,00	0,20	11/16/2017	12:26:01
12	Ca	2,00E-08	24868,00	65,30	97,50	0,25	11/16/2017	16:19:13
13	K	2,00E-08	6545,80	73,90	112,60	0,49	3/2/2017	13:31:21
14	Mn	2,00E-08	5028,60	125,10	117,10	0,43	3/2/2017	13:10:54

Mineral Chemistry: Garnet Zoning						Mineral Chemistry: Garnet Zoning									
Sample	LC-004	LC-004	LC-004	LC-004	LC-004	Sample	LC-022B	LC-022B	LC-022B	LC-022B	LC-022B	LC-022B	LC-022B	LC-022B	
Spot	12	13	14	15	16	Spot	67	68	69	70	71	72	73	74	
Site	Rim	Core	Core	Core	Rim	Site	Rim	Rim	Core	Core	Core	Core	Rim	Rim	
SiO <sub>2</sub>	37,35	37,05	37,01	37,32	37,26	SiO <sub>2</sub>	37,70	37,08	36,86	37,12	37,07	37,21	37,02	36,41	
TiO <sub>2</sub>	0,01	0,02	0,04	0,03	0,00	TiO <sub>2</sub>	0,00	0,04	0,03	0,02	0,02	0,02	0,01	0,00	
Al <sub>2</sub> O <sub>3</sub>	21,10	20,83	20,86	20,93	21,19	Al <sub>2</sub> O <sub>3</sub>	21,21	20,81	20,81	20,72	20,77	20,80	20,81	20,64	
Cr <sub>2</sub> O <sub>3</sub>	0,01	0,02	0,00	0,05	0,02	Cr <sub>2</sub> O <sub>3</sub>	0,00	0,00	0,03	0,08	0,06	0,05	0,00	0,02	
Fe <sub>2</sub> O <sub>3</sub>						Fe <sub>2</sub> O <sub>3</sub>									
FeO	32,91	30,99	29,40	31,14	33,49	FeO	32,40	31,10	29,75	29,44	29,93	30,46	30,97	32,74	
MnO	2,97	4,69	6,12	3,84	3,07	MnO	4,28	6,07	7,67	7,93	7,30	6,37	5,35	3,98	
MgO	3,88	3,27	2,61	3,27	3,81	MgO	4,10	3,57	3,27	3,11	3,29	3,51	3,70	3,86	
CaO	1,86	3,07	3,99	3,39	1,93	CaO	1,20	1,74	1,74	1,60	1,74	1,80	1,75	1,22	
Total	100,11	99,96	100,04	100,04	100,79	Total	100,95	100,48	100,21	100,06	100,25	100,28	99,65	98,89	
Alm	72,44	67,26	63,98	68,49	72,23	Alm	70,77	66,78	64,13	64,82	65,05207	66,28	67,79	71,34	
Spes	6,73	10,73	13,99	8,72	6,97	Spes	9,62	13,86	17,62	18,09	16,67854	14,49	12,24	9,26	
Pyr	15,48	13,14	10,48	13,07	15,25	Pyr	16,20	14,33	13,19	12,47	13,23107	14,06	14,91	15,82	
Gros	5,24	8,52	11,14	9,52	5,31	Gros	3,36	4,78	4,81	4,51	4,847194	4,99	4,90	3,39	
Uvar	0,00	0,01	0,00	0,01	0,00	Uvar	0,00	0,00	0,01	0,01	0,009396	0,01	0,00	0,00	
Andr	0,10	0,34	0,40	0,18	0,23	Andr	0,06	0,24	0,24	0,10	0,178609	0,16	0,16	0,20	
Ca-Ti Grt	0,00	0,00	0,01	0,01	0,00	Ca-Ti Grt	0,00	0,01	0,01	0,00	0,003128	0,00	0,00	0,00	
XCa	0,05	0,09	0,12	0,10	0,06	XCa	0,03	0,05	0,05	0,05	0,050383	0,05	0,05	0,04	

Mineral Chemistry: Garnet Zoning										Mineral Chemistry: Garnet Zoning							
Sample	LC-030	LC-030	LC-030	LC-030	LC-030	LC-030	LC-030	LC-030	LC-030	Sample	LC-039	LC-039	LC-039	LC-039	LC-039	LC-039	LC-039
Spot	13	14	15	16	17	18	19	20	21	Spot	36	37	38	39	40	41	42
Site	Rim	Rim	Core	Core	Core	Core	Core	Rim	Rim	Site	Rim	Rim	Core	Core	Core	Rim	Rim
SiO <sub>2</sub>	37,33	36,89	36,85	36,93	36,82	36,91	37,01	36,80	37,05	SiO <sub>2</sub>	37,01	37,19	37,59	37,25	37,35	37,50	37,36
TiO <sub>2</sub>	0,00	0,00	0,00	0,00	0,00	0,00	0,00	0,00	0,00	TiO <sub>2</sub>	0,05	0,10	0,13	0,13	0,06	0,05	0,00
Al <sub>2</sub> O <sub>3</sub>	20,98	20,59	20,67	20,56	20,73	20,71	20,81	20,89	20,84	Al <sub>2</sub> O <sub>3</sub>	20,82	20,80	20,98	20,79	20,65	20,89	20,56
Cr <sub>2</sub> O <sub>3</sub>	0,00	0,00	0,04	0,04	0,01	0,00	0,07	0,00	0,00	Cr <sub>2</sub> O <sub>3</sub>	0,00	0,00	0,01	0,05	0,02	0,00	0,04
Fe <sub>2</sub> O <sub>3</sub>										Fe <sub>2</sub> O <sub>3</sub>							
FeO	31,43	31,88	30,93	28,50	28,48	28,97	31,19	32,44	32,20	FeO	23,36	23,61	23,81	24,14	24,75	24,18	23,94
MnO	3,99	2,81	4,74	7,55	7,98	7,27	4,63	2,41	2,87	MnO	11,44	11,03	11,49	11,00	12,11	11,25	13,84
MgO	3,63	3,02	2,70	1,98	2,00	2,05	2,80	3,25	3,74	MgO	2,52	2,64	2,64	2,69	2,71	2,77	2,34
CaO	2,56	3,63	3,58	3,99	4,00	3,85	3,25	3,22	2,68	CaO	4,86	4,89	4,48	4,59	3,23	4,10	2,42
Total	99,99	98,88	99,51	99,59	100,12	99,83	99,80	99,14	99,43	Total	100,19	100,29	101,18	100,69	100,93	100,92	100,57
Alm	69,09	70,80	67,78	63,13	61,89	63,88	68,71	71,93	70,62	Alm	49,67	50,32	51,00	51,14	52,50	51,90	52,38
Spes	9,06	6,46	10,89	17,32	18,36	16,69	10,60	5,54	6,56	Spes	26,16	25,08	25,83	24,94	27,42	25,39	31,36
Pyr	14,49	12,20	10,91	7,98	8,09	8,26	11,28	13,16	15,06	Pyr	10,12	10,55	10,45	10,75	10,81	11,02	9,32
Gros	7,22	10,31	10,03	11,31	11,18	10,88	9,15	9,12	7,52	Gros	13,41	13,46	12,33	12,54	8,85	11,34	6,80
Uvar	0,00	0,00	0,01	0,02	0,00	0,00	0,02	0,00	0,00	Uvar	0,00	0,00	0,00	0,02	0,00	0,00	0,01
Andr	0,14	0,23	0,37	0,24	0,47	0,29	0,25	0,25	0,24	Andr	0,62	0,54	0,34	0,55	0,39	0,34	0,13
Ca-Ti Grt	0,00	0,00	0,00	0,00	0,00	0,00	0,00	0,00	0,00	Ca-Ti Grt	0,02	0,04	0,05	0,05	0,02	0,02	0,00
XCa	0,07	0,11	0,10	0,12	0,12	0,11	0,09	0,09	0,08	XCa	0,14	0,14	0,13	0,13	0,09	0,12	0,07